The Interaction and Steering of Nematicons

Benjamin D. Skuse

Doctor of Philosophy
University of Edinburgh
2010

Declaration

I declare that this thesis was composed by myself and that the work contained therein is my own, except where explicitly stated otherwise in the text.

(*Benjamin D. Skuse*)

To Marjorie

Abstract

The waveguiding effect of spatial solitary waves in nonlinear optical media has been suggested as a potential basis for future all-optical devices, such as optical interconnects. It has been shown that low power ($\sim mW$) beams, which can encode information, can be optically steered using external electric fields or through interactions with other beams. This opens up the possibility of creating reconfigurable optical interconnects.

Nematic liquid crystals are a potential medium for such future optical interconnects, possessing many advantageous properties, including a "huge" nonlinear response at comparatively low input power levels. Consequently, a thorough understanding of the behaviour of spatial optical solitary waves in nematic liquid crystals, termed nematicons, is needed. The investigation of multiple beam interaction behaviour will form an essential part of this understanding due to the possibility of beam-on-beam control. Here, the interactions of two nematicons of different wavelengths in nematic liquid crystals, and the optical steering of nematicons in dye-doped nematic liquid crystals will be investigated with the aim of achieving a broader understanding of nematicon interaction and steering.

The governing equations modelling nematicon interactions are nonintegrable, which means that nematicon collisions are inelastic and radiative losses occur during and after collision. Consequently numerical techniques have been employed to solve these equations. However, to fully understand the physical dynamics of nematicon interactions in a simple manner, an approximate variational method is used here which reduces the infinite-dimensional partial differential equation problem to a finite dynamical system of comparatively simple ordinary differential equations. The resulting ordinary differential equations are modified to include radiative losses due to beam evolution and interaction, and are then quickly solved numerically, in contrast to the original governing partial differential equations. Nöther's Theorem is applied to find various conservation laws which determine the final steady states, aid in calculating shed radiation and accurately compute the trajectories of nematicons. Solutions of the approximate equations are compared with numerical solutions of the original governing equations to determine the accuracy of the approximation. Excellent agreement is found between full numerical solutions and approximate solutions for each physical situation modelled. Furthermore, the results obtained not only confirm, but explain theoretically, the interaction phenomena observed experimentally. Finally, the relationship between the nature of the nonlinear response of the medium, the trajectories of the beams and radiation shed as the beams evolve is investigated.

Acknowledgements

First and foremost I wish to thank Professor Noel Smyth for his guidance and support for the past four years. His enthusiasm, patience, knowledge and kindness have been an inspiration and I could not have completed this work without him. I also wish to thank Professor David Parker for suggesting I apply for this PhD. Without his encouragement life would be very different now! Professor Tim Minzoni reinvigorated my interest in all things scientific with his enthusiasm and bottomless knowledge of the history of science. He and his family welcomed me, a foreign stranger, into their home and showed me such kindness that will never be forgotten. Finally the help, advice and support from numerous friends and family members cannot go unmentioned. Thanks go particularly to Julian Wagstaff, Evgeni Ovcharov and of course my parents, Jacqueline and David Skuse.

Contents

List of Abbreviations

CCD - Charge Coupled Device

CNLS - Coupled Nonlinear Schrödinger Equation

DD-NLC - Dye-Doped Nematic Liquid Crystal

FFT - Fast Fourier Transform

IST - Inverse Scattering Transform

LCD - Liquid Crystal Display

NIR - Near Infrared

NLC - Nematic Liquid Crystal

NLS - Nonlinear Schrödinger Equation

ODE - Ordinary Differential Equation

PDE - Partial Differential Equation

PVA - Polyvinyl Alcohol

SOS - Spatial Optical Soliton

TIR - Total Internal Reflection

XPM - Cross-phase modulation

Chapter 1

Introduction

1.1 Solitary Waves - 'Solitons'

The first written record of a soliton can be found in James Scott Russell's *Report on Waves* which describes the "*large solitary elevation*" Scott Russell famously observed on Edinburgh's Union Canal in 1834 [1]. Boussinesq, Lord Rayleigh and Korteweg & de Vries developed mathematical models supporting Scott Russell's observation of what was later termed a *solitary wave* before the turn of the 20th century, but it was not until the mid-1960s that the term 'soliton' was coined and the inverse scattering transform (IST) developed, from which exact multiple soliton solutions of various nonlinear equations could be computed. Strictly speaking Scott Russell observed a solitary wave, whereas developments in the 1960s largely focused on idealised solitary waves, or solitons. A soliton is defined as a solution of an integrable nonlinear differential equation for which

- *the solution is a stable solitary wave*, i.e. a localised wave of permanent form.
- *interactions between solitons are elastic*, i.e. the soliton can collide with other solitons yet emerge unchanged except for a phase shift, with no radiative losses.

This exacting definition meant that solitons were difficult to create in experimental situations, so in the physical and experimental literature the definition was extended to include periodically varying localised waves and localised waves where propagation and collisions resulted in radiative losses. Whilst the qualitative behaviour of these experimental solitons was similar, they no longer quantitatively satisfied the original definition of a soliton. A more encompassing description of what a soliton is has been used in optics and related literature over the past few decades and can be summarised by the following;

A soliton is a solution of a nonlinear partial differential equation for which

- the solution is a localised wave which retains its basic form over a long time or large distance.
- interactions between solitons can be elastic or inelastic, but solitons emerge from collisions with a similar size and shape or fuse together creating a larger localised wave with a similar shape.

A broad spectrum of interesting nonlinear phenomena involving localised structures could then be classed under a 'catch-all' term using this definition. The localised structures presented here conform to such a definition.

Developments in nonlinear wave theory in the 1960s were the prelude to a great surge of interest in nonlinear optics from the 1970s to the present day. The development of low loss glass for optical communications sparked the initial theoretical interest, with Hasegawa & Tappert predicting that optical fibres could support the propagation of stable temporal solitons in 1973 [2, 3], later confirmed in 1980 experimentally [4]. Such developments in the field, combined with the increasing knowledge of various useful soliton properties, such as the low losses associated

with soliton propagation and their intrinsic nonlinear nature, attracted both researchers and members of the communications industry whose aim was to improve fibre optic communication technology. This indirectly resulted in the discovery of various new types of temporal and spatial solitons in a huge variety of different materials.

There are a number of differences between temporal and spatial solitons worth mentioning before continuing further. Temporal solitons can form in media exhibiting weak nonlinearities and are described, or at least approximated, as being stable. Generally temporal solitons are easily modelled using a linear approximation. Contrary to this, spatial solitons form in media with a strong nonlinearity and their stability is not guaranteed [5]. A full nonlinear description must therefore be found. Whilst temporal solitons are formed via a balance between nonlinear self-phase modulation and linear dispersion, spatial solitons rely on balancing nonlinear self-focusing and linear diffractive spreading. Diffractive spreading can be countered by an increase in the refractive index of the medium in the vicinity of the beam, which focuses the beam and causes a waveguiding effect. If the beam itself causes the refractive index change in the medium then the beam traps itself in its own waveguide, a property known as nonlinear local self-focusing, where the term 'local' refers to the self-focusing response of the medium being greatest where the beam intensity is high and decaying to zero outside of the near vicinity of the beam.

In recent years a great deal of attention has turned to spatial optical solitons (SOS) in nonlinear optical media. There are three main reasons for this change in direction. Firstly, in contrast to media supporting temporal solitons, the large nonlinearities associated with media capable of supporting SOS do not allow linear models to approximately describe soliton behaviour. Hence, a more refined approach is required. Secondly, a huge variety of materials support SOS propagation. Soliton evolution is directly affected by the properties of the medium. Thus solitons in different media are governed by different equations, allowing great scope for original research. Lastly, interest has been stoked further by the potential applications of SOS in technology. For example, SOS in liquid crystals have been proposed as candidates for use in optoelectronic devices, such as logic gates [6]. This thesis focuses attention particularly on SOS in a highly promising nonlinear medium, the nematic liquid crystal (NLC), adding theoretical understanding to experimental observations and contributing to the ever-growing rich tapestry of knowledge in soliton theory.

1.2 Nematic Liquid Crystals and Nematicons

Solitons have been observed in a huge range of nonlinear materials, from the first solitons discovered in water by John Scott Russell to solitons describing the macroscopic dynamics of Bose-Einstein condensates [5]. One of the most interesting materials capable of supporting solitons is the nematic liquid crystal (NLC), due to its uniquely controllable nonlinear response and extensive use in technology, for example the liquid crystal display (LCD).

In a NLC, a beam can self-focus due to a regular local nonlinearity which was described above and/or a nonlocal reorientational nonlinearity. The nonlocal nonlinearity is defined and discussed below, but it suffices here to say that it is highly tuneable and consequently SOS have been observed that have been induced by a regular local nonlinearity, a nonlocal nonlinearity or a combination of both [7, 8, 9]. Other materials such as plasmas and atomic vapours, ion gases, thermoelastic media and photorefractive crystals exhibit nonlocal soliton formation [10, 11, 12], however none of these nonlocal media possess the same mechanism driving nonlocality as that of the NLC.

Liquid crystals display characteristics of liquids, yet retain some degree of long range molecular order similar to crystals. A nematic liquid crystal is a type of thermotropic liquid crystal. As the name suggests, thermotropic liquid crystals come into being by changing the temperature of the medium. At low temperature a material will form an anisotropic crystal, raising the temperature leads to the formation of smectic liquid crystals that have a well-defined positional and orientational molecular order, a further rise in temperature leads to the nematic phase and above this all order is lost and the medium forms an isotropic liquid. The nematic phase is characterised by a high degree of molecular orientational order and no positional order. As a result, NLCs exhibit a fluidity in motion but with the optical properties of a crystal. There are

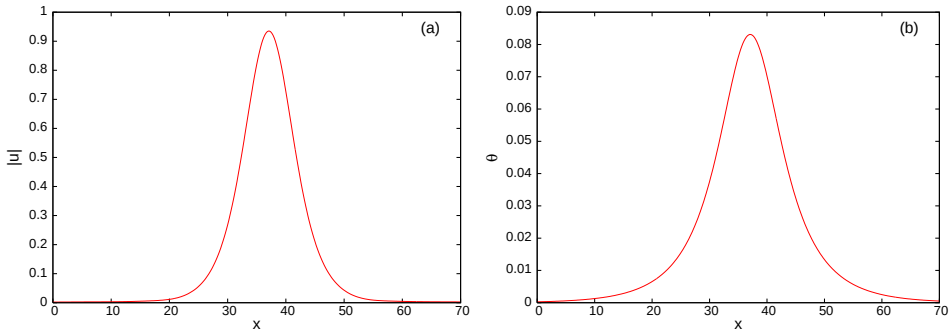

Figure 1.1: Numerically calculated steady nematicon. Cross-sections of (a) the nematicon beam profile and (b) the perturbation θ of the refractive index of the NLC caused by the beam and extending beyond it.

several advantageous properties that LCs, and in particular NLCs, possess. Liquid crystals in general are chemically stable and can be kept in the LC phase over a wide range of temperatures. NLCs have the advantage that their refractive index is easily changed by electric fields, magnetic fields and boundary conditions [13]. With such easily tuned nonlinearities, NLCs have become relatively common media for optical experimentation.

Nematic molecules are rod-like and tend to align in a certain direction via elastic intermolecular forces. When an electric or magnetic field is applied to the medium the rod-like molecules form dipoles and rotate in response to the torque induced by the dipole-field interaction, resulting in a large refractive index change in the liquid crystal. The electric field of a light beam can also induce the same reorientational response as a static/low-frequency applied electric field. The resulting refractive index change extends beyond the vicinity of the beam, which is demonstrated in Figure 1.1 for a single nematicon propagating in a nonlocal NLC. The beam profile is given in Figure 1.1(a). The perturbation of the molecular orientation, or refractive index change , caused by the beams' presence, θ, shown in Figure 1.1(b), clearly extends beyond the tail of the beam itself. This nonlinear reorientational response occurs in other optical media, such as thermoelastic media [14], but the degree of control via electric fields is unique to NLCs and, as a result, is the source of unique nonlinear effects. Local nonlinearities, on the other hand, are far more common. NLCs are capable of local and nonlocal reactions. As a result of this, the analysis of nematicons requires appropriate equations that model nematicon propagation and interaction in both local and nonlocal regimes. These equations will be shown to be strongly related to the nonlinear Schrödinger (NLS) equation, which is the simplest equation governing soliton evolution in a nonlinear optical medium and is written

$$i\frac{\partial u}{\partial z} + \frac{1}{2}\nabla^2 u + |u|^2 u = 0, \tag{1.1}$$

where u represents the envelope of the electric field of the beam and z is the propagation direction. The Laplacian ∇^2 can refer to the second derivative of u with respect to the spatial variable x transverse to z for $(1+1)$-D solitons, or $\partial^2 u/\partial x 2 + \partial^2 u/\partial y^2$ for $(2+1)$-D solitons, where the term '$(1+1)$-D soliton' refers to a soliton which is limited to one spatial transverse dimension, e.g. x and one propagation (time-like) direction z. Solitons can be modelled in (1+1) dimensions in planar waveguides, such as the homeotropically-aligned thin film waveguide used by Karpierz *et al* to observe nematicons [13]. A $(2+1)$-D soliton has two transverse spatial dimensions, x & y, and a propagation direction z. These $(2+1)$-D solitons will be the focus of the present work. It is worth noting that the coefficient $1/2$ in the NLS equation is solely included to simplify calculations. The second (Laplacian) term represents linear diffraction as the beam evolves. Nonlinear self-focusing is represented by the final term. A balance between the two terms results in the emergence of a stable soliton.

The (1+1)-D NLS equation is integrable and possesses exact solutions. It has a stable soliton solution which can be found via the IST or, more easily, analytically and is given exactly by

$$u(x,z) = a\,\mathrm{sech}(ax)e^{ia^2 z/2}, \tag{1.2}$$

where a is the amplitude of the soliton. Conversely stable soliton solutions cannot be found for the $(2+1)$-D NLS equation because solutions blow-up in finite z above an amplitude threshold or decay into radiation below the threshold. For the $(2+1)$-D nematicon equations presented in this work, nonlinearities have a complicated dependence on molecular reorientation, the optical beam(s) and changes to the nematic refractive index. As a consequence the $(2+1)$-D NLS equation is an inappropriate equation to model nematicon evolution. Stable evolution in $(2+1)$ dimensions can, however, be achieved in materials whose nonlinear response is saturable. It will be shown that the thermal and reorientational nonlinearities characteristic of NLCs have this saturating property. The complex interactions between the beam(s) and the medium can be modelled by coupling a NLS-like equation to equations representing this interaction. A more appropriate basic equation encompassing various nematicon evolution phenomena then is the generalised NLS equation

$$i\frac{\partial u}{\partial z} + \frac{1}{2}\left(\frac{\partial^2 u}{\partial x^2} + \frac{\partial^2 u}{\partial y^2}\right) + F(|u|^2)u = 0, \tag{1.3}$$

where the specific form of F depends on the relation u has with the nematic refractive index change, which can be defined separately. Even though equations of the type (1.3) may not necessarily be exactly integrable and will therefore not have an infinite number of conserved quantities, stable solitary wave solutions can be found which possess a finite number of conserved quantities [11]. Each nematicon regime presented in this work will have equations of this general form which govern the propagation of the light beam(s). Two-colour nematicon equations only differ in that each of the NLS-like equations representing each of the beams will have a nonlinearity F with a dependence on the other beam due to coupling. The specific form of F for each nematicon regime investigated will be discussed in the Background section of each chapter and a brief derivation of the general nematicon governing equations will be given in Section 2.1.

A reorientational nonlinearity causes a very strong refractive index change in the medium, particularly when considering the relatively low power levels ($\sim 2mW$) used to excite a nonlinear reaction [6]. The saturating nature of the nonlinearity additionally means that nematicons are easy to generate for a large range of power levels. This combination of properties suggests that there is potential for using nematicons in optoelectronic components. However, whilst the nonlinear effect is strong, several orders of magnitude greater than that of comparable media [9], it is also slow ($\sim 0.1s$) [6]. NLCs in their present form have little chance of finding commercial optoelectronic applications in telecommunications, where GHz switching rates are the minimum. For example, current electrical interconnects switch at microsecond speeds, whereas optical interconnects created using solitons in NLCs react over seconds [15]. The issue of the slowness of the NLC nonlinear reaction is not addressed in this work, but should be kept in mind as any claims of potential applications for SOSs in NLCs are made under the assumption that nonlinear reaction times will be improved significantly in the future, a condition which is far from guaranteed. There is a large amount of materials research being conducted now with the specific aim of increasing the speed of the NLC nonlinear response. In the meantime NLCs are still highly useful, providing an ideal test bed for investigations into novel optical soliton dynamics.

1.3 Experimentally Observed Nematicons

Nematicons (SOSs in NLCs) have been extensively studied by experimentalists since early investigations of the nonlocal, nonlinear self-focusing of beams in NLCs by Braun *et al* in 1993 [7]. "*Self-waveguiding structures*", most likely nematicons, were observed by Warenghem *et al* in capillaries filled with dye-doped NLC in 1998 [8], but it was not until 2000 that $(2+1)$-D nematicons were first observed in bulk NLC by Peccianti *et al* [9]. A beam was shown to propagate unchanged over a distance of $1.4mm$, which is more than 20 times the distance at which the beam would be expected to diffract. This SOS in a NLC was later given the title "*nematicon*" in 2003 [6]. Investigations by experimental researchers in the Nonlinear Optics and Optoelectronics Lab (Nooel) in the University of Rome "Roma Tre" and various other

institutions have revealed substantial differences between soliton behaviour in local nonlinear media and NLCs. These differences can be attributed to the large saturable reorientational nonlocal nonlinearity described in the previous section.

The experimental scheme naturally varies slightly depending on the particular behaviour under investigation. However a general overview of how nematicons are produced is useful, particularly when comparing theoretical results with experimental observations. A cell is filled with a commercially available nematic such as E7 or 5CB. The NLC cell is treated as a bulk medium, with boundary effects being neglected, when the wavelength of the light and the width of the initial beam are smaller than the dimensions of the cell in the (x, y)-plane and the beam propagates far from the cell boundaries. Nematic molecules in the bulk nematic can be given a homeotropic or planar initial alignment. Here only NLCs with an initial planar alignment will be considered. By applying an external static/low-frequency electric field (also known as bias) the mean molecular orientation (termed director) can be adjusted. This is known as a pre-tilt of the director. The pre-tilt is decided by the relative strength of the torque, which forces molecules to align in the direction of the external applied field, and the strength of inter-molecular forces struggling to keep molecules in their original alignment. The introduction of a pre-tilt field is necessary to lower the minimum optical beam power required to provoke a reorientational response in the nematic, known as the Fréedericksz transition threshold. A pre-tilt in the direction of polarisation of the electric field of the input beam then allows the initial beam to evolve into a nematicon at a lower optical power, since the increase in refractive index required to self-focus the beam is reduced due to the initial increase in refractive index caused by the pre-tilt. Not only is there a saving in power consumption (since beams require less power to form nematicons when an appropriate pre-tilt is introduced), but this also reduces the unwanted effects of thermal local nonlinearities on nematicons. An ideal pre-tilt forms an angle of $\pi/4$ with respect to the direction of propagation of an initial beam, as then the Fréedricksz threshold is zero [16]. It is worth noting that a pre-tilt can also be achieved by different methods usually involving a change in the anchoring conditions of the nematic molecules at the boundary of the NLC cell, which affects the molecular orientation in the bulk NLC. One method involves coating the glass slide interfaces bounding the cell with Polyvinyl alcohol (PVA) and then rubbing them. Doing so affects the molecular anchoring and mean orientation at the boundaries and has a knock-on effect with respect to the orientation of molecules in the bulk cell [15, 17]. Another method is to mix the NLC with a small amount of dye dopant [16]; an external beam shone into the dye-doped nematic liquid crystal (DD-NLC) causes an interaction between dye molecules and molecules on the inner surface of the glass interface at the boundary of the DD-NLC layer. This interaction can be tuned to change anchoring conditions of nematic molecules at the boundaries which also changes the molecular orientation throughout the illuminated region of the bulk DD-NLC, allowing an increase or decrease of the refractive index according to the wavelength and/or intensity of the external beam [16]. The effect that an illumination has on a propagating nematicon in a DD-NLC layer is the focus of Chapter 5.

Whichever way a pre-tilt is achieved it must have a component in the same plane as that of the electric field of the beam to have any effect, due to the birefringent nature of NLCs. As an example, an x-polarised input beam will diffract if the applied electric field is in the y direction since the pre-tilt will be in the (y, z)-plane. There will be no pre-tilt in the (x, z)-plane meaning that the Fréedericksz threshold cannot be overcome, molecular reorientation cannot occur and the beam will not self-focus [18]. Of course, if the beam had an optical power high enough to overcome the Fréedericksz threshold without a pre-tilt it could self-focus and form a nematicon but additional local nonlinearities would play a significant role and the possibility of strong self-focusing increases the chances of the nematicon becoming unstable [9].

Figure 1.2 shows experimental results taken from Ref. [9] for which a linearly x-polarised Gaussian input beam was launched from a laser into a bulk planar NLC cell. Beam propagation was monitored in the (y, z)-plane using a charge coupled device (CCD) camera attached to a microscope which collected light scattered in the x direction. Figure 1.2 (a) reveals that with no pre-tilt field a weak beam could not overcome the Fréedericksz transition threshold and diffracted at $z \approx 55\mu m$. However, when an external static/low-frequency electric field was applied a pre-tilt was induced, eliminating the Fréedrick's effect and allowing nonlinear molecular reorientation to cause self-focusing which, in Figure 1.2 (b), balanced diffraction

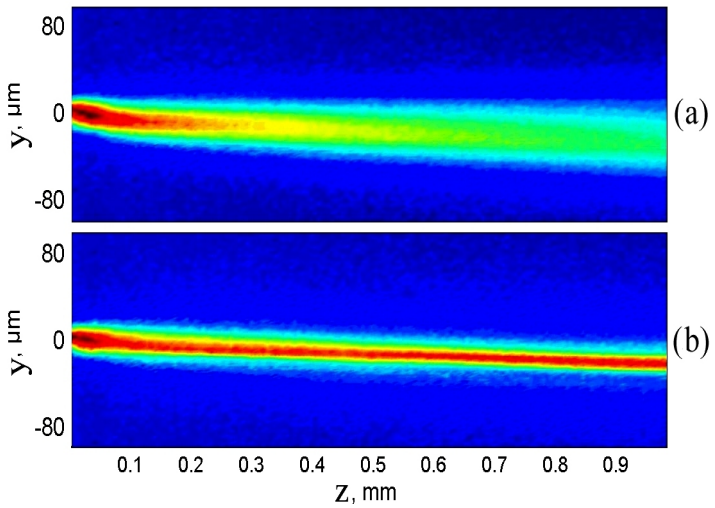

Figure 1.2: Experimental results of beams with input power $4.2mW$ where (a) no external static/low-frequency electric field is applied, and (b) a field of $0.8V$ at $1kHz$ is applied across the $75\mu m$ cell. Permission of use of image taken from Ref. [9] kindly given by Prof. G. Assanto.

and lead to a stable solitary wave propagating unchanged over a distance of $1mm$, roughly 20 times the diffraction length observed in Figure 1.2 (a). It is noticeable that the beam did not propagate in the z direction but at an angle to the z axis. This angular path deviation is known as 'walk-off' and will be discussed later.

Once formed nematicons exhibit a wide range of interesting behaviour. For example, nematicons have been observed confining beams with equal polarisation. These "*probe*" beams can have different wavelengths, different intensities and different input angles, yet still remain trapped in the nematicon waveguide [19]. Speckled light, white light and distorted beams have been employed as input beams and yet still a nematicon can form [6]. As shown in Figure 1.2, nematicons additionally experience a 'walk-off' effect which could be used to all-optically steer a nematicon. More complex experiments have been conducted which show equally interesting nematicon behaviour. Two or more identical nematicons have been colaunched exhibiting attraction, walk-off, interlacing, spiralling and fusion [12, 19, 20, 21]. Similar phenomena have been both predicted and experimentally verified for two colaunched nematicon beams of different wavelengths [17, 22, 23, 24], known as two-colour nematicons. Beam dynamics of two-colour nematicons will be studied in depth in Chapters 3 & 4.

The phenomenon that has been termed 'walk-off' throughout the introduction will be clarified here. Walk-off can be defined as *"an effective angular deviation of propagation direction from the initial input alignment"* [25, 26]. The walk-off of an individual initial beam is due to the birefringent nature of the nematic molecules because they have different optical properties parallel and perpendicular to their axis. The refractive index is then tensorial and the dispersion relation has two components; the ordinary component which is parallel to the input beam and the extraordinary component which has walk-off. The refractive index of the extraordinary beam is affected by reorientation, and so this beam can form a solitary wave. Walk-off is linearly related to the optical beam power. Peccianti *et al* [18] highlighted the tuneability of walk-off subject to various external field powers, revealing that appropriately polarised input beams form nematicons and have output positions with respect to x and y arranged in a semi-circle when external field power is raised from $0V$ to saturation of the nonlinearity, i.e. from when there is no pre-tilt until the nematic molecules are perpendicular to the direction of the external electric field. Walk-off angles were observed of up to $7°$ [18].

The first observations of nematicons were modelled with respect to the crystal axes (x, y, z) and walk-off was deemed a paraxial phenomenon in most theoretical models, i.e. walk-off of the beam from the z axis was assumed to be negligible [6, 9, 19, 20, 27, 28, 29]. Whilst these

theoretical models accounted for many phenomena, such as unusual beam interactions caused by nonlocality [19], it was not until the propagation of nematicons was considered in a frame of reference paraxial to the direction of beam propagation subject to walk-off that theoretical models accurately portrayed nematicon evolution [16, 17]. For an initial beam with no particular polarisation for which the walk-off is a constant δ with respect to z, this is equivalent to a rotation of the (x, y, z) coordinate system by the walk-off angle δ [17], resulting in a new 'ray' coordinate system (r, t, s) [19]. When the walk-off is not constant, for example due to a varying pre-tilt field, the ray is not straight and the ray direction must be locally solved [19].

If the principal optical axis, and therefore the pre-tilt δ, are in the (x, z)-plane, the electric field of the beam is polarised in the x direction, and the input beam direction is parallel to z, then walk-off is in the (x, z)-plane solely, with no y component. A suitable 'ray' coordinate system equivalent to the one above is (x, t, s); a rotation of (x, y, z) about x by the walk-off angle in the (x, z)-plane, δ. This experimental set-up was used to observe two-colour nematicons in Ref. [17].

In the present work pre-tilts and beam polarisations have been taken as above, but rather than use 'ray' coordinates the (x, y, z) coordinate system has been used and walk-off has been incorporated implicitly by a phase factor transformation of the electric fields of the beam(s) in the governing equations [23]. A full account of this transformation is given in Chapter 3. One major consequence of incorporating walk-off into the governing equations is that any other walk-off observed in these models is an additional effect which has not been accounted for in previous models. The nature of any additional walk-off will be analysed and explained for each regime presented in Chapters 3, 4 & 5.

1.4 Aim of Thesis

Theoretical models, both numerical and analytical, predicting the various nematicon phenomena described above have been put forward before. Some have even been compared to experimental data and good agreement has been found [9, 15, 17, 19]. Yet no analytical model had been proposed, to the author's knowledge, which accurately portrayed nematicon evolution over large distances until the work of García-Reimbert *et al* in 2006 [30]. In this work the evolution of a single nematicon in a bulk NLC was analysed numerically and analytically in the local nonlinear response regime. To study beam behaviour analytically they employed an extended variational method yielding modulation equations for the beam parameters from an averaged Lagrangian formulation of approximated governing equations for a nematicon in the local limit [30]. The most important features of the method are the inclusion of

- a shelf of diffractive radiation which travels with the beam as it propagates, and has been shown to form as a nematicon evolves from numerical simulations, see Figure 1.3.
- diffractive losses radiated from the beam over large z, resulting in a damping of oscillations of the beam parameters such as amplitude, width and position, as the beam settles to a steady nematicon.

This technique was first proposed by Kath & Smyth when studying $(1+1)$-D soliton evolution in a nonlinear optical fibre governed by the NLS equation [31]. It was found, in this work and the work of García-Reimbert *et al*, that the mechanism allowing the initial pulse/beam to settle to a steady state soliton was radiation loss. In a related piece of work, Smyth & Kath used the same extended variational technique to show that two symmetric interacting initial beams in a birefringent nonlinear optical fibre emit radiation during collision and that this shed radiation was responsible for the initial beams settling to a steady vector soliton, when this is energetically allowed [32], which had previously been reported by Yang using a completely different method [33].

In this thesis the extended variational method of Kath & Smyth will be adapted to model nematicon beam(s) evolution in a NLC bulk medium over a large z distance. Two beam collisions, the formation and propagation of two-colour vector nematicons and single beam steering via a DD-NLC refractive index defect will be explored analytically and numerically. In the analytical method the radiation shelf travelling with the beam(s), predicted by previous

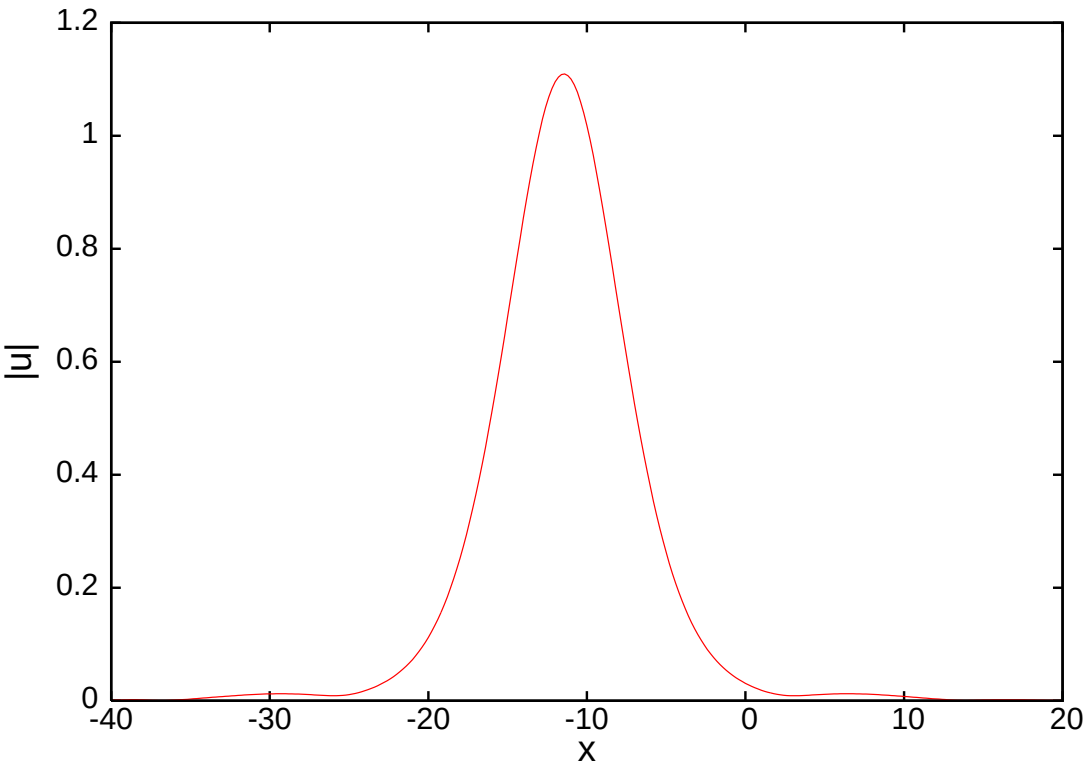

Figure 1.3: Numerically calculated $(2+1)$-D nematicon exhibiting a shelf of radiation during evolution in z with $y = 0$.

numerical results (and seen in Figure 1.3), and the effect of diffractive radiative losses as the beam(s) evolve will be included to explain nematicon evolution over large z. It will also be shown that numerical and analytical solutions of the nematicon equations agree very well for all nematicon regimes investigated.

The thesis is organised as follows. Chapter 2 begins with a brief discussion about the basic equations governing nematicon evolution. The important principles underlying the analytical method used to solve these nematicon governing equations are then explained. This is followed by a review of the numerical method employed to solve the nematicon governing equations. Using the techniques outlined in Chapter 2, Chapter 3 explores the formation and evolution of two-colour nematicons in a NLC with a nonlocal nonlinear response. Approximate modulation equations will be found and their solutions compared with numerical solutions of the nematicon governing equations. In Chapter 4 the same methods are used to investigate two-colour nematicons propagating in a NLC with a local response. A comparison between nematicons propagating in the local and nonlocal nonlinear response regimes will be given and differences between the solutions will be highlighted. Again the accuracy of the analytical model will be tested against numerical solutions of the two-colour nematicon governing equations. Equations modelling a single nematicon's evolution as it propagates through a bulk DD-NLC with a refractive index defect will be discussed in Chapter 5, using the same methods outlined above. Chapters 3, 4 & 5 will additionally have a focus on the effects of walk-off, as this is an important property of nematicon propagation, particularly when discussed in the context of future applications of spatial optical solitons in the optoelectronics industry. Finally, a general analysis of the results, main outcomes, methodology and possible future research will be conducted in Chapter 6.

Chapter 2

Methods

2.1 The Governing Equations

The equations governing soliton evolution, and any other electromagnetic wave evolution, in any material medium are all essentially based on the classical Maxwell's equations. A full solution of Maxwell's four partial differential equations (PDEs) would be prohibitively time consuming and could only be done via numerical methods. Additionally, for the beams travelling in a nonlocal nematic liquid crystal (NLC) there are other effects to consider due to the interaction of the beams with the nematic medium [34]. To avoid these problems an asymptotic analysis of Maxwell's equations can be conducted, from which simpler PDEs are derived to model beam dynamics. Such an analysis was undertaken by Peccianti *et al* around the time that nematicons were first discovered and the equations governing the electric field of the light beam in the presence of a static/low-frequency electric field were found to closely resemble the $(2+1)$-D nonlinear Schrödinger (NLS) equation [9]. These governing equations cast nematicon evolution as a propagation problem in the time-like coordinate z. For a single optical beam Assanto *et al* [6, 19] and Peccianti *et al* [18] showed that the equations for the electric field of an optical beam and the optical axis, or director, in the presence of an applied static/low-frequency electric field are a coupled system consisting of an NLS-like equation for the beam and a Poisson equation for the director, these equations being

$$2ik\frac{\partial E}{\partial Z} + \nabla^2_{XY}E + k_0^2\varepsilon_a\left(\sin^2\phi - \sin^2\hat{\theta}\right)E = 0, \tag{2.1}$$

$$4K\nabla^2\phi + 2\Delta\epsilon_{RF}E_S^2\sin(2\phi) + \varepsilon_0\varepsilon_a\sin(2\phi)|E|^2 = 0, \tag{2.2}$$

where E is the magnitude of the electric field of the beam, $\phi = \hat{\theta} + \theta$ is the total mean director rotation induced by the static/low-frequency electric field and the beam. $\hat{\theta}$ is the pre-tilt and θ the optically-induced reorientation of the director, where $\theta \ll \hat{\theta}$. k is the propagation constant (wavenumber) of the beam and $k_0 = 2\pi/\lambda$ is the input wavenumber of the beam with λ its input wavelength. The constants $\varepsilon_a = n_{\shortparallel}^2 - n_\perp^2$ and ε_0 are the birefringence and permittivity of free space respectively, ($n_{\shortparallel}$ and $n_\perp$ being the refractive indices for an optical beam parallel and normal to the director alignment [19]). E_S is the static/low frequency external electric field and $\Delta\epsilon_{RF}$ is the static/low frequency anisotropy. K is the Frank constant which measures the elasticity of the medium and is taken equal for splay, twist and bend deformations of the NLC molecules. A full derivation of these equations for the reorientation of the beam can be found in Ref. [19] and a full derivation from Maxwell's equations of similar governing equations was presented by Karpierz whilst studying nematicons in a waveguide [13].

Using the nondimensional variables x, y, z and u, with $X = Ax$, $Y = Ay$, $Z = Bz$ and $E = Cue^{i\psi z}$, where ψ is used to eliminate constant factors in the electric field equation, the

governing equations can be nondimensionalised to

$$iu_z + \frac{1}{2}\nabla_{xy}^2 u - \cos(2\phi)u = 0, \tag{2.3}$$

$$\nu\nabla^2\phi + p\sin(2\phi) + 2|u|^2\sin(2\phi) = 0, \tag{2.4}$$

where

$$\nu = \frac{8Kk}{\varepsilon_0\varepsilon_a}, \qquad p = \frac{4\Delta\epsilon_{RF}E_S^2}{\varepsilon_0\varepsilon_a}, \tag{2.5}$$

and the constants A, B, C and ψ have been chosen appropriately. Equation (2.3) is called the Foch-Leontovich equation. These equations can be further simplified by separating the contributions to the total director orientation ϕ of the pre-tilt $\hat{\theta}$ and the reorientation θ. At the boundaries of the cell ($x = \pm L$) $\phi = 0$. To obtain analytically tractable equations, this director equation will now be expanded by perturbing about the pre-tilt angle $\hat{\theta}$ [35]. Without a beam being present, the director angle satisfies the equation

$$\nu\nabla^2\hat{\theta} + p\sin(2\hat{\theta}) = 0, \qquad \phi(-L) = \phi(L) = 0. \tag{2.6}$$

It is possible to adjust p (which is the square of the static/low-frequency electric field) so that $\phi > \pi/4$ in the centre of the liquid crystal cell [27, 28]. This is justified as ϕ varies from $\phi = 0$ at the boundaries to a possible $\phi = \pi/2$ when the static/low-frequency field is strong and the molecules align with the direction of the field. By decomposing the director angle $\phi = \hat{\theta} + \theta$, the director equation (2.4) can be expanded to give

$$\nu\nabla^2\hat{\theta} + \nu\nabla^2\theta + p\sin 2\hat{\theta}\cos 2\theta + p\cos 2\hat{\theta}\sin 2\theta + 2|u|^2\sin 2\hat{\theta}\cos 2\theta + 2|u|^2\cos 2\hat{\theta}\sin 2\theta = 0. \tag{2.7}$$

The maximal self-focusing response is achieved when the Fréedericksz threshold is zero, which occurs at a pre-tilt of $\hat{\theta} = \pi/4$. The static/low-frequency electric field can be adjusted so that the pre-tilt angle $\hat{\theta}$ is above $\pi/4$ but close to it. On using the static director equation (2.6), the director equation (2.7) becomes

$$\nu\nabla^2\theta + p\cos 2\hat{\theta}\sin 2\theta + 2|u|^2\sin 2\hat{\theta}\cos 2\theta = 0, \tag{2.8}$$

to first order in small $|\theta|$. Since the pre-tilt $\hat{\theta}$ is a slowly-varying function, a suitable re-scaling of variables allows the factors $\cos 2\hat{\theta}$ and $\sin 2\hat{\theta}$ to be scaled out. It should be noted that it is important that $\cos 2\hat{\theta} < 0$ since the static/low-frequency field has been chosen so that $\hat{\theta} > \pi/4$, but close to $\pi/4$, in the centre of the cell. After re-scaling, this director equation becomes

$$\nu\nabla^2\theta - q\sin 2\theta + 2|u|^2\cos 2\theta = 0, \tag{2.9}$$

where q is the scaled p. For small director deviation θ this director equation is the same as that derived by Conti *et al* [27] for a single nematicon travelling through a NLC with an applied static/low-frequency electric field.

In a similar manner, the Foch-Leontovich equation (2.3) can be nondimensionalised and rewritten in the form

$$iu_z + \frac{1}{2}\nabla_{xy}^2 u + \sin(2\theta)u = 0. \tag{2.10}$$

Equations (2.10) & (2.9) are the basic equations describing nematicon evolution which will be used and developed to investigate a wide range of nematicon behaviour in both the local and nonlocal limits. There are no exact solutions of equations (2.10) & (2.9). The nematicon governing equations in the cases that will be presented in this work are variants of these equations and consequently have no exact solutions either. To determine the evolution of these beams one can solve the governing equations numerically, which yields few insights into nematicon dynamics and its underlying mechanisms yet provides an accurate portrayal of beam evolution, or one can solve the governing equations approximately.

2.2 Approximate Method

The approximate method that will be used in this work is a variational method which yields modulation equations for each of the nematicon parameters and allows the incorporation of the diffractive radiation shed as the beams evolve. This technique has the potential to be inaccurate if the simplifications imposed on the governing equations and beam profile remove key features of the true beam evolution or form. However, if the governing equations are solved approximately and compare well to numerically determined solutions, one can gain insight into the mechanics of beam formation, propagation and dynamical behaviour. The variational method is a highly useful tool, which has been used in the scientific investigation of dynamical systems for decades. Anderson was the first to apply the method to problems involving optical solitons governed by the NLS equation in 1983 [34, 36] and the method has been utilised in a variety of different areas of optics ever since.

To define the variational method the governing equations must first be rewritten in their equivalent Lagrangian formulation, $L(u_z, u_{\mathbf{x}}, u)$, where $\mathbf{x}$ represents the spatial coordinates of the system, in this case not including the time-like coordinate z. The Lagrangian formulation describes the system in terms of its kinetic and potential energy. The averaged Lagrangian $\mathcal{L}$ can then be defined by

$$\mathcal{L} = \int L d\mathbf{x}, \tag{2.11}$$

The variational method is based around the principle of stationary action which, when applied to the action of a system, allows the equations of motion to be found. The action is a functional which takes the trajectory of the system as its argument and whose integrand is the averaged Lagrangian

$$A = \int_{z_0}^{z_f} \mathcal{L} dz, \tag{2.12}$$

where z is a time-like evolution coordinate and z_0 and z_f are the initial and final z points respectively. The principal of stationary action states that the action must be stationary in the sense that the action does not vary to first order when small perturbations are applied to the trajectory

$$\delta A = \delta \int_{z_0}^{z_f} \mathcal{L} dz = 0. \tag{2.13}$$

In other words, the physical system must always take the trajectory whereby the action is stationary. By this reasoning variations of the averaged Lagrangian may be taken for a defined trial function which are equivalently a perturbation of the true beam trajectory.

If the principle of stationary action is satisfied by the averaged Lagrangian, the next step is to insert an appropriate trial function (also known as an ansatz) into the averaged Lagrangian, as the exact nematicon solution is not known. The choice of trial function is not dictated by any mathematical rules and has no direct relationship with the (unknown) nematicon steady state solution. It must be chosen either as a good match to solutions obtained from numerical simulations or by experience, or a combination of both. Generally speaking, trial functions take the form of a basic beam profile with certain parameters ($p_i(z)$ say, where $i = 1, \ldots, N$ and N is the total number of parameters) such as amplitude, width and phase, which are allowed to vary with z. Once the trial function is inserted into the averaged Lagrangian, the resultant averaged Lagrangian equation is a function of the variable parameters and their derivatives [34]. Consequently, variational equations, also known as modulation equations, of the form

$$\frac{d}{dz}\frac{\partial \mathcal{L}}{\partial (dp_i/dz)} - \frac{\partial \mathcal{L}}{\partial p_i} = 0, \tag{2.14}$$

representing modulations of the beam parameters can be extracted from the averaged Lagrangian and these modulation equations can then be solved by simple numerical methods.

Nöther's theorem states that for any differentiable symmetry of the action of a conservative physical system there exists a corresponding conservation equation relating to some fundamental property of the system. The principle of stationary action and, by association, the variational method are therefore closely linked to the infinite number of conservation equations found in

integrable systems. In fact, each of the variational equations can be obtained by calculating the corresponding conserved quantity associated with the governing equations [25].

The basic variational method, outlined above, has been used to approximate a variety of physical systems, yet the inherent need for the system to be conservative has limited the usefulness of such approximations. An extension to the averaged Lagrangian method was first introduced by Kath & Smyth [31]. In this work they analysed $(1+1)$-D solitons in nonlinear optic fibres. They had noticed that variational approximations matched physical systems well over small intervals of the evolutionary variable (z or time) but the approximation gradually became less accurate over greater intervals. They concluded that numerical solutions were exhibiting losses to radiation and that these losses were the reason for the inaccuracy of the variational method over larger intervals. Kath & Smyth linked these losses to the evolution of parameters from oscillatory states to the steady state. Their technique consists of utilising the well known variational method for conservative systems, shown above, but with the addition of a radiation loss term incorporated into one or more of the modulation equations [31, 32]. The inclusion of loss terms allows oscillations of various parameters to settle to steady values in a manner which closely matches that of numerical simulations. It was later found that this extended variational method has a wide range of applications, particularly in the field of optical solitons.

2.2.1 A Simple System excluding Shed Radiation

To demonstrate the extended variational method, a simpler case, related to the models that will be described in this thesis, is examined for which minimal technical details are given. The $(1+1)$-D NLS equation governs the evolution of pulses travelling in polarisation-preserving, single-mode nonlinear optical fibers [5, 31] and is given in nondimensional form by

$$i\frac{\partial u}{\partial z} + \frac{1}{2}\frac{\partial^2 u}{\partial x^2} + |u|^2 u = 0, \tag{2.15}$$

where u is the slowly varying envelope of the electric field, z is the direction along the fibre and x is time. In an optical fibre x would normally be replaced by t and would represent the normalised time. This equation would then yield temporal soliton solutions with nonlinearity acting against dispersion [25]. However, here the $(1+1)$-D NLS equation is introduced as a simple starting point to demonstrate the analytical methods used in the following chapters.

The NLS equation (2.15) has the corresponding Lagrangian formulation

$$L = i(u^* u_z - u u_z^*) - |u_x|^2 + |u|^4, \tag{2.16}$$

where the superscript * denotes the complex conjugate. One can check the validity of any Lagrangian by taking variations with respect to the function(s) it contains. This action returns the original governing equation(s). For the current example, taking variations of equation (2.16) with respect to u yields the complex conjugate of the governing equation (2.15), from which equation (2.15) is easily obtained. As mentioned earlier, the NLS equation possesses an infinite number of conservation equations. These conservation equations are derived from the integrals of motion [5, 25], some important examples of which are

$$P = \int_{-\infty}^{\infty} |u|^2 dx, \quad M = i\int_{-\infty}^{\infty} (u_x^* u - u_x u^*)\, dx, \quad H = \frac{1}{2}\int_{-\infty}^{\infty} \left(|u_x|^2 - |u|^4\right) dx. \tag{2.17}$$

These equations represent mass (P), momentum (M) and the total energy or Hamiltonian (H) respectively. Conservation equations for mass, momentum and energy are then

$$\frac{d}{dz}\int_{-\infty}^{\infty} |u|^2 dx = 0, \quad \frac{d}{dz}\frac{i}{2}\int_{-\infty}^{\infty} (u_x^* u - u_x u^*)\, dx = 0, \quad \frac{dH}{dz} = \frac{d}{dz}\int_{-\infty}^{\infty} \left(|u_x|^2 - |u|^4\right) dx = 0. \tag{2.18}$$

The relationship between these conserved quantities and the Lagrangian is obvious when the two are compared. They are associated with invariances of the Lagrangian; mass conservation relates to invariances with respect to phase changes, momentum conservation to invariances

with respect to translations in x and the Hamiltonian to invariances with respect to translations in z [31, 37]. These three conservation equations will be shown to play a central role in the calculation of radiative losses for all nematicon regimes presented in the following chapters.

The next step in the approximate method is to choose a trial function, or ansatz, that represents a soliton-like pulse whose parameters vary realistically. An ansatz that has independently varying amplitude a, width w and phase σ is therefore desirable. The form of the exact solution (1.2) of the NLS equation suggests that a sech profile will match the soliton profile well. Also, from numerical simulations conducted by Kath & Smyth [31], it was shown that a low amplitude shelf of radiation, shed by a pulse as it evolves, develops in its vicinity. The existence of this shelf of low wavenumber radiation under the pulse was further demonstrated from soliton perturbation theory and perturbed inverse scattering [31, 33]. A simple argument to show why it occurs can be obtained from group velocity. The group velocity for linear waves for the NLS equation is $c_g = k$, so that low wavenumber waves have low group velocity and thusly remain in the vicinity of the soliton. The shelf and pulse continually interact [31, 32]. To account for this interaction a parameter representing variations of the amplitude of the shelf (g) is also included. With these considerations a suitable trial function is

$$u = a\,\mathrm{sech}(x/w)e^{i\sigma} + ige^{i\sigma}, \tag{2.19}$$

where a, w, σ and shelf amplitude g are all functions of z. Soliton perturbation theory and perturbed inverse scattering show that the shelf and the soliton are $\pi/2$ out of phase [31, 33] which is accounted for by i. The radiation shelf travelling with the pulse cannot continue to be flat, so it is assumed to be zero outside a certain undetermined length, ℓ. Hence it is required that the radiation shelf is non-zero when $-\ell < x < \ell$. The form of the radiation outside of this region will be taken up below.

Whilst a suitably chosen trial function can incorporate radiation shed by the pulse yet still travelling in its vicinity, radiation shed to the far field as the pulse propagates is not naturally included. Dispersive radiation is essential for soliton pulses to evolve to their steady state. Without its inclusion pulse parameters oscillate indefinitely around their fixed points. This is not a critical problem when modelling pulse behaviour over small t, but makes a big difference over longer time intervals, particularly when multiple pulses (beams) are continually interacting, as will be shown and discussed in Chapters 3 & 4.

Substituting the trial function (2.19) into the averaged Lagrangian given by

$$\mathcal{L} = \int_{-\infty}^{\infty} L dx, \tag{2.20}$$

yields

$$\mathcal{L} = \pi g\left(w\frac{da}{dz} + a\frac{dw}{dz}\right) - \pi a w\frac{dg}{dz} - 2a^2 w\frac{d\sigma}{dz} - \ell g^2\frac{d\sigma}{dz} - \frac{a^2}{3w} + \frac{2a^4 w}{3}, \tag{2.21}$$

where ℓ is the length of the shelf of radiation travelling with the pulse, still to be determined. Variations of the averaged Lagrangian are taken for each of the pulse parameters

$$\delta a: \quad -\pi w\frac{dg}{dz} - 2aw\frac{d\sigma}{dz} - \frac{a}{3w} + \frac{4}{3}a^3 w = 0, \tag{2.22}$$

$$\delta w: \quad -2\pi a\frac{dg}{dz} - 2a^2\frac{d\sigma}{dz} + \frac{a^2}{3w^2} + \frac{2}{3}a^4 = 0, \tag{2.23}$$

$$\delta\sigma: \quad \frac{d}{dz}\left(2a^2 w + \ell g^2\right) = 0, \tag{2.24}$$

$$\delta g: \quad \pi\frac{d}{dz}(aw) - \ell g\frac{d\sigma}{dz} = 0, \tag{2.25}$$

which can be rewritten, after suitable rearrangement, as

$$\frac{dg}{dz} = -\frac{2a}{3\pi}\left(a^2 - \frac{1}{w^2}\right), \tag{2.26}$$

$$\frac{d}{dz}(aw) = \frac{\ell g}{\pi}\left(a^2 - \frac{1}{2w^2}\right), \tag{2.27}$$

$$\frac{d\sigma}{dz} = a^2 - \frac{1}{2w^2}, \tag{2.28}$$

$$\frac{d}{dz}\left(\frac{a^2}{w} - 2a^4 w\right) = 0. \tag{2.29}$$

There is still a quantity to determine however; the length of the radiation shelf ℓ. With this in mind, linearising the equations about their fixed point determines the nature of the fixed point. The fixed point is easily found to be a centre and as such soliton solutions orbit, or oscillate, around it, where the period of oscillation is determined by ℓ [31]. Kath & Smyth presented numerical solutions of pulse profiles which revealed that the radiation shelf has small amplitude, $|g| \ll a$, and is relatively flat in comparison to the pulse itself [31]. Consequently the nonlinear term in the NLS can be neglected for this shelf and the linearised NLS equation

$$i\frac{\partial u}{\partial z} + \frac{1}{2}\frac{\partial^2 u}{\partial x^2} = 0, \tag{2.30}$$

can be used to determine the governing equation for the shelf g as

$$ig_z - \sigma_z g + \frac{1}{2}g_{xx} = 0. \tag{2.31}$$

At the edge of the shelf, $x \sim \ell$, it is clear that $g_{xx} \sim 0$, so equation (2.31) reduces to

$$ig_z = \sigma_z g, \tag{2.32}$$

which expresses that the period of oscillation of the shelf of radiation matches the oscillation period of the pulse [31, 38]. Kath & Symth [31] then obtained an expression for the length of the shelf in terms of the fixed point $\hat{a}$

$$\ell = \frac{3\pi^2 \hat{w}}{8}, \quad \text{where} \quad \hat{a} = \hat{a}(\hat{w}), \quad \hat{w} = \frac{1}{\hat{a}}. \tag{2.33}$$

The fixed point $\hat{a}$ is found from the energy conservation equation (2.29) as

$$\hat{a} = \left(2a_0^4 w_0 - \frac{a_0^2}{w_0}\right)^{1/3}, \tag{2.34}$$

with a_0 and w_0 the initial values of a and w. Equations (2.26)–(2.29) form a complete system of evolution equations now that ℓ has been defined, but radiation losses have been neglected so far.

Before tackling the problem of incorporating radiation loss into the modulation equations it is worth summarising what has been shown so far. The various nematicon regimes presented in Chapters 3, 4 & 5 are analysed using the exact same technique presented here. This section has been included to show the standard variational method applied to a simple system in order that the critical decisions and important details can be highlighted. These points are universal to the technique and consist of

- deriving equations that accurately model the particular dynamical system of interest.
- choosing an appropriate trial function which has parameters that vary realistically.

There are also several key details common to the variational method for determining the evolution of both NLS solitons and nematicons;

- trial functions have the same form, with a sech profile for the pulse/beam and a term representing a shelf of radiation.
- shelf amplitude is small in comparison to that of the pulse/beam.
- the length of the radiation shelf is determined by matching the soliton oscillation frequency to the frequency of shelf oscillations.
- soliton solutions oscillate about the fixed point, which is a centre.
- solitons require radiative losses to damp oscillations around the centre and fall to their steady state.

The final point is discussed in more detail for the simple NLS system in the following section.

2.2.2 A Simple System including Shed Radiation

Radiation shed by the pulses as they evolve must be included if agreement between numerical and approximate solutions is to be good over large z. More specifically, the critical points of a Hamiltonian system such as the one described are always centres and, as a consequence, the pulse trajectory will infinitely oscillate about the fixed point in a stable orbit unless the motion of the pulse is coupled to the radiation field, which will cause a damping of oscillations, allowing the pulse to settle [31].

Radiation outside the vicinity of the pulse has been shown numerically to be of low amplitude in comparison to the amplitude of the pulse itself [31]. Hence the nonlinear term in the governing equation can be neglected and a linearised pulse equation governs evolution outside of the pulse vicinity, namely

$$i\frac{\partial u}{\partial z} + \frac{1}{2}\frac{\partial^2 u}{\partial x^2} = 0. \tag{2.35}$$

The exact solution of this linearised NLS equation yields the form of the radiation shed by the pulse. However, the complete details of this solution are not needed, only the amount of conserved quantities shed in radiation. Since loss of mass is the major contributor to radiation shed by the pulse, it is not surprising that the conservation of mass equation plays the most important role in the calculation of shed radiation [31]. Mass density is $\rho = |u|^2$ and mass flux density is $J = \frac{i}{2}(uu_x^* - u^*u_x)$. Hence the conservation of mass equation is given by

$$\frac{\partial \rho}{\partial z} + \frac{\partial J}{\partial x} = \frac{\partial}{\partial z}|u|^2 + \frac{\partial}{\partial x}\frac{i}{2}(uu_x^* - u^*u_x) = 0, \tag{2.36}$$

which, when integrated in x, is

$$\frac{d}{dz}\int_{-\infty}^{\infty} |u|^2 dx = 0, \tag{2.37}$$

for both the linearised NLS equation and the NLS equation itself. The mass conservation equation will be shown to be integral to the calculation of mass flux, and therefore radiation loss [31].

If $\Lambda = \ell/2$ represents the length from the centre of the pulse to the edge of the radiation shelf then the mass radiated to the right of the pulse will be radiated into the region $\Lambda < x < \infty$ and is therefore given by

$$\frac{d}{dz}\int_{\Lambda}^{\infty} |u|^2 dx = \mathrm{Im}(u^*u_x)|_{x=\Lambda}. \tag{2.38}$$

By taking the Laplace transform of the linearised NLS equation (2.35) and manipulating the result appropriately an equation for u_x in terms of u can be found. The linearised NLS equation has the Laplace transform

$$i\zeta\tilde{u} + \frac{1}{2}\frac{d^2\tilde{u}}{dx^2} = 0 \quad \text{with} \quad \tilde{u}(\zeta) = \int_0^{\infty} e^{-\zeta z} u dz = \mathcal{L}\{u(z)\}, \tag{2.39}$$

where $\mathcal{L}\{u(z)\}$ is the Laplace transform of u in z. The solution $\tilde{u}$ of this ordinary differential equation (ODE) in Laplace space and its derivative with respect to x respectively are

$$\tilde{u} = Ae^{-\sqrt{-2i\zeta}x} \quad \text{where} \quad x > \Lambda, \qquad \frac{d\tilde{u}}{dx} = -\sqrt{2\zeta}e^{-\frac{i\pi}{4}}\tilde{u}. \tag{2.40}$$

The convolution theorem is then applied to invert the Laplace transform, yielding

$$u_x = -\sqrt{2}e^{-\frac{i\pi}{4}}\frac{d}{dz}\int_0^z \frac{u(\Lambda, s)}{\sqrt{\pi\,(z-s)}}ds, \tag{2.41}$$

at $x = \Lambda$. Therefore equation (2.38) may be rewritten

$$\frac{d}{dz}\int_\Lambda^\infty |u|^2 dx = \mathrm{Im}\left(- u^*(\Lambda, z)\sqrt{2}e^{-i\pi/4}\frac{d}{dz}\int_0^z \frac{u(\Lambda, s)}{\sqrt{\pi(z-s)}}ds\right). \tag{2.42}$$

On noting that the mass radiated to the left and right are the same due to the symmetry of the problem and that the mass lost to dispersive radiation has to come from mass contained in the vicinity of the pulse, $-\Lambda < x < \Lambda$, for which the mass conservation equation (2.36) has already been obtained, a modified total mass conservation equation where the mass in the vicinity of the pulse is equated to the mass radiated away from the pulse is derived and given by

$$\frac{d}{dz}\left(2a^2w + 2\Lambda g^2\right) = 2\sqrt{2}\,\mathrm{Im}\left(u^*(\Lambda, z)e^{-i\pi/4}\frac{d}{dz}\int_0^z \frac{u(\Lambda, s)}{\sqrt{\pi(z-s)}}ds\right). \tag{2.43}$$

Yet $u(\Lambda, s)$, the radiation at the edge of the shelf, is still to be identified. From numerical solutions it was found that the shelf of radiation has low amplitude and is relatively flat in comparison to the pulse. Therefore it can be assumed that its phase is slowly varying relative to the shed radiation and can be approximated as being constant [31]. If this approximation is taken then $u(\Lambda, s)$ and $u^*(\Lambda, s)$ can be replaced by $r = |u(\Lambda, s)|$ and equation (2.43) is

$$\frac{d}{dz}\left(2a^2w + 2\Lambda g^2\right) = -2r\frac{d}{dz}\int_0^z \frac{r}{\sqrt{\pi(z-s)}}ds. \tag{2.44}$$

At the edge of the shelf $x = \Lambda$, $u(\Lambda, z)$ is given by

$$u(\Lambda, z) = \left(a\,\mathrm{sech}(\frac{\Lambda}{w}) + ig - \hat{a}\,\mathrm{sech}(\frac{\Lambda}{\hat{w}})\right)e^{i\sigma z}. \tag{2.45}$$

Then r may be defined as

$$r = |u(\Lambda, z)| = \sqrt{\left(a\,\mathrm{sech}(\frac{\Lambda}{w}) - \hat{a}\,\mathrm{sech}(\frac{\Lambda}{\hat{w}})\right)^2 + g^2}. \tag{2.46}$$

Expanding the real part of the shelf in the above expression for $r = |u(\Lambda, z)|$ in a Taylor series about the fixed point to first order yields

$$\left(a\,\mathrm{sech}(\frac{\Lambda}{w}) - \hat{a}\,\mathrm{sech}(\frac{\Lambda}{\hat{w}})\right)^2 \approx \frac{a^2w - \hat{a}^2\hat{w}}{\Lambda}, \tag{2.47}$$

which is the mass difference between the solitary wave and the fixed point soliton [38]. Substituting equation (2.47) into equation (2.46) for $r = |u(\Lambda, z)|$ gives

$$r^2 = |u(\Lambda, z)|^2 \approx \frac{1}{\Lambda}\left(a^2w - \hat{a}^2\hat{w} + \Lambda g^2\right), \tag{2.48}$$

allowing the calculation of the integral in equation (2.44).

What remains is to incorporate mass loss into the variational equations (2.26)–(2.29). Since

pulse damping is a function of g and mass loss and the height of the shelf g are both zero initially, it is natural to include the loss term, denoted δ, in the variational equation for g [31, 32]. With this inclusion the approximate evolution equations for a NLS soliton are

$$\frac{dg}{dz} = -\frac{2a}{3\pi}\left(a^2 - \frac{1}{w^2}\right) - 2\delta g, \tag{2.49}$$

$$\frac{d}{dz}(aw) = \frac{2\Lambda g}{\pi}\left(a^2 - \frac{1}{2w^2}\right), \tag{2.50}$$

$$\frac{d\theta}{dz} = a^2 - \frac{1}{2w^2}, \tag{2.51}$$

$$\frac{d}{dz}\left(\frac{a^2}{w} - 2a^4 w\right) = 0, \tag{2.52}$$

where

$$\delta = \frac{9\pi^2}{128\Lambda r}\frac{d}{dz}\int_0^z \frac{r}{\sqrt{\pi(z-s)}}ds, \tag{2.53}$$

$$r^2 = |u(\Lambda, z)|^2 = \frac{1}{\Lambda}\left(a^2 w - \hat{a}^2\hat{w} + \Lambda g^2\right). \tag{2.54}$$

The modulation equations (2.49)–(2.52) are now complete and can be solved numerically via the Runge-Kutta method or an equivalent iterative method.

2.2.3 A Single Nematicon System

Whilst the example of a temporal soliton pulse governed by a $(1+1)$-D NLS equation is of great importance to understanding the method of approximation, particularly when considering the incorporation of radiation loss, there are two major differences between this and the method for approximately solving equations governing nematicon propagation which require highlighting and clarification before proceeding further. Firstly, the evolution equations presented in this work model $(2+1)$-D spatial soliton beams. Moving from 1 to 2 spatial transverse dimensions extends the modulation equations and complicates the calculation of radiation loss. Secondly, an interaction between nematic molecules and the optical beam, discussed in Chapter 1, introduces a second governing equation required to model the evolution of the director, which must be coupled to the familiar NLS-like equation governing beam evolution. For the approximate modulation equations to be simple enough for a meaningful analysis of beam evolution to be made, these governing equations and the associated Lagrangian must be simplified which adds another layer of approximation to the approximate method. An additional complication arises from the inclusion of a director equation into the calculation of the already simplified averaged Lagrangian requiring that further approximations are needed for it to be evaluated.

Complications to the calculation of the modulation equations associated with the inclusion of a director equation will be highlighted for each particular regime presented in Chapters 3, 4 & 5, but the difficulties common to each regime encountered when calculating radiation loss in higher dimensions are presented here since the radiation calculation varies little from case to case.

To highlight the differences between calculating radiation loss for a $(1+1)$-D NLS solitary wave and that of $(2+1)$-D nematicons, the propagation of a typical $(2+1)$-D nematicon in the local regime will be presented briefly, followed by a detailed study of the changes required to include diffractive radiation losses. The local regime has been chosen as nonlocality causes an additional complication to the radiation shelf calculation which will be discussed in Chapter 3. The radiation calculation for nematicons in the local regime was presented in full by García-Reimbert *et al* [30]. However the author suggests that a full summary of this calculation is essential if a complete understanding of the modulation method is to be obtained, since the additional beams of Chapters 3 & 4 and the index defect of Chapter 5 add more equations, variables and parameters to an already complicated problem. Furthermore, radiation losses are calculated in an identical fashion for all of the regimes presented in this work, so one detailed analysis of the calculation here, with adjustments mentioned in the relevant chapters for each

regime, is the most efficient way of presenting the calculation.

The equations governing single nematicon evolution were derived in Section 2.1 and are

$$i\frac{\partial u}{\partial z} + \frac{1}{2}\nabla^2 u + \sin(2\theta)\, u = 0, \tag{2.55}$$

$$\nu\nabla^2\theta - q\sin(2\theta) + 2|u|^2\cos(2\theta) = 0, \tag{2.56}$$

which can, in the local limit with ν small and small $|u|$, be simplified to the higher-order NLS equation [30]

$$i\frac{\partial u}{\partial z} + \frac{1}{2}\nabla^2 u + \frac{2}{q}|u|^2 u - \frac{4}{q^3}|u|^6 u = 0, \tag{2.57}$$

where u is the envelope of the electric field and ν and q are constants whose physical meanings were touched upon previously and will be explained further in Chapter 3. The Laplacian ∇^2 is in the (x, y)-plane and the beam initially propagates in the z direction. Using the same modulation technique as for the one-dimensional NLS equation, described in Section 2.2.1, the governing equations are converted to the equivalent Lagrangian formulation. To calculate the double integral averaged Lagrangian

$$\mathcal{L} = \int_{-\infty}^{\infty}\int_{-\infty}^{\infty} L\, dxdy, \tag{2.58}$$

a suitable trial function is chosen

$$u = a\,\mathrm{sech}\,\frac{\sqrt{x^2+y^2}}{w}e^{i\sigma} + ige^{i\sigma}, \tag{2.59}$$

where beam amplitude a, beam width w, phase σ and shelf amplitude g are functions of z. This trial function is then inserted into $\mathcal{L}$. Variations are taken with respect to each of the parameters a, w, σ and g. As for the $(1+1)$-D NLS soliton, nematicons form a radiation shelf travelling under and with the beam during propagation. The existence of this shelf was shown numerically for single nematicons by García-Reimbert *et al* [30] and Minzoni *et al* [39] and can also be clearly seen in Figure 1.3. This shelf is in $(2+1)$-D and therefore forms a disc under the beam whose radius is given by ℓ. To simplify some of the calculations Λ is introduced, whose relation to ℓ is $\Lambda = \frac{1}{2}\ell^2$ [30]. The modulation equations for a single nematicon are then found to have exactly the same structure as those for the NLS soliton, with a few changes to coefficients, namely

$$\frac{d}{dz}\left(I_2 a^2 w^2 + \Lambda g^2\right) = 0, \tag{2.60}$$

$$\frac{d}{dz}\left(I_1 a w^2\right) = \Lambda g\frac{d\sigma}{dz}, \tag{2.61}$$

$$I_1\frac{dg}{dz} = \frac{I_{22}a}{2w^2} - \frac{I_4 a^3}{q} + \frac{3I_8 a^7}{q^3}, \tag{2.62}$$

$$I_2\frac{d\sigma}{dz} = -\frac{I_{22}}{w^2} + \frac{3I_4 a^2}{q} - \frac{7I_8 a^6}{q^3}. \tag{2.63}$$

The Is are various constants given by integrals [30]. These constants are defined later (see (3.18) & (4.16)). Now that the modulation equations (2.60)–(2.63) are known a detailed analysis of the shed radiation can be presented.

The linearised NLS equation (2.35) is the equation governing radiation shed to the far field for the NLS solitary wave. Similarly, by linearising the governing Schrödinger-like equation (2.57) and assuming circular symmetry, radiation propagating away from the nematicon beam is governed in polar coordinates by

$$i\frac{\partial u}{\partial z} + \frac{1}{2}\frac{\partial^2 u}{\partial\chi^2} + \frac{1}{2\chi}\frac{\partial u}{\partial\chi} = 0, \tag{2.64}$$

where $\chi^2 = x^2 + y^2$. Since the governing equation for shed radiation is now linearised what

follows is identical for single nematicons in both local and nonlocal regimes [30, 39] because radiative losses are too small to have a non-negligible nonlinear interaction with the medium.

Equation (2.64) is solved coupled with a boundary condition ($S(z)$) at the edge of the shelf which matches the shelf of radiation with shed radiation, i.e. $u = S(z)$ on $\chi = \ell$, for the purpose of finding the mass flux to radiation. The shelf radius ℓ has already been assumed to be slowly varying so for the purposes of calculating radiation it will be assumed to be constant. Mass conservation in standard form is given as

$$\frac{d}{dz}\int_{-\infty}^{\infty}\chi|u|^2 d\chi = 0, \tag{2.65}$$

equivalent to equation (2.37) for the NLS solitary wave. Thus the mass flux into the far field is radiated from the edge of the shelf into the region $\ell < \chi < \infty$ and is given by

$$\frac{d}{dz}\int_{\ell}^{\infty}\chi|u|^2 d\chi = \mathrm{Im}\left(\chi u^* u_\chi\right)|_{\chi=\ell}, \tag{2.66}$$

on neglecting higher-order terms. Again an expression relating u and u_χ must be found and $R = |u(\Lambda, z)|$ calculated.

The Laplace transform of the linearised NLS-like equation (2.64) is

$$2i\zeta\chi\tilde{u} + \chi\frac{d^2\tilde{u}}{d\chi^2} + \frac{d\tilde{u}}{d\chi} = 0 \quad \text{with} \quad \tilde{u}(\zeta) = \int_0^{\infty} e^{-\zeta z} u dz = \mathcal{L}\{u(z)\}, \tag{2.67}$$

Setting $\chi = \alpha r$, equation (2.67) may be rewritten

$$2i\zeta\alpha^2 r\tilde{u} + r\frac{d^2\tilde{u}}{dr^2} + \frac{d\tilde{u}}{dr} = 0. \tag{2.68}$$

A suitable choice of α allows equation (2.68) to be given in the form

$$r\frac{d^2\tilde{u}}{dr^2} + \frac{d\tilde{u}}{dr} - r\tilde{u} = 0 \quad \text{with} \quad \alpha = \frac{e^{i\pi/4}}{\sqrt{2\zeta}}. \tag{2.69}$$

The solution of this equation is the modified Bessel function of order 0

$$\tilde{u} = AK_0(r) = AK_0[\sqrt{2\zeta}e^{-i\pi/4}\chi], \tag{2.70}$$

where A is some constant. From this description of $\tilde{u}$, $\tilde{u}_\chi$ can also be found

$$\tilde{u}_\chi = -\sqrt{2\zeta}e^{i\pi/4}AK_1, \tag{2.71}$$

where K_1 is the modified Bessel function of order 1. The undefined constant A can be eliminated to leave

$$\tilde{u}_\chi = -\frac{\sqrt{2\zeta}e^{i\pi/4}\tilde{u}K_1}{K_0}. \tag{2.72}$$

Utilising the convolution theorem, as was done for the earlier NLS soliton example, the inverse Laplace transform of equation (2.72) yields

$$u_\chi|_{\chi=\ell} = -\frac{1}{2i\pi}\int_C \sqrt{2s}e^{-\frac{i\pi}{4}}\frac{K_1\left[\ell\sqrt{2s}e^{-\frac{i\pi}{4}}\right]}{K_0\left[\ell\sqrt{2s}e^{-\frac{i\pi}{4}}\right]}\tilde{S}e^{sz}ds, \tag{2.73}$$

where S is the as yet undetermined boundary condition for u at $\chi = \ell$, $\tilde{S}$ the Laplace transform of S, s is the Laplace transform variable and the contour C lies to the right of all singularities of the integrand [30]. Equation (2.73) gives the flux product

$$u^* u_\chi = S(z)^* \int_0^z G\left(z - z'\right) S(z')dz', \tag{2.74}$$

where G, the Green's function, is given by

$$G(\tau) = -\frac{1}{2i\pi}\int_C \sqrt{2s}e^{\frac{-i\pi}{4}}\frac{K_1\left[\ell\sqrt{2s}e^{-\frac{i\pi}{4}}\right]}{K_0\left[\ell\sqrt{2s}e^{-\frac{i\pi}{4}}\right]}e^{s\tau}ds. \tag{2.75}$$

From observations made for the $(1+1)$-D NLS soliton [31], S can be assumed to have slowly varying phase ϕ and equation (2.74) may be rewritten as

$$u^*u_\chi = R(z)\int_0^\infty G(z-z')R(z')dz', \quad \text{where} \quad S(z) = R(z)e^{i\phi z}. \tag{2.76}$$

This equation can be used to provide an accurate calculation of the radiation flux, but the Green's function is not suitably explicit for the analysis of radiation loss.

Since K_1 is the derivative with respect to s of K_0, the Green's function G (equation (2.75)) can be rearranged to

$$G(\tau) = \frac{1}{2i\pi}\int_C \frac{2s}{\ell}\frac{d}{ds}\ln\left(K_0\left[\ell\sqrt{2s}e^{-\frac{i\pi}{4}}\right]\right)e^{s\tau}ds. \tag{2.77}$$

Taking the asymptotic expansion of the Bessel function K_0 as $s \to 0$, corresponding to z large, an approximation of K_0 is obtained as

$$K_0(\psi) \sim -\ln(\frac{\psi}{2}) \quad \text{where} \quad \psi \to 0. \tag{2.78}$$

This approximation misses the early transient of the shelf formation and is only accurate for relatively large z, where the Laplace transform variable $s \to 0$. However, radiation damps the nematicon over large z so the approximation is valid on the scales of interest for the regimes that will be presented in this work. Inserting this asymptotic approximation into the equation for the Green's function then yields

$$G(\tau) = -\frac{1}{2i\pi\ell}\int_C \frac{2e^{s\tau}}{\ln s + \ln\Lambda - i\pi/2}ds. \tag{2.79}$$

The Green's function G can now be calculated. The integral in equation (2.79) is evaluated along the inverse Laplace transform contour C. The contour C is closed around the branch point of $\ln s$. Since a large z approximation has been taken, the integral is then asymptotically evaluated using the method of stationary phase, otherwise known as the saddle-point approximation. Transforming the variable s such that $\mathrm{Re}\, s = -e^\xi$ deforms the contour on the branch cuts and leads to the explicit expression

$$G(\tau) = \frac{1}{4\ell}\int_{-\infty}^\infty \frac{e^{-e^\xi\tau+\xi}}{\left(\frac{\xi}{2}+\frac{\ln\Lambda}{2}\right)^2 - (i\pi/2)\left(\frac{\xi}{2}+\frac{\ln\Lambda}{2}\right)+\frac{3\pi^2}{16}}d\xi. \tag{2.80}$$

A standard stationary phase analysis can then be made by letting

$$4\ell G(\tau) = \int_{-\infty}^\infty g(\xi)e^{f(\xi)}d\xi, \tag{2.81}$$

where

$$f(\xi) = -e^\xi\tau + \xi, \quad g(\xi) = \left(\left(\frac{\xi}{2}+\frac{\ln\Lambda}{2}\right)^2 - \frac{i\pi}{2}\left(\frac{\xi}{2}+\frac{\ln\Lambda}{2}\right)+\frac{3\pi^2}{16}\right)^{-1}, \tag{2.82}$$

to asymptotically evaluate the integral for large τ, estimating the major contributions to the integral. The integral is dominated by the highest stationary point of f, which will be a saddle point (since the integral is evaluated in the complex plane). The result is derived from the

Taylor series of f about the point ξ_0, where ξ_0 is chosen such that $df(\xi_0)/d\xi = 0$, namely

$$4\ell G(\tau) \approx g(\xi_0) e^{f(\xi_0)} \left(\frac{2\pi}{|d^2 f(\xi_0)/d\xi^2|} \right)^{1/2}. \tag{2.83}$$

The asymptotic form of the Green's function for large τ is then equation (2.83). It is then simple to approximate u_χ for large z, which is given after some algebra by

$$u_\chi = -\frac{\sqrt{2\pi}}{4\ell e} \int_0^z \frac{R(z')}{(z-z') \left(\left\{ \frac{1}{2} \ln(\frac{z-z'}{\Lambda}) - \frac{i\pi}{4} \right\}^2 - \frac{\pi^2}{4} \right)} dz'. \tag{2.84}$$

Mass flux is then found in exactly the same manner as equation (2.44) was found for a NLS solitary wave. From equation (2.66) for mass flux to radiation the modified mass conservation equation is

$$\frac{d}{dz} \int_0^\ell \chi |u|^2 d\chi = \frac{d}{dz} \left(a^2 w^2 I_2 + \Lambda g^2 \right) = \mathrm{Im} \left\{ \frac{\sqrt{2\pi} R(z)}{4e} \int_0^z \frac{R(z')}{\left(\left\{ \frac{1}{2} \ln \left(\frac{z-z'}{\Lambda} - \frac{i\pi}{4} \right) \right\}^2 - \frac{\pi^2}{4} \right)} \frac{dz'}{(z-z')} \right\}. \tag{2.85}$$

The function $R(z)$ representing the height of the shelf still needs to be determined and is found in the exact same manner that r was found in the $(1+1)$-D NLS soliton case. Namely, the area of the shelf is equated to the difference in mass between the solution at z and the fixed point solitary wave so that

$$|R|^2 \Lambda = \left(I_2 a^2 w^2 - I_2 \hat{a}^2 \hat{w}^2 + \Lambda g^2 \right). \tag{2.86}$$

All that remains to be done is to incorporate the mass loss found into the variational equation for g, equation (2.62). This is an identical process to that shown before for the NLS equation and the final modified equation is

$$I_1 \frac{dg}{dz} = \frac{I_{22} a}{2w^2} - \frac{I_4 a^3}{q} + \frac{3 I_8 a^7}{q^3} - 2\delta g, \tag{2.87}$$

where δ is the loss coefficient calculated below. $R^2 = g^2$ at the fixed point so the conservation of mass equation (2.60) is

$$\frac{d}{dz} \left(a^2 w^2 I_2 \right) + 2\Lambda g \frac{dg}{dz} = -\mathrm{Im} \left\{ \ell R u_\chi |_{\chi=\ell} \right\}. \tag{2.88}$$

At the fixed point it is also reasonable to assume that the main contribution to the left hand side of equation (2.87) comes from the loss term [38]. If this assumption is taken then

$$\frac{dg}{dz} \sim -\frac{2\delta g}{I_1}, \tag{2.89}$$

and equation (2.88) yields

$$-\frac{4\Lambda}{I_1} \delta g^2 = -\frac{4\Lambda}{I_1} \delta R^2 = -\mathrm{Im} \left\{ \ell R u_\chi |_{\chi=\ell} \right\}. \tag{2.90}$$

Consequently, the loss coefficient δ is calculated as

$$\delta = \frac{I_1 \ell}{4\Lambda R} \mathrm{Im} \left\{ u_\chi |_{\chi=\ell} \right\} = -\frac{\pi\sqrt{2\pi} I_1}{32 e R \Lambda} \int_0^z \frac{R(z') \ln[\frac{z-z'}{\Lambda}]}{\left(\left(\left\{ \frac{1}{4} \ln \left[\frac{z-z'}{\Lambda} \right] \right\}^2 + \frac{3\pi^2}{16} \right)^2 + \frac{\pi^2}{16} \left\{ \ln \left[\frac{z-z'}{\Lambda} \right] \right\}^2 \right)} \frac{dz'}{(z-z')}. \tag{2.91}$$

With this definition of δ the modulation equations (2.60), (2.61) and (2.63) with the extended equation (2.87) form a full set of modulation equations approximating single nematicon evolution in the local regime. The extended variational approximation yielding modulation equations governing NLS soliton and nematicon evolution has been fully presented. The numerical tech-

nique used to solve these equations is the subject of the next section.

2.2.4 Numerical Method of Solving Approximate Equations

Analysis of the modulation equations uncovers interesting information about beam evolution and conserved quantities, yet these equations still need to be solved numerically to be compared with their counterpart numerical solutions of the full governing equations. The modulation equations found in sections 2.2.2 & 2.2.3 and in subsequent chapters are all first order ODE systems which can be solved easily using the standard fourth order Runge-Kutta method or a suitable equivalent technique.

Generally an ODE system obtained via the variational method may be rewritten in the form of a matrix equation

$$\mathbf{A}\mathbf{x}' = \mathbf{b}, \tag{2.92}$$

where $\mathbf{A}$ is the matrix of coefficients of $\mathbf{x}'$, which is the vector of derivatives of each of the beam parameters as a function of z. $\mathbf{b}$ is the vector of the inhomogeneous right hand sides of each of the differential equations. To solve equation (2.92) using the Runge-Kutta method the system must be inverted. To this end, the LU decomposition is utilised. $\mathbf{A}$ can be factorised into lower and upper triangular matrices respectively

$$\mathbf{A}\mathbf{x}' = \mathbf{L}\mathbf{U}\mathbf{x}' = \mathbf{b}. \tag{2.93}$$

Introducing $\mathbf{y} = \mathbf{U}\mathbf{x}'$, equation (2.93) can be replaced by the coupled system of first order ODEs

$$\mathbf{L}\mathbf{y} = \mathbf{b}, \qquad \mathbf{U}\mathbf{x}' = \mathbf{y}. \tag{2.94}$$

These triangular matrices $\mathbf{L}$ and $\mathbf{U}$ can be inverted more easily than $\mathbf{A}$. Numerical forward substitution is used to solve for $\mathbf{y}$ and then backward substitution solves $\mathbf{U}\mathbf{x}' = \mathbf{y}$ for $\mathbf{x}'$. The main advantage of using the LU decomposition over simply inverting the matrix $\mathbf{A}$ is that there is an efficiency gain of about a factor of three. Then for each b_i in $\mathbf{b} = (b_1 \quad b_2 \ldots b_n)$, where n is the number of differential equations, the triangular matrices are quickly solved. If Gaussian elimination were used to compute $\mathbf{x}'$ for each b_i the computation would be dramatically slowed by having to perform Gaussian elimination n times [40].

The system (2.92) is now solved using the standard fourth order Runge-Kutta scheme for $\mathbf{x}'$ using the initial values of the beam parameters. For the vector of parameters $\mathbf{x}$ the initial value problem is defined as

$$\mathbf{x}' = \mathbf{f}(z, \mathbf{x}), \quad \mathbf{x}(z_0) = \mathbf{x}_0, \tag{2.95}$$

where $\mathbf{f}$ is the operator $\mathbf{A}^{-1}\mathbf{b}$, yet to be calculated. With these definitions the fourth order Runge-Kutta algorithm is summarised as

$$\begin{aligned} \mathbf{x}_{m+1} &= \mathbf{x}_m + \frac{1}{6}\left(\mathbf{a}_1 + 2\mathbf{a}_2 + 2\mathbf{a}_3 + \mathbf{a}_1\right), \\ z_{m+1} &= z_m + h. \end{aligned} \tag{2.96}$$

The estimates of the slope a_i of the solution, within the step of length h, are given by

$$\begin{aligned} \mathbf{a}_1 &= \mathbf{f}(z_m, x_m), \\ \mathbf{a}_2 &= \mathbf{f}(z_m + \frac{1}{2}h, x_m + \frac{1}{2}h\mathbf{a}_1), \\ \mathbf{a}_3 &= \mathbf{f}(z_m + \frac{1}{2}h, x_m + \frac{1}{2}h\mathbf{a}_2), \\ \mathbf{a}_2 &= \mathbf{f}(z_m + h, x_m + h\mathbf{a}_3). \end{aligned} \tag{2.97}$$

$\mathbf{x}_m$ are the values of the n parameters at the position z_m after m steps and $\mathbf{x}_{m+1}$ are the values of the parameters $\mathbf{x}$ at the next z step determined by the step length h. This method is fourth order accurate in h and solves the ODE system, yet once again the incorporation of radiation shed as the beam evolves brings with it complications.

A Simple System including Radiation

For the simple NLS solitary wave described in Section 2.2.2, the loss term δ was given by

$$\delta = \frac{9\pi^2}{128\Lambda r}\frac{d}{dz}(\Gamma) = \frac{9\pi^2}{128\Lambda r}\frac{d}{dz}\int_0^z \frac{r}{\sqrt{\pi(z-s)}}ds. \tag{2.98}$$

The integral Γ can easily be evaluated using the Trapezoidal Rule over most of the interval, except at the upper limit $z = s$, where it is singular. Miksis & Ting developed a numerical method to solve general integral-differential systems [41]. In this work they circumvented the difficulties of calculating an integral with a singularity by separating the integral into two parts; one integral is calculated using the composite Trapezoidal Rule as there is no singularity in its range, the other lies in an interval near and including the singularity, expressed as a sum of integrals easily approximated by a linear polynomial, apart from the term involving z which is solved using standard Picard iteration.

For the NLS soliton example given above, the integral Γ is then given by

$$\Gamma = \Gamma_1 + \Gamma_2 = \int_0^L \frac{r(s)}{\sqrt{\pi(z-s)}}ds + \int_L^z \frac{r(s)}{\sqrt{\pi(z-s)}}ds. \tag{2.99}$$

Γ_1 is calculated directly using the composite Trapezoidal Rule since there is no singularity in the range of integration. L, the integral change-over point, is chosen far enough away from z to ensure that the integrand in Γ_1 is smooth, but close enough to z so that it contains the major part of the region of integration. This is done because the composite Trapezoidal Rule is more accurate over identical step lengths than the method for evaluating Γ_2 near the singularity.

Γ_2 may be expressed as a sum of integrals

$$\Gamma_2 = \sum_{i=k}^{n}\int_{z_i}^{z_{i+1}} \frac{r(s)}{\sqrt{\pi(z-s)}}ds, \tag{2.100}$$

where k is chosen so that $z_k = L$. The linear polynomial approximation for r on each interval $z_i < s < z_{i+1}$ is given by

$$r(s) \approx r(z_i) + (s - z_i)\frac{r(z_{i+1}) - r(z_i)}{z_{i+1} - z_i}, \tag{2.101}$$

which is then inserted into equation (2.100). The resulting integral is then evaluated exactly, giving

$$\begin{aligned}\Gamma_2 = \sum_{i=k}^{n}\Bigg(2\left(r(z_i) + \left(\frac{r(z_{i+1}) - r(z_i)}{z_{i+1} - z_i}\right)(z - z_i)\right)\left(\sqrt{z - z_i} - \sqrt{z - z_{i+1}}\right) \\ + \frac{2}{3}\frac{r(z_{i+1}) - r(z_i)}{z_{i+1} - z_i}\left((z - z_{i+1})^{3/2} - (z - z_i)^{3/2}\right)\Bigg).\end{aligned} \tag{2.102}$$

Miksis & Ting used variable step sizes to take advantage of the smooth nature of the integrand of Γ_1 [41]. By taking a small step size for Γ_2 near the singularity and then increasing the step size for Γ_1 over $0 < s < L$ they managed to increase computational efficiency. But this is impossible for the calculation of the radiation loss coefficient δ presented here since r has only been calculated at each z step and is therefore not the smooth continuous function required for variable step sizes. Splitting of the integral in this manner is still necessary and advantageous, however, as by choosing the integral change-over point L to be as close to z as possible the more accurate composite Trapezoidal Rule can be used to calculate most of the integral and only a small range of s requires the less accurate linear polynomial approximation near the singularity.

A Single Nematicon System

The radiation loss integral for a single nematicon, which is identical to the loss integrals for each of the cases presented in this work, was given by

$$\delta = -\frac{\pi\sqrt{2\pi}I_1}{32eR\Lambda}\,\Gamma = -\frac{\pi\sqrt{2\pi}I_1}{32eR\Lambda}\int_0^z \frac{R(z')\ln[\frac{z-z'}{\Lambda}]}{\left(\left\{\frac{1}{4}\ln\left[\frac{z-z'}{\Lambda}\right]\right\}^2+\frac{3\pi^2}{16}\right)^2+\frac{\pi^2}{16}\left\{\ln\left[\frac{z-z'}{\Lambda}\right]\right\}^2\right)}\frac{dz'}{(z-z')}. \tag{2.103}$$

It seems natural to use the method of Miksis & Ting once again. However this method is valid for integrals of the form

$$\int_0^z \frac{f(z')}{(z-z')^a}dz', \tag{2.104}$$

where f is some non-singular function and $0 < a < 1$, or at least has a singularity which can be integrated exactly. If $a \geq 1$ the integral is divergent. The denominator of the integrand of equation (2.103) has $a = 1$, yet this integral is convergent as $z \to z'$ since the denominator includes terms involving squared logarithms. A careful analysis of the singularity near $z = z'$, taking account of the logarithms in the denominator, shows that the singularity is integrable. An extended version of the method of Miksis & Ting can be used to evaluate the integral near the singularity [30]. As a result, the integral Γ is split into two parts, as for the numerical calculation of the radiation loss term for the NLS soliton, with the denominator approximated by its leading order singularity as $z' \to z$. Now that radiation has been calculated, the nematicon modulation equations can be numerically solved and their solutions compared with numerical solutions of the full governing equations. The method used to solve the full nematicon equations will be outlined in the next section.

2.3 Numerical Method

For any deductions to be made from the solutions of the modulation equations, the validity of such solutions must be established as they have been derived under a number of approximations. This is done by calculating numerical solutions of the full governing nematicon equations and comparing them with the modulation solutions.

Naturally a numerical method must be chosen with proven accuracy and efficiency. For this reason a pseudo-spectral method based on the method developed by Fornberg & Whitham [42] will be used. Fornberg & Whitham's Fourier method has been analysed and compared with other numerical techniques by various authors and has been found to be competitive, yielding accurate solutions with low computational cost compared to other popular methods, such as finite difference or finite element methods. Furthermore, García-Reimbert *et al* [43] compared an alternative finite difference method to the method which will be used here and described below. In this work they analysed the full governing single nematicon equations (2.55)–(2.56) which were solved using the method of the present work and using a standard method based on the Dufort-Frankel finite difference scheme to solve equation (2.55) and a Gauss-Siedel iteration with successive over relaxation to solve equation (2.56). Identical step sizes were taken and it was found that agreement was excellent [43].

The numerical scheme presented here is developed somewhat from that derived by Fornberg & Whitham in that the z integration has been calculated using a fourth order Runge-Kutta method in Fourier space, as opposed to the original stepping in z of Fornberg & Whitham which was calculated using a second order scheme in physical space. Additionally, a damping layer has been included at the boundaries to reduce the effects of wave reflection there on the solitary wave, as proposed by If *et al* [44]. The nematicons presented in this thesis have governing equations which include a director equation similar to equation (2.56), which also needs to be solved. This is achieved using a standard fast Fourier transform (FFT)-based boundary value numerical method [45].

The $(1 + 1)$-D NLS equation will be used as an example once again to highlight the main features of the full numerical method. Later the numerical method for the $(2 + 1)$-D nematicon governing equation will be discussed. Any further adjustments to the numerical scheme for any

particular regime presented in this thesis will be included in the Results section of the specific chapter.

To damp any waves reflected at the boundaries, damping terms around these boundaries are added to the NLS equation (2.15). This adjustment adds an additional term to the NLS which simulates dispersive radiation travelling away from the beam indefinitely. Radiation is absorbed just before it reaches the boundary, in effect simulating an infinite grid. With the addition of this damping term the adjusted NLS equation is

$$\begin{aligned} &iu_z + \frac{1}{2}u_{xx} + |u|^2 u + i\varepsilon(x)u = 0 \quad \text{where,} \\ &\varepsilon(x) = \varepsilon_0 \left[\operatorname{sech}^2\left(\eta(x - L/2)\right) + \operatorname{sech}^2\left(\eta(x + L/2)\right)\right]. \end{aligned} \tag{2.105}$$

L is the computational domain length, so that the boundaries are $x = -L/2$ and $x = L/2$. ε_0 and $1/\eta$ are the strength and width of the damping layer, respectively. The inclusion of a damping term allows smaller spatial intervals to be chosen, which in turn allows greater computational speed. To solve the modified NLS equation (2.105) it must first be transformed into Fourier space via the Fourier transform, which yields

$$\frac{d\bar{u}}{dz} + \frac{i}{2}\omega^2 \bar{u} - iF\left\{|u|^2 u\right\} + F\left\{\varepsilon u\right\} = 0, \tag{2.106}$$

where the Fourier transform of $u(x, z)$ and its inverse respectively are defined by

$$\bar{u}\left(\omega, z\right) = F\left\{u\right\} = \frac{1}{\sqrt{2\pi}} \int_{-\infty}^{\infty} u\left(x, z\right) e^{-i\omega x} dx, \quad u(x, z) = F^{-1}\left\{\bar{u}\right\} = \frac{1}{\sqrt{2\pi}} \int_{-\infty}^{\infty} \bar{u}(\omega, z) e^{i\omega x} d\omega. \tag{2.107}$$

Equation (2.106) can now be rewritten in Fourier space by multiplying by an integrating factor, $e^{i\omega^2 z/2}$, from which the name of the method was taken, and which yields a first order ODE

$$\frac{d}{dz}\left(\bar{u} e^{i\omega^2 z/2}\right) = \left(iF\left\{|u|^2 u\right\} + F\left\{\varepsilon u\right\}\right) e^{i\omega^2 z/2}. \tag{2.108}$$

To solve equation (2.108) for $u(x, z)$ numerically requires the equation to be discretised. The discrete form of equation (2.108) is given by

$$\frac{d}{dz}\left(\bar{u}_j e^{i\omega_j^2 z/2}\right) = \left(iF\left\{|u|^2 u\right\} + F\left\{\varepsilon u\right\}\right) e^{i\omega_j^2 z/2}, \tag{2.109}$$

where

$$\omega_j = \frac{2\pi j}{L}, \qquad j = \frac{-N}{2} + 1, \ldots, \frac{N}{2}. \tag{2.110}$$

N is the number of spatial points and $u(x, t)$ is now numerically defined on these points. It can be solved using the standard forward FFT algorithm to calculate the Fourier transforms, then the Runge-Kutta method or an equivalent iterative method in Fourier space to calculate $\bar{u}$ at the next z step. Finally $\bar{u}$ is multiplied by the inverse integrating factor and then the backward FFT algorithm calculates the inverse Fourier transform of $\bar{u}$, namely u. These algorithms, and further details of the method, will be described below for a nematicon.

The $(2+1)$-D single nematicon governing equations including a damping term are given by

$$i\frac{\partial u}{\partial z} + \frac{1}{2}\nabla^2 u + \sin\left(2\theta\right) u + i\varepsilon u = 0, \tag{2.111}$$

$$\nu\nabla^2\theta - q\sin\left(2\theta\right) + 2|u|^2\cos\left(2\theta\right) = 0. \tag{2.112}$$

Taking the Fourier transform of equation (2.111) yields

$$\frac{\partial \bar{u}}{\partial z} - \frac{i}{2}\omega_x^2 \bar{u} - \frac{i}{2}\omega_y^2 \bar{u} - iF\left\{u \sin 2\theta\right\} + F\left\{\varepsilon u\right\} = 0, \tag{2.113}$$

where ω_x is the Fourier transform dummy variable corresponding to spatial variable x and ω_y the dummy variable corresponding to y. The integrating factor method is used in an identical

fashion to that for the NLS example to reduce equation (2.113) to

$$\frac{d}{dz}\left(\bar{u}e^{i\omega_x^2 z/2}\right) = \left(i\left[\frac{1}{2}\omega_y^2\bar{u} + F\left\{u\sin 2\theta\right\}\right] - F\left\{\varepsilon u\right\}\right)e^{i\omega_x^2 z/2}. \tag{2.114}$$

Assuming u is known for a given z then $\bar{u}$, the Fourier transform of u, is also calculable. At each z step the Fourier transform of the second derivative of u with respect to y can then be calculated. $F\left\{u\sin 2\theta\right\}$ requires the computation of θ which is found from the director equation (2.112). To solve this equation it is rewritten in the form

$$\nu\nabla^2\theta - 2q\theta = q\sin 2\theta - 2q\theta - 2|u|^2\cos 2\theta, \tag{2.115}$$

with boundary conditions

$$\begin{aligned} &\frac{\partial^2\theta}{\partial x^2} = 0 \quad \text{if} \quad x = 0, \qquad \frac{\partial^2\theta}{\partial y^2} = 0 \quad \text{if} \quad y = 0, \\ &\theta \to 0 \quad \text{as} \quad x \to \infty, \quad y \to \infty. \end{aligned} \tag{2.116}$$

It was found that equation (2.115) had better convergence properties than the original director equation (2.112) [30, 35, 39]. $\partial^2\theta/\partial x^2$ is solved using standard second order finite differences. On taking FFTs in the x direction this reduces to a two-point boundary value problem in y which is solved using a standard Picard iteration, where the right hand side is evaluated at the previous iteration. The other term $\{\varepsilon u\}$ is solved simply in physical space. $u\sin 2\theta$ and εu are transformed from physical space to Fourier space via the FFT algorithm.

Equation (2.114) can now be considered a first order ODE in Fourier space which, upon discretisation, will be solved using the fourth order Runge-Kutta scheme. Discretising equation (2.114) yields the single nematicon equivalent of equation (2.108) for a NLS soliton, namely

$$\frac{d}{dz}\left(\bar{u}_{jk}e^{i\omega_j^2 z/2}\right) = \left(\frac{i}{2}\omega_k^2\bar{u}_{jk} + iF\left\{u\sin 2\theta\right\} - F\left\{\varepsilon u\right\}\right)e^{i\omega_j^2 z/2}, \tag{2.117}$$

where

$$\omega_j = \frac{2\pi j}{L_x}, \qquad \omega_k = \frac{2\pi k}{L_y}, \tag{2.118}$$

$$j = \frac{-N_x}{2} + 1, \ldots, \frac{N_x}{2}, \qquad k = \frac{-N_y}{2} + 1, \ldots, \frac{N_y}{2}. \tag{2.119}$$

L_x, N_x are the interval length and number of points respectively in the x direction and L_y, N_y the same in the y direction.

Fornberg & Whitham used a leapfrog z stepping scheme whereby u_z was approximated by $u_z \approx u(x, z+\Delta z) - u(x, z-\Delta z)/2\Delta z$ [42]. Here however the calculation of u_z is more accurately performed in Fourier space using the fourth order Runge-Kutta method. To calculate u at the next space step $(z + \Delta z)$, the right hand side of equation (2.117) is calculated at z, $z + \Delta z/2$ and $z + \Delta z$. Equation (2.117) is estimated for the smallest step $\Delta z/2$ to be

$$\frac{d}{dz}(\phi_{jk}) = \frac{d}{dz}\left(\bar{u}_{jk}\left(n\Delta z\right)\right)e^{\frac{i}{4}\omega_j^2\Delta z}\eta(u_{jk})e^{\frac{i}{4}\omega_j^2\Delta z} = G(u, z), \tag{2.120}$$

where

$$\phi = \bar{u}e^{i\omega_x^2 z/2}, \quad \eta(u) = \frac{i}{2}\omega_y^2\bar{u} + iF\left\{u\sin 2\theta\right\} - F\left\{\varepsilon u\right\}, \tag{2.121}$$

and n is the current step. The nonlinear part of equation (2.117) is calculated exactly in physical space, then transformed to Fourier space numerically using the forward FFT algorithm.

With these definitions the Runge-Kutta method takes ϕ_{jk}^n, the Fourier transform of u multiplied by the integrating factor at the current step n, and computes ϕ_{jk}^{n+1} at the next z step $n + 1$. The algorithm is explained in detail as follows;

- $$U_1 = \phi_j^n + \frac{\Delta z}{2} G(u, z).$$

  u is known at z therefore $G(u, z)$ is easily calculated. U_1 is an Euler step of length $\Delta z/2$, yielding an estimate of ϕ at $z + \Delta z/2$.

- $$U_2 = \phi_j^n + \frac{\Delta z}{2} G(F^{-1}(U_1), z + \frac{\Delta z}{2}).$$

  If U_1 is multiplied by the inverse integrating factor and then the inverse Fourier transform of U_1 is taken, an estimate of u at $z + \Delta z/2$ is found. Consequently $G(u, z + \Delta z/2)$ can be calculated.

- $$U_3 = \phi_j^n + \Delta z G(F^{-1}(U_2), z + \frac{\Delta z}{2}).$$

  U_2 is known at $z + \Delta z/2$ therefore $G(F^{-1}(U_2), z + \Delta z/2)$ is easily calculated. Notice that U_3 is an Euler step of length Δz, yielding an estimate of ϕ at $z + \Delta z$.

- $$U_4 = -\phi_j^n + \frac{\Delta z}{2} G(F^{-1}(U_3), z + \Delta z).$$

  If U_3 is multiplied by the inverse integrating factor and then the inverse Fourier transform of U_3 is taken, an estimate of u at $z + \Delta z$ is found. Consequently $G(F^{-1}(U_3), z + \Delta z)$ can be calculated.

The solution at $n + 1$, ϕ_{jk}^{n+1}, is given by a weighted average of the estimates U_1–U_4, namely

$$\phi_{jk}^{n+1} = \frac{1}{3}U_1 + \frac{2}{3}U_2 + \frac{1}{3}U_3 + \frac{1}{3}U_4. \tag{2.122}$$

u^{n+1}, which is u at the next z step, is then extracted from ϕ_{jk}^{n+1} by multiplying by the integrating factor and then inverting $\bar{u}$ using the backward FFT algorithm to return u to physical space. This process is repeated until the final z value has been reached.

In this chapter the analytical method for approximating nematicon dynamics has been described along with the numerical scheme used to solve the resultant modulation equations. A description of the numerical method used to solve the full nematicon governing equations has also been given. How to extend these methods to more complicated nematicon regimes can now be investigated.

Chapter 3

Two-Colour Nematicons in the Nonlocal Limit

3.1 Background

Unlike soliton collisions in integrable systems, collisions in nonintegrable systems display unusual and interesting features. Collision effects for solitons governed by nonlinear Schrödinger-like (NLS-like) equations can depend on several parameters including wavelengths, intensities, collision angles and relative phases of the beams. In most media in-phase beams attract, possibly leading to beam fusion where the two beams form a single vector soliton with large parameter oscillations. In certain circumstances an additional beam may form and 3 solitons emerge from the collision [11]. Otherwise the beams pass through one another emerging intact but with oscillations of the beam parameters, a positional shift and some losses to radiation. Generally, out of phase beams repel one another [5, 39]. One interesting feature of the nonlocal nematic liquid crystal (NLC) reorientational response is that the interaction is always attractive because there is always an attractive positive refractive index perturbation caused by one beam on the other that extends beyond the beams themselves to the overlap of the respective refractive index perturbations. This nonlocal attraction counteracts any repulsion in cases where beams are out of phase, making the interaction between nematicons predominantly phase-independent [19, 20, 28, 39].

The first step in the observation of two-colour nematicons was made by Peccianti *et al* where waveguiding of weak signals by nematicons was reported [9]. In this work a single nematicon caused a refractive index change in the NLC, creating a self-induced waveguide in which a weak signal was passively steered. Later, Assanto *et al* conducted experiments with two symmetric nematicons of similar intensity co-propagating in a NLC. They noted that the interaction was always attractive and that *"no phase dependence was observed"* [19]. The same group led by Prof. Assanto once again were the first to discover nematicon interaction and co-propagation between two light beams of different colours, termed 'two-colour nematicons' [17]. Nonlinear self-focusing of individual beams caused by the reorientational response of the nematic has been shown to prompt a walk-off effect which displays a linear relation between the walk-off angle and initial beam power, with increased power producing a greater walk-off angle. In the two-colour nematicon experiments, when two beams were colaunched the addition of nonlinear cross-phase modulation (XPM) between the two beams enhanced the nonlinear response, allowing a vector nematicon to form from which a combined vector walk-off could be calculated. Varying the wavelengths (colours) of the beams introduced aperiodic breathing features and had an effect on walk-off yet the beams were stable, in contrast to predictions made by Shen *et al* for two-colour solitons in nonlocal Kerr-type nonlinear materials [46]. Additionally, the authors presented governing equations which were solved numerically. Comparisons between experimental data and numerical solutions of the governing equations were excellent [17]. An experimental observation of a two-colour nematicon with wavelengths $632.8nm$ (red) and $1064nm$ (near infrared (NIR)) for each colour respectively, is shown in Figure

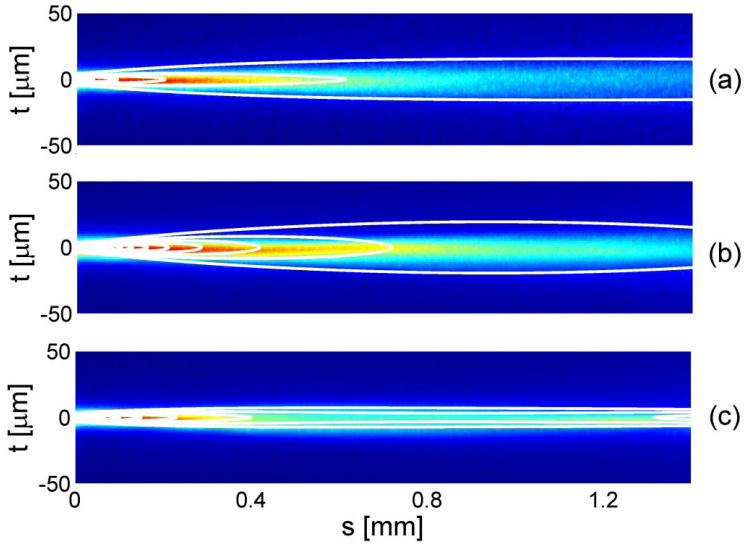

Figure 3.1: Experimental results and superimposed numerical contour maps for (a) two co-launched beams with negligible XPM diffracting, (b) a single beam diffracting and (c) two colaunched beams interacting to form a two-colour nematicon. Permission of use of image taken from Ref. [17] kindly given by Prof. G. Assanto.

3.1(c), with a contour map of the intensity profile calculated by Alberucci *et al* represented by the white lines [17]. It should be noted that walk-off is not seen in these figures as the (x, y, z) coordinate system has been replaced by a system (x, t, s) which is a rotation about the x axis accounting for the combined walk-off of the vector soliton. Figure 3.1(a) shows two copolarised beams, one weak $(0.1mW)$ and the other relatively strong $(1.2mW)$, colaunched into a NLC cell. The strong beam cannot self-focus to form a waveguide for the weak beam and, as a result, they both diffract. A single red beam of average power $(0.4mW)$ is launched into the cell in Figure 3.1(b) and diffracts. However, when an average power $(0.4mW)$ red beam is colaunched with a strong $(1.2mW)$ NIR beam, XPM allows the two beams to form a vector soliton, or two-colour nematicon, as seen in Figure 3.1(c) [17].

The experimental setup did not include an externally applied electric field as it was assumed that additional walk-off effects would be observed in this regime [17]. However other investigations into nematicon behaviour have been conducted with an externally applied electric field so it is of interest to discover whether additional walk-off is indeed observed under these new conditions and, if so, what the nature of this additional effect is. From a mathematical point of view, when there is no static/low-frequency applied electric field the nematic response does not have a pulse shape, so the appropriate boundary conditions at the cell walls must be accounted for [47]. With an applied field the nematic response is localised. Consequently the boundaries can be ignored for small beam to cell width ratios, resulting in a much simpler mathematical analysis [48]. Another motivation for the present work is that nematicon experimental results have so far been limited to *mm* distances, meaning that investigations of the role that radiative losses play in the evolution of the beams have not been carried out [9]. To this end, large propagation distances will be investigated which have the added advantage of showing beam evolution approaching or reaching the steady state [39].

A model including an externally applied electric field incorporating the walk-off observed by Alberucci *et al* will be introduced. This means that any further walk-off effects observed here would be in addition to the ones described by Alberucci *et al* and would therefore be of a different nature arising from the added externally applied electric field. Therefore to differentiate between the two types of walk-off, the walk-off observed by Alberucci *et al* will be described as 'Poynting vector walk-off' and any walk-off observed in this work will be named 'momentum walk-off.'

Let us consider two polarised, coherent light beams of different colours (wavelengths) prop-

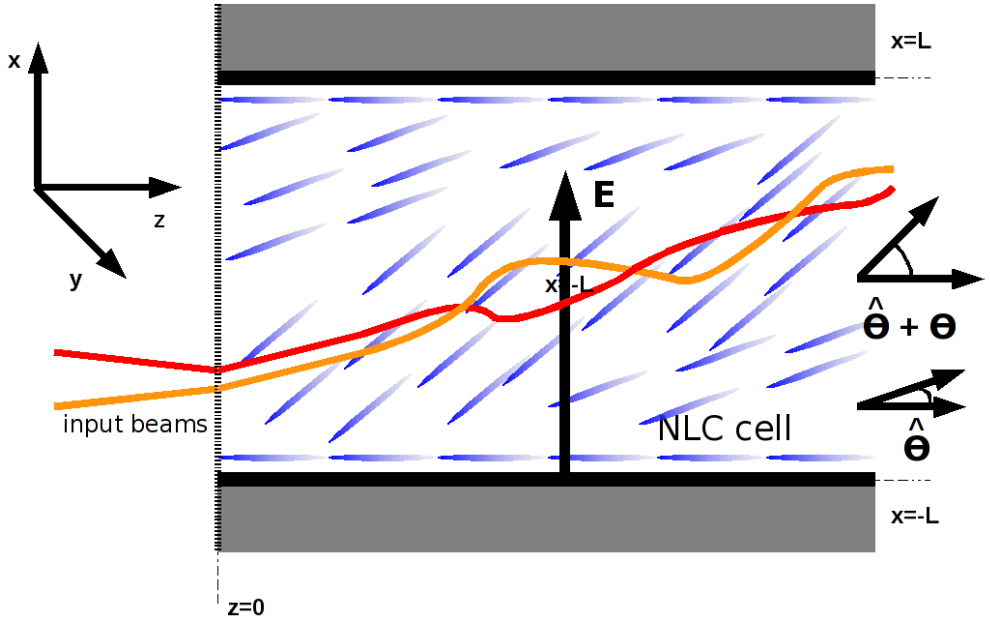

Figure 3.2: Schematic diagram of a liquid crystal cell with two x polarised light beams of different colours interacting.

agating through a planar nematic liquid crystal cell, taking the direction down the cell to be the z direction, with the (x, y)-plane orthogonal to this, as illustrated in Figure 3.2. The input light beams are polarised so that their electric fields are in the x direction. The Fréedericksz threshold is overcome by applying a static/low-frequency electric field in the x direction which causes the optical director angle to be pre-tilted by an angle $\hat{\theta}$ to the z direction. When light beams are incident the optical director angle is perturbed by a further angle θ.

Alberucci *et al* derived the equations for two-colour nematicon propagation in the absence of an applied static/low-frequency electric field [17]. These equations can be extended to include an applied static/low-frequency electric field in a similar way to that described in Section 2.1 for a single nematicon. The equations governing the propagation of two-colour nematicons then consist of coupled nonlinear Schrödinger-like (CNLS-like) equations for each colour and a director (Poisson) equation which is the two beam equivalent of equation (2.9) derived before. In nondimensional form these equations are

$$i\frac{\partial u}{\partial z} + \frac{1}{2}D_u\nabla^2 u + A_u u \sin 2\theta = 0, \tag{3.1}$$

$$i\frac{\partial v}{\partial z} + \frac{1}{2}D_v\nabla^2 v + A_v v \sin 2\theta = 0, \tag{3.2}$$

$$q\sin 2\theta - 2\cos 2\theta\left(A_u|u|^2 + A_v|v|^2\right) = \nu\nabla^2\theta, \tag{3.3}$$

where the Laplacian ∇^2 is in the (x, y)-plane. A_k and D_k are coupling and diffraction coefficients respectively, where $k = u, v$. q is proportional to the square of the pre-tilting field [17]. The parameter ν measures the strength of the elastic response of the nematic, and so measures its degree of nonlocality, with a nonlocal response corresponding to ν large. The variables u and v are the complex-valued, slowly varying envelopes of the electric fields of the two beams, modified by a phase factor which accounts for Poynting vector walk-off. Peccianti *et al* showed that Poynting vector walk-off is a departure of propagation direction from z in the x direction [49]. If Poynting vector walk-off were to be included in the current model, equations (3.1) and

(3.2) would become

$$i\frac{\partial U}{\partial z} + i\tan\Delta_u\frac{\partial U}{\partial z} + \frac{1}{2}D_u\nabla^2 U + A_u U\sin 2\theta = 0, \tag{3.4}$$

$$i\frac{\partial V}{\partial z} + i\tan\Delta_v\frac{\partial V}{\partial z} + \frac{1}{2}D_v\nabla^2 V + A_v V\sin 2\theta = 0. \tag{3.5}$$

U and V are then the field envelopes of the beams without the Poynting vector walk-off factored out. As Δ_u and Δ_v are the walk-off angles for each colour beam then the phase transformation

$$U = ue^{((i/2)z\tan^2\Delta_u - ix\tan\Delta_u)/D_u}, \quad V = ve^{((i/2)z\tan^2\Delta_v - ix\tan\Delta_v)/D_v},$$

eliminates the Poynting vector walk-off terms, and so validates the application of equations (3.1)–(3.3) to study additional deviation of propagation direction relative to the Poynting vector walk-off.

It is important to note that if $v = 0$ and $A_u = D_u = 1$ equations (3.1)–(3.3) reduce to the governing equations (2.55) & (2.56) found in Section 2.2.3 for a single beam propagating in a NLC [30, 39].

3.2 Analysis

3.2.1 Modulation Equations

In the nonlocal, ν large, limit it can be seen from the director equation (3.3) that θ, the optically induced deviation of the optical director angle from the pre-tilt angle $\hat{\theta}$, is small at low input beam powers. In this $|\theta|$ small limit the governing equations may be approximated by

$$i\frac{\partial u}{\partial z} + \frac{1}{2}D_u\nabla^2 u + 2A_u u\theta = 0, \tag{3.6}$$

$$i\frac{\partial v}{\partial z} + \frac{1}{2}D_v\nabla^2 v + 2A_v v\theta = 0, \tag{3.7}$$

$$2q\theta - 2\left(A_u|u|^2 + A_v|v|^2\right) = \nu\nabla^2\theta. \tag{3.8}$$

Since no exact solutions of (3.6)–(3.8) exist, alternative methods must be used to study the evolution of two-colour nematicons. By applying the approximate variational method described in Chapter 2 modulation equations are derived for the beam parameters, solutions of which will be compared with numerical solutions of the full governing equations (3.1)–(3.3).

Following the variational approximation method outlined in Chapter 2 the two-colour nematicon governing equations (3.6)–(3.8) have the Lagrangian

$$L = \sum_{k=u,v}\left[i\left(k^*k_z - kk_z^*\right) - D_k|\nabla k|^2 + 4A_k\theta|k|^2\right] - \nu|\nabla\theta|^2 - 2q\theta^2. \tag{3.9}$$

Appropriate trial functions are then inserted into the averaged Lagrangian

$$\mathcal{L} = \int_{-\infty}^{\infty}\int_{-\infty}^{\infty} L\,dxdy, \tag{3.10}$$

from which variational equations, termed modulation equations, are derived for the beam parameters. Gaussians have been widely employed as trial functions for spatial optical solitons (SOS) in the highly nonlocal limit. These trial functions are valid approximations to the nematicon profile in the limit of infinite nonlocality, which is not the experimental regime. Generally, experimental values of ν have been shown to be of the order of $\nu = 200$ [50]. The $(1+1)$-D NLS equation yields exact hyperbolic secant solutions. Additionally, sech trial functions have been successfully employed to find approximate modulation solutions for the CNLS equation [32, 51] and $(2+1)$-D nematicon NLS-like and CNLS-like equations [30, 35, 39, 43, 46]. Since the integrals involved in equation (3.10) need to be evaluated analytically, trial functions are required to be reasonably simple, yet this requirement must be balanced against the need for

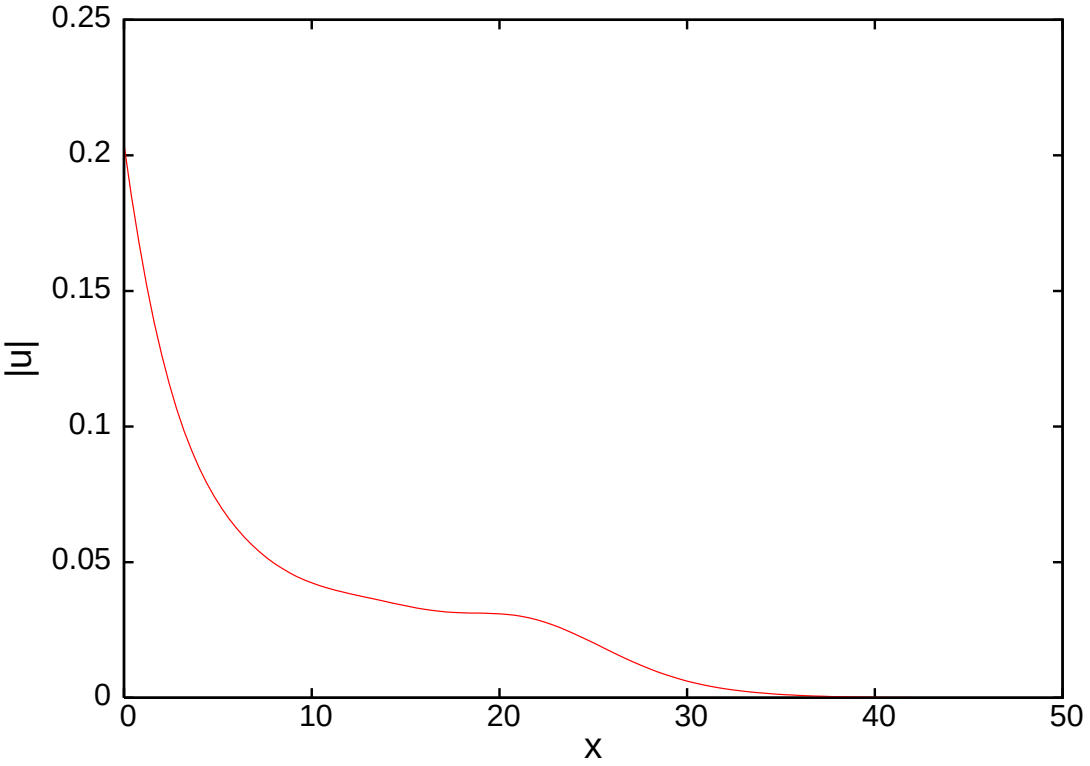

Figure 3.3: Numerical solution of the full governing equations (3.1)–(3.3) showing the radiation shelf profile of a u colour beam at $z = 60$, $y = 0$. The amplitude of the beam is $a \approx 1.1$.

some complexity in order to at least model basic features of beam evolution and interaction [34]. Suitable trial functions are then

$$\begin{aligned} k &= a_k \operatorname{sech} \frac{\chi_k}{w_k}\, e^{i\psi_k} + i g_k e^{i\psi_k}, \quad k = u, v, \\ \theta &= \sum_{k=u,v} \alpha_k \operatorname{sech}^2 \frac{\chi_k}{\beta_k}, \end{aligned} \tag{3.11}$$

where

$$\chi_k = \sqrt{(x - \xi_k)^2 + y^2}, \quad \psi_k = \sigma_k + V_k (x - \xi_k), \tag{3.12}$$

and the nematicon parameters are functions of z, these being the electric field amplitudes a_k and widths w_k, nematicon positions ξ_k, velocities V_k, phases σ_k, shelf amplitudes g_k and director beam amplitudes α_k and widths β_k. The first terms in the trial functions for u and v represent varying soliton-like beams, while the second terms represent the diffractive radiation of low wavenumber which accumulates under the evolving nematicons. The radiation shelves travelling with the beams protrude from the beam tails, as demonstrated in Figure 3.3 which shows a numerical solution of the u colour beam after significant evolution. This beam has an amplitude ($a_u \approx 1.1$) much larger than the observed shelf amplitude ($g_u \approx 0.04$) so the shelf can be assumed to be approximately flat, which has been done in the trial function. It is also clear from observation that the radiation shelf is finite, in this case becoming negligibly small around $x \approx 35$. It is assumed then that g_k are non-zero in the discs $0 \leq \sqrt{(x - \xi_k)^2 + y^2} \leq R_k$. The form of the diffractive radiation outside of these discs will be discussed at the end of this section. The director beam is the sum of the director beams associated with the individual light beams. These director beams have been chosen to have a sech^2 profile due to the $|k|^2$ terms in equation (3.8). Numerical simulations further confirm this shape to be a good fit to the actual director beam profile.

Modulation equations for the nematicon parameters are now found by substituting the trial functions (3.11) into the averaged Lagrangian (3.10), modulation equations being obtained as

variational equations with respect to the nematicon parameters. Upon substitution, all of the resulting integrals can be evaluated except those consisting of a product of hyperbolic secants with different widths, of the form

$$\int_{-\infty}^{\infty}\int_{-\infty}^{\infty}\theta|k|^2\,dxdy. \tag{3.13}$$

These integrals can be evaluated numerically, but the solution would be a function of the nematicon amplitude and therefore not a fixed number [30]. Essentially then this would defeat the object of finding a simple finite dimensional ordinary differential equation (ODE) system approximating a partial differential equation (PDE) system with infinitely many dimensions of freedom.

To avert this potential problem the concept of an 'equivalent' Gaussian is used, as in Minzoni *et al* [30] and García-Reimbert *et al* [39], whereby, for these integrals only, the sech trial functions are replaced by Gaussians as

$$\operatorname{sech}\frac{\chi_k}{\beta_k}\to e^{-\chi_k^2/(A\beta_k)^2}\quad\text{and}\quad\operatorname{sech}\frac{\chi_k}{w_k}\to e^{-\chi_k^2/(Bw_k)^2}, \tag{3.14}$$

so that the problematic cross integrals can be approximately evaluated in closed form. The scaling parameters A and B will be determined by matching the Taylor series of the resulting averaged Lagrangian using Gaussians with the Taylor series of the known averaged Lagrangian using sech trial functions in the *symmetric* limit $A_u = A_v$ and $D_u = D_v$ with $\xi_u = \xi_v$. Both are expanded in the highly nonlocal limit $w_k \ll \beta_k$.

Since Gaussians were used to evaluate integrals of the form (3.13) it is natural then to also investigate the potential of using Gaussians as trial functions, as noted previously. Indeed, in experiments the input beams used have a Gaussian profile [17], so one could argue that the final steady state nematicon profile could be close to a Gaussian shape. Section 3.3 reviews solutions using both trial functions and details the drawbacks of the latter approach.

With the equivalent Gaussian approximate evaluation of the problematic integrals the averaged Lagrangian (3.10) for the sech trial function is given by

$$\begin{aligned}\mathcal{L} &= \mathcal{L}_I-\sum_{k=u,v}\big[2(I_2a_k^2w_k^2-\Lambda_kg_k^2)(\sigma_k'-V_k\xi_k')+2I_1a_kw_k^2g_k'-2I_1w_k^2g_ka_k'-4I_1a_kw_kg_kw_k'\\ &\quad+ID_ka_k^2+D_k(I_2a_k^2w_k^2-\Lambda_kg_k^2)V_k^2+4\nu I_{42}\alpha_k^2+2qI_4\alpha_k\beta_{k^2}\big],\end{aligned} \tag{3.15}$$

where $'$ denotes differentiation with respect to z and $\Lambda_k = R_k^2/2$. The interaction component $\mathcal{L}_I$ of the averaged Lagrangian is

$$\begin{aligned}\mathcal{L}_I &= A_uA^2B^2a_u^2w_u^2\left(\frac{\alpha_u\beta_u^2}{Q_1}+\frac{\alpha_v\beta_v^2}{Q_2}e^{-2\gamma_1}\right)+A_vA^2B^2a_v^2w_v^2\left(\frac{\alpha_v\beta_v^2}{Q_3}+\frac{\alpha_u\beta_u^2}{Q_4}e^{-2\gamma_2}\right)\\ &\quad-\frac{2\nu\alpha_u\alpha_v\beta_u^2\beta_v^2}{Q_5}(1-4\gamma_3)\,e^{-2\gamma_3}-\frac{q\alpha_u\alpha_v\beta_u^2\beta_v^2A^2}{Q_5}e^{-2\gamma_3}.\end{aligned} \tag{3.16}$$

In these equations

$$\begin{aligned}&Q_1=A^2\beta_u^2+B^2w_u^2,\quad Q_2=A^2\beta_v^2+B^2w_u^2,\quad Q_3=A^2\beta_v^2+B^2w_v^2,\quad Q_4=A^2\beta_u^2+B^2w_v^2,\\ &Q_5=\beta_u^2+\beta_v^2,\quad \rho=\xi_u-\xi_v,\quad \gamma_1=\frac{\rho^2}{Q_2},\quad \gamma_2=\frac{\rho^2}{Q_4},\quad \gamma_3=\frac{\rho^2}{A^2Q_5},\\ &\Lambda_u=R_u^2/2,\quad A=\frac{I_2\sqrt{2}}{\sqrt{I_{32}}},\quad B=\sqrt{2I_2}.\end{aligned} \tag{3.17}$$

The integrals I_i and I_{ij} are

$$
\begin{aligned}
I_1 &= \int_0^\infty x \operatorname{sech} x \, dx = 2C, \\
I_2 &= \int_0^\infty x \operatorname{sech}^2 x \, dx = \ln 2, \\
I_{22} &= \int_0^\infty x \operatorname{sech}^2 x \tanh^2 x \, dx = \frac{1}{3}\ln 2 + \frac{1}{6}, \\
I_{32} &= \int_0^\infty x^3 \operatorname{sech}^2 x \, dx = 1.3523145016\ldots, \\
I_{42} &= \frac{1}{4}\int_0^\infty x \left[\frac{d}{dx}\operatorname{sech}^2 x\right]^2 dx = \frac{2}{15}\ln 2 + \frac{1}{60},
\end{aligned}
\tag{3.18}
$$

where C is the Catalan constant $C = 0.915965594\ldots$. It is immediately apparent that without the interaction component L_I, equation (3.15) is the averaged Lagrangian for two separate single nematicons [39].

Taking variations with respect to each of the nematicon parameters yields the modulation equations

$$\delta\sigma_u : \quad \frac{d}{dz}\left(I_2 a_u^2 w_u^2 + \Lambda_u g_u^2\right) = 0, \tag{3.19}$$

$$\delta V_u : \quad \left(\frac{d\xi_u}{dz} - D_u V_u\right)\left(a_u^2 w_u^2 I_2 - \Lambda_u g_u^2\right) = 0, \tag{3.20}$$

$$\delta g_u : \quad \frac{d}{dz}\left(a_u w_u^2 I_1\right) - \Lambda_u g_u \left(\frac{d\sigma_u}{dz} - V_u\frac{d\xi}{dz} + \frac{1}{2}D_u V_u^2\right) = 0, \tag{3.21}$$

$$
\begin{aligned}
\delta a_u : \quad & -2I_2 a_u w_u^2 \left(\frac{d\sigma_u}{dz} - V_u\frac{d\xi_u}{dz}\right) - I_1 w_u^2 \frac{dg_u}{dz} - I_1 \frac{d}{dz}\left(g_u w_u^2\right) \\
& + 2I_1 g_u w_u \frac{dw_u}{dz} - D_u I a_u - D_u I_2 a_u w_u^2 V_u^2 \\
& + A_u A^2 B^2 a_u w_u^2 \left(\frac{\alpha_u \beta_u^2}{A^2\beta_u^2 + B^2 w_u^2} + \frac{\alpha_v \beta_v^2}{A^2\beta_v^2 + B^2 w_u^2} e^{-\frac{2(\xi_u - \xi_v)^2}{A^2\beta_v^2 + B^2 w_u^2}}\right) = 0,
\end{aligned}
\tag{3.22}
$$

$$
\begin{aligned}
\delta w_u : \quad & -2I_2 a_u^2 w_u \left(\frac{d\sigma}{dz} - V_u\frac{d\xi}{dz}\right) - 4I_1 a_u w_u \frac{dg_u}{dz} - D_u I_2 a_u^2 w_u V_u^2 \\
& + A_u A^2 B^2 a_u^2 w_u \left(\frac{A^2 \alpha_u \beta_u^4}{\left(A^2\beta_u^2 + B^2 w_u^2\right)^2}\right. \\
& \left. + \frac{\alpha_v \beta_v^2}{\left(A^2\beta_v^2 + B^2 w_u^2\right)^2}\left(A^2\beta_v^2 + \frac{2B^2 w_u^2\left(\xi_u - \xi_v\right)}{A^2\beta_v^2 + B^2 w_u^2}\right) e^{-\frac{2(\xi_u - \xi_v)^2}{A^2\beta_v^2 + B^2 w_u^2}}\right) = 0,
\end{aligned}
\tag{3.23}
$$

$$
\begin{aligned}
\delta\xi_u : \quad & -\frac{d}{dz}\left(I_2 a_u^2 w_u^2 V_u + \Lambda_u g_u^2\right) - \frac{4A_u A^2 B^2 \alpha_v \beta_v^2 a_u^2 w_u^2 \left(\xi_u - \xi_v\right)}{\left(A^2\beta_v^2 + B^2 w_u^2\right)^2} e^{-\frac{2(\xi_u - \xi_v)^2}{A^2\beta_v^2 + B^2 w_u^2}} \\
& - \frac{4A_v A^2 B^2 \alpha_u \beta_u^2 a_v^2 w_v^2 \left(\xi_u - \xi_v\right)}{\left(A^2\beta_u^2 + B^2 w_v^2\right)^2} e^{-\frac{2(\xi_u - \xi_v)^2}{A^2\beta_u^2 + B^2 w_v^2}} + \frac{4q\alpha_u \alpha_v \beta_u^2 \beta_v^2 \left(\xi_u - \xi_v\right)}{\left(\beta_u^2 + \beta_v^2\right)^2} e^{-\frac{2(\xi_u - \xi_v)^2}{A^2\left(\beta_u^2 + \beta_v^2\right)}} \\
& + \frac{8\nu\alpha_u \alpha_v \beta_u^2 \beta_v^2 \left(\xi_u - \xi_v\right)}{A^2\left(\beta_u^2 + \beta_v^2\right)^3}\left(3 - \frac{4\left(\xi_u - \xi_v\right)^2}{A^2\left(\beta_u^2 + \beta_v^2\right)}\right) e^{-\frac{2(\xi_u - \xi_v)^2}{A^2\left(\beta_u^2 + \beta_v^2\right)}} = 0,
\end{aligned}
\tag{3.24}
$$

plus the symmetric equivalent variational equations for the v colour beam and also algebraic equations representing the variations of the parameters α_u, α_v and β_u, β_v which are not presented here for brevity, but will be presented in a suitably rearranged form below.

In total 16 equations govern the 8 parameters for each of the two beams. The modulation equations (3.19)–(3.24) are reduced by rearrangement to simpler first order ODE modulation

equations

$$\frac{d}{dz}\left(I_2 a_u^2 w_u^2 + \Lambda_u g_u^2\right) = 0, \tag{3.25}$$

$$I_1 \frac{d}{dz}\left(a_u w_u^2\right) = \Lambda_u g_u \left(\sigma_u - \frac{1}{2} D_u V_u^2\right), \tag{3.26}$$

$$\frac{d\xi_u}{dz} = D_u V_u, \tag{3.27}$$

$$2I_1 \frac{dg_u}{dz} = \frac{D_u I_{22} a_u}{w_u^2} - A_u A^2 B^4 a_u w_u^2 \left(\frac{\alpha_u \beta_u^2}{Q_1^2} + \frac{\alpha_v \beta_v^2}{Q_2^2} e^{-2\gamma_1}\left(1 - 2\gamma_1\right)\right), \tag{3.28}$$

$$\begin{aligned} I_2 a_u^2 w_u^2 \left(\frac{d\sigma_u}{dz} - \frac{1}{2} D_u V_u^2\right) = &-I_{22} D_u a_u^2 A_u A^2 B^2 a_u^2 w_u^2 \left[\alpha_u \beta_u^2 \left(A^2 \beta_u^2 + 2B^2 w_u^2\right) Q_1^{-2}\right. \\ &\left. + \alpha_v \beta_v^2 \left(\left(A^2 \beta_v^2 + 2B^2 w_u^2\right) Q_2 - B^2 w_u^2 \rho_2^2\right) Q_2^{-3} e^{-\gamma_1}\right], \end{aligned} \tag{3.29}$$

$$\begin{aligned} \frac{d}{dz}\left[\left(I_2 a_u^2 w_u^2 + \Lambda_u g_u^2\right) V_u\right] = &-\frac{4A_u A^2 B^2 a_u^2 w_u^2 \alpha_v \beta_v^2 \rho}{Q_2^2} e^{-2\gamma_1} - \frac{4A_v A^2 B^2 a_v^2 w_v^2 \alpha_u \beta_u^2 \rho}{Q_4^2} e^{-2\gamma_2} \\ &+ \frac{8\nu \alpha_u \alpha_v \beta_u^2 \beta_v^2 \rho}{A^2 Q_5^3}\left(3 - 4\gamma_3\right) e^{-2\gamma_3} + \frac{4q\alpha_u \alpha_v \beta_u^2 \beta_v^2 \rho}{Q_5^2} e^{-2\gamma_3}, \end{aligned} \tag{3.30}$$

and the algebraic equations for variations with respect to α and β reduce to

$$\begin{aligned} 4\left(2\nu I_{42} + q I_4 \beta_u^2\right)\alpha_u &= A_u A^2 B^2 a_u^2 w_u^2 \beta_u^2 Q_1^{-1} + A_v A^2 B^2 a_v^2 w_v^2 \beta_u^2 Q_4^{-1} e^{-2\gamma_2} \\ &\quad - \frac{\alpha_v \beta_u^2 \beta_v^2}{Q_5}\left[\frac{2\nu}{Q_5}\left(1 - \frac{4\rho^2}{A^2 Q_5}\right) + qA^2\right] e^{-2\gamma_3}, \end{aligned} \tag{3.31}$$

$$\begin{aligned} 2qI_4 \alpha_u &= A_u A^2 B^4 a_u^2 w_u^4 Q_1^{-2} + A_v A^2 B^2 a_v^2 w_v^2 \left(B^2 w_v^2 + 4A^2 \beta_u^2 \rho^2 Q_4^{-1}\right) Q_4^{-2} e^{-2\gamma_2} \\ &\quad - \frac{2\nu \alpha_v \beta_v^2}{Q_5^3}\left[\beta_v^2 - \beta_u^2 - \frac{2\rho^2}{A^2 Q_5}\left(2\beta_v^2 - \beta_u^2 + \frac{4\beta_u^2 \rho^2}{A^2 Q_5}\right)\right] e^{-2\gamma_3} \\ &\quad - q\alpha_v \beta_v^2 \left(A^2 \beta_v^2 + 2\beta_u \rho^2 Q_5^{-1}\right) Q_5^{-2} e^{-2\gamma_3}, \end{aligned} \tag{3.32}$$

plus the symmetric modulation equations and algebraic equations for the v colour.

The modulation equations (3.25)–(3.32) form a conservative system as loss to diffractive radiation has been neglected so far. A number of details of the evolution of the nematicons can be found from conservation equations resulting from this neglect of shed radiation. The three fundamental conserved quantities are mass, momentum and the Hamiltonian, H, which is related to energy. Equation (3.30) is the momentum conservation equation and equation (3.25) the mass conservation equation for the u colour beam. For these equations the term including g_u describes the momentum and mass respectively that seeps from the u colour beam into the radiation shelf. 'Mass' does not refer to any physical mass but, in an optical context is defined as the optical power or intensity of the light beam [31]. Other conserved quantities are more difficult to interpret physically so it is sensible and far simpler to regard these quantities as resulting from the application of Nöther's Theorem to invariances of the Lagrangian (3.9) [24, 31]. Adding the momentum equation (3.30) in the u colour to its symmetric counterpart in the v colour gives the equation for total momentum conservation in the system as

$$\frac{d}{dz}\sum_{k=u,v}\left(I_2 a_k^2 w_k^2 + \Lambda_k g_k^2\right) V_k = 0. \tag{3.33}$$

In addition to this momentum conservation equation, the modulation equations also possess an energy conservation equation by Nöther's Theorem applied to the Lagrangian (3.9) using invariances in z [25]. The averaged form of the energy conservation equation for an individual

beam k is then

$$\frac{dH}{dz} = \frac{d}{dz}\int_{-\infty}^{\infty}\int_{-\infty}^{\infty}\left[\nu|\nabla\theta|^2 + 2q\theta^2 + \sum_{k=u,v}\left(D_k|\nabla k|^2 - 4A_k\theta|k|^2\right)\right]dxdy = 0. \tag{3.34}$$

Inserting the trial functions (3.11) into equation (3.34) and using the mass and momentum equations (3.25) and (3.30) and their v colour counterparts then gives the total energy conservation equation

$$\begin{aligned}\frac{dH}{dz} = \frac{d}{dz}\Big(&-A_uA^2B^2\alpha_v a_u^2 w_u^2\beta_v^2 Q_2^{-1}e^{-2\gamma_1} - A_vA^2B^2\alpha_u a_v^2 w_v^2\beta_u^2 e^{-2\gamma_2}Q_4^{-1}\\ &+ 2\nu\alpha_u\alpha_v\beta_u^2\beta_v^2\left(1-4\rho^2A^{-2}Q_5^{-1}\right)Q_5^{-2}e^{-2\gamma_3} + qA^2\alpha_u\alpha_v\beta_u^2\beta_v^2Q_5^{-1}e^{-2\gamma_3}\\ &+ \sum_{k=u,v}\Big[I_{22}D_k a_k^2 + D_k\left(I_2a_k^2w_k^2 + \Lambda_k g_k^2\right)V_k^2\\ &- \frac{A_kA^2B^2\alpha_k a_k^2w_k^2\beta_k^2}{(A^2\beta_k^2 + B^2w_k^2)} + 4\nu I_{42}\alpha_k^2 + 2qI_4\alpha_k^2\beta_k^2\Big]\Big) = 0.\end{aligned} \tag{3.35}$$

The modulation equations (3.25)–(3.32) have a family of fixed point solutions which are the steady nematicon solutions of the governing equations. The final steady nematicon states for the two beams are determined by energy conservation [39]. There are two types of fixed points. The first type occurs when the nematicons interact but at some point pass through and travel away from one another, resulting in separate single nematicons, where $|\xi_u - \xi_v| \to \infty$ as $z \to \infty$. The second type interact indefinitely, forming a coupled vector nematicon as $z \to \infty$ with $\xi = \xi_u = \xi_v$. In the present work the case of interest is the coupled vector nematicon since the large z interaction provides a greater range of dynamical behaviour, such as walk-off and beam fusion. On a more fundamental level this case is of interest because two-colour vector solitons may find a use in all-optical interconnects in future communications devices, so their evolution and interaction is of particular importance.

Denoting fixed point values of the beam parameters by a $\hat{}$ superscript and boundary values at $z = 0$ by a subscript 0, we then have $\hat{\xi}_u = \hat{\xi}_v$, $\hat{g}_u = \hat{g}_v = 0$ and $g_{u0} = g_{v0} = 0$ since the shelf does not exist initially, and steady state nematicons have no radiation shelf. Using the momentum conservation equation (3.33), the mass conservation equation (3.25), the position equation (3.27) and their v colour counterparts, the combined momentum walk-off of the vector nematicon is

$$\hat{\xi}' = \hat{\xi}_u' = \hat{\xi}_v' = \frac{D_uD_vM_0}{I_2\left(D_ua_{v0}^2w_{v0}^2 + D_va_{u0}^2w_{u0}^2\right)}, \tag{3.36}$$

where

$$M_0 = I_2\sum_{k=u,v}a_{k0}^2w_{k0}^2V_{k0}, \tag{3.37}$$

is the initial total momentum, which is conserved. Equation (3.36) will be useful in revealing the extent to which radiative losses influence momentum walk-off.

The final quantities to determine are the shelf radii Λ_k. In previous work the shelf radius of a nematicon has been calculated by linearising the modulation equations about the fixed point $g = 0$, resulting in a simple harmonic oscillator equation whose frequency is matched to the known nematicon frequency at the fixed point [30, 31, 33, 39, 43]. Rearrangement then leads to an expression for the shelf radius. In this case however the calculation is intractable. To simplify the calculation somewhat certain approximations can be made. In experiments the diffraction coefficients D_k and the coupling coefficients A_k take similar values. For instance, for the experiments of Alberucci *et al* the diffraction coefficients were 0.805 for red ($632.8nm$) and 0.823 for NIR ($1064nm$) light [17]. By taking $D_u = D_v$ and $A_u = A_v$ and using the energy conservation equation (3.36) appropriately, an approximation to the fixed points of the modulation equations can then be found [24]. As stated before, these fixed points are required to find the shelf radii Λ_u & Λ_v whose calculation is fully presented in Appendix A. The final

result is

$$\Lambda_k = \frac{-\hat{\Sigma}_k' I_1^2 \hat{w}_k \left(\hat{w}_k + 2\hat{a}_k \varphi\right)}{\Theta}, \tag{3.38}$$

where $\hat{\Sigma}_k'$, φ and Θ depend on the fixed point beam parameters in a complicated way. The definitions of these terms are given in Appendix A.

3.2.2 Radiation Calculation

To complete the modulation equations the effect of shed diffractive radiation needs to be incorporated. García-Reimbert *et al* [30] calculated the diffractive radiation shed by a single nematicon as it evolves and included the effect of this shed radiation in the modulation equations for nematicon evolution in the local limit. These calculations have also been presented in Chapter 2. If it is assumed that the shed radiation from one beam does not interact with the shed radiation from the other beam, then radiative losses for the two beams can be treated as for two non-interacting single nematicons. Radiative losses are governed by the linearised electric field equations since radiative losses are of small amplitude and consequently have a negligible nonlinear interaction with the nematic. These linearised equations are the same equations for both local and nonlocal nematicons, as noted by Minzoni *et al* [39]. The linearised form of the field equations (3.6) and (3.7) are just two uncoupled equations for a single nematicon and are in fact Schrödinger's equation. They can be written in polar coordinates as

$$i\frac{\partial u}{\partial z} + \frac{1}{2r} D_u \frac{\partial}{\partial r}\left(r\frac{\partial u}{\partial r}\right) = 0, \tag{3.39}$$

$$i\frac{\partial v}{\partial z} + \frac{1}{2r} D_v \frac{\partial}{\partial r}\left(r\frac{\partial v}{\partial r}\right) = 0. \tag{3.40}$$

Equations (3.39) & (3.40) are solved using Laplace transforms, as shown in Chapter 2, and differ from equation (2.64) only by the linear diffraction coefficients D_k. However, there is a complication in the calculation of the radiation shelf here in that there is an additional component to the shelf relating to its nonlocal interaction with the director beam [39]. In the local regime the refractive index perturbation of the medium is localised to the close vicinity of the beam. Contrasting this, for highly nonlocal regimes the director beam, also known as optical axis beam or refractive index perturbation, is broader than the optical beam with an extended tail, as shown in Figure 1.1. This causes the electric fields of the beams to have long, low, flat tails as well. Consequently there is an inner component of the shelf due to the interaction of the beam with the radiation travelling with the beam, and an outer component created by the director beams reaction to the optical axis. The radiation shelf components travelling and interacting with the beams were discussed in Section 3.2.1, and have radii R_u, R_v, whereas the components relating to the shelves' interactions with the director have separate radii, which will be denoted ρ_u, ρ_v.

Minzoni *et al* estimated the values of ρ_k, where $k = u, v$, from numerical solutions [39]. In this work they judged that the half-widths of the optical director beams $\beta_{k1/2}$ are approximately related to the radii ρ_k by $\rho_k = 7\beta_{k1/2}$, where a half-width $\beta_{k1/2}$ of a director beam of width β_k is defined by

$$\beta_{k1/2} = \beta_k \operatorname{sech}^{-1}\left(1/\sqrt{2}\right). \tag{3.41}$$

Since the original shelf radii R_k were described by their areas modulo 2π, $\Lambda_k = R_k^2/2$, analogous relations will be used for the outer shelves

$$\tilde{\Lambda}_k = \frac{1}{2}\rho_k^2 = \left(7\beta_{k1/2}\right)^2. \tag{3.42}$$

As shown in Chapter 2, mass shed from the beams forms the major contribution of the radiation shed as the beams propagate. Therefore the mass conservation equations for the linearised equations (3.39) & (3.40) are required and are given by

$$i\frac{\partial}{\partial z}\left(r|k|^2\right) + \frac{1}{2} D_k \frac{\partial}{\partial r}\left(rk^* k_r - rkk_r^*\right) = 0. \tag{3.43}$$

The mass flux lost to dispersive radiation from the beams is found in this case by integrating the mass equation from the edge of the *outer* shelf $r = \rho_k$ to infinity

$$\frac{d}{dz}\int_{\rho_k}^{\infty} r|k|^2 dr = D_k \,\mathrm{Im}\left(rk^* k_r\right)|_{r=\rho_k} + \bigcirc[\rho_k(z)]. \tag{3.44}$$

In order to determine this mass loss, shed radiation must be matched to the shelves under the beams at the boundary between them. Following the steps carried out in Section 2.2.3 and being careful to include the diffraction coefficients D_k, the final result is that the mass conservation equation (3.25) and equation (3.28) for the radiation shelf height g_u, plus their symmetric equivalents in the v colour, gain a loss term

$$\begin{aligned}
\frac{d}{dz}\left(I_2 a_u^2 w_u^2 + \Lambda_u g_u^2\right) &= -2D_u\delta_u\tilde{\Lambda}_u\kappa_u^2, &(3.45)\\
I_1\frac{dg_u}{dz} &= \frac{1}{2}D_u I_{22} a_u w_u^{-2} - \frac{1}{2}A_u A^2 B^4 a_u w_u^2\left[\alpha_u\beta_u^2 Q_1^{-2}\right.\\
&\quad \left.+\alpha_v\beta_v^2 Q_2^{-2} e^{-2\gamma_1}\left(1-2\gamma_1\right)\right] - 2D_u\delta_u g_u. &(3.46)
\end{aligned}$$

For a single nematicon radiative losses were accounted for by including a loss term in the modulation equation for g (see Section 2.2.3), which coupled the rate of mass loss to the equation for the shelf height g. Here, both the mass conservation equation and the equation for g have been modified because two nematicons not only incur losses from their propagation but also losses via interactions with one another.

With the replacement of the original shelf radii Λ_k with the outer shelf radii $\tilde{\Lambda}_k$ in the loss calculation, the loss coefficient δ_u is found in an identical fashion to that described in Chapter 2 and is

$$\begin{aligned}
\delta_u &= -\frac{\sqrt{2\pi}I_1}{2e\kappa_u\tilde{\Lambda}_u}\int_0^z \pi\kappa_u(z')\ln((z-z')/\tilde{\Lambda}_u)\left[\left\{\left[\frac{1}{2}\ln((z-z')/\tilde{\Lambda}_u)\right]^2 + \frac{3\pi^2}{4}\right\}^2\right.\\
&\quad \left.+\pi^2\left[\ln((z-z')/\tilde{\Lambda}_u)\right]^2\right]^{-1}\frac{dz'}{(z-z')}. &(3.47)
\end{aligned}$$

Finally

$$\kappa_u^2 = \frac{1}{\tilde{\Lambda}_u}\left[I_2 a_u^2 w_u^2 - I_2\hat{a}_u^2\hat{w}_u^2 + \tilde{\Lambda}_u g_u^2\right], \tag{3.48}$$

gives the difference between the u colour beam mass at z and its mass at the fixed point.

Equations (3.26), (3.27), (3.29)–(3.32), (3.45) and (3.46), plus their symmetric equivalents for the v colour, form the full set of 12 modulation equations and four algebraic equations approximating the evolution of the two-colour nematicons.

3.2.3 Adjustments to Numerical Methods

The numerical scheme used to solve the modulation equations varies little from that given in Section 2.2.4 for a single nematicon in the local regime. Modulation equations (3.26), (3.27), (3.29), (3.30), (3.45) & (3.46) plus their symmetric equivalents for the v colour beam are solved using the fourth order Runge-Kutta method. The parameters α_k and β_k are found by rearranging appropriately, then solving exactly, equations (3.31) & (3.32) and their v colour counterparts. The shelf radii Λ_k are calculated using equation (3.38) at each z step.

Whereas the modulation equations for the single nematicon included the energy conservation equation, here the mass equation is retained with a loss term representing radiation shed by the beams, equation (3.45).

The full two-colour nematicon equations (3.1) and (3.2) were solved using a pseudo-spectral method similar to that of Fornberg and Whitham [42]. The director equation (3.3) was solved as a boundary value problem using a Fourier method. These methods are described in more detail in Section 2.3 where they are applied to a single nematicon problem, and few changes need to be made here. The additional field equation for the v colour beam is solved in an

identical manner to the u beam simultaneously, where θ at the previous z step has been used in their calculation. u and v are then used to calculate θ at the current step.

Although no results have been presented for Gaussian trial functions, the modulation equations and the numerically solved full governing equations with Gaussian trial functions were solved for comparison to the sech trial functions. The modulation equations are identical to those of the hyperbolic secant trial function except that the I_i, I_{ij} integrals have different values (see Section 4.2.1 in Chapter 4). Consequently these modulation equations are solved in an identical manner to that described above. The full governing equations with Gaussian trial functions were solved numerically using the same scheme as for the sech trial functions, only requiring a change of the initial beam profile.

3.3 Results

In this section numerical solutions of the full two-colour nematicon equations (3.1)–(3.3) will be compared with solutions of the modulation equations. The full governing equations were numerically solved using step sizes $\Delta x = \Delta y = 0.4$ and $\Delta z = 0.005$, with spatial intervals 102.4 in the x and y directions respectively. Comparisons were taken for different step sizes and it was found that smaller step sizes did not increase the accuracy to any great extent, especially to graphical accuracy. This combination was the most efficient, with excellent accuracy and reasonable speed. The ample computational domain, combined with damping boundaries, discussed in Chapter 2, ensured that waves reflected at the boundaries had an insignificant impact on the beams. The modulation equations were solved with an equal z stepping of $\Delta z = 0.005$.

Equations (3.6)–(3.8) are approximations to the nematicon equations (3.1)–(3.3) where it has been assumed that θ, the optical director angle perturbation, is small enough that the first terms of the Taylor series of $\sin 2\theta$ and $\cos 2\theta$ may be taken. This assumption is, however, only valid in highly nonlocal media for which $\nu > 100$ for nondimensional optical powers of $O(1)$, since the angle θ decreases as the degree of nonlocality ν increases [23]. Minzoni *et al* found that the θ small limit could be achieved at $\nu = 10$ for a single nematicon [39]. $\nu \approx 10$ is not valid in this case as the optical beams induce a larger combined reorientation of the director angle from equation (3.3). Many experiments have been conducted in nematic media with nonlocality $\nu \approx 200$. As a result, $\nu = 500$ has been taken which is a value at the upper end of the experimental range [18, 27], and is large enough that the small θ approximation is valid.

Gaussian trial functions require much higher values of ν than hyperbolic secant trial functions for θ to be sufficiently small that the approximate equations (3.6)–(3.8) are valid. It was found that Gaussian trial functions required $\nu > 2000$, which is well outside the experimental range. Hence no results for Gaussian trial functions will be reported here. Above $\nu = 2000$ the solutions were very similar to those for the hyperbolic secant ansatz. This is in accord with the Snyder & Mitchell asymptotic solution which shows that a Gaussian becomes a better approximation to the nematicon profile as ν increases [52]. Here the Snyder & Mitchell model is invalid since their assumption is that soliton width and separation are negligible in comparison to the spatial extent of the director beam [52]. This is the situation only in extreme cases of highly nonlocal media where $\nu \to \infty$.

Diffraction and coupling coefficients for the two beams were taken that had similar relations as experimental values. For example, for red and NIR beams the diffraction coefficients had the relation $D_{red} \approx 0.98 \times D_{NIR}$. It then follows that the nondimensionalised diffraction coefficients of the present work should be given the values $D_u = 1$, $D_v = 0.98$. Similarly $A_u = 1$ and $A_v = 0.95$ were chosen as coupling coefficients for the u and v beams respectively. In the following analysis numerical solutions of the full governing equations [(3.1)–(3.3)] are referred to as 'full numerical solutions' and numerical solutions of the modulation equations [(3.26), (3.27), (3.29), (3.30), (3.45) & (3.46) and the equivalent equations for the v colour beam] are termed 'modulation solutions.'

Figure 3.4 shows a comparison between the full numerical and modulation solutions for boundary values for which the beams evolved into a bound vector nematicon. It can be seen from Figure 3.4(a) that the position comparison is good. The mean momentum walk-off as given by the modulation and full numerical solutions is in near perfect agreement, and there is little

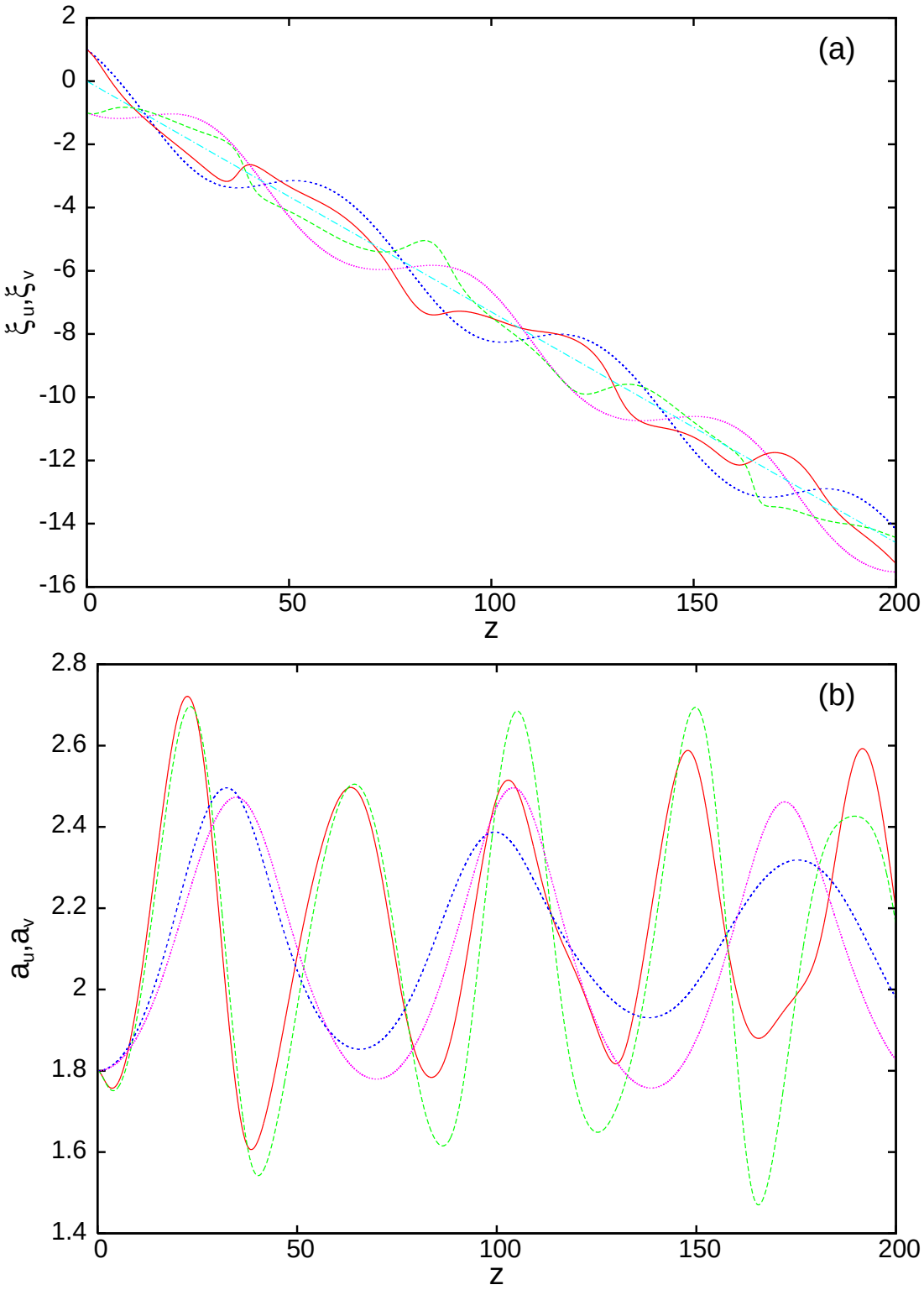

Figure 3.4: Comparisons for the initial values $a_u = a_v = 1.8$, $w_u = w_v = 3.0$, $\xi_u = 1.0$, $\xi_v = -1.0$, $V_{u0} = -0.1$, $V_{v0} = -0.05$ with $\nu = 500$, $q = 2$, $A_u = 1.0$, $A_v = 0.95$, $D_u = 1.0$, $D_v = 0.98$. Full numerical solution for the u colour (——)[red] and v colour (—— ——)[green] beams; solution of modulation equations for the u colour (– – –)[blue] and v colour (- - -)[violet] beams; momentum conservation result (3.36) (– · – · – ·) [turquoise]. (a) Positions, (b) Amplitudes.

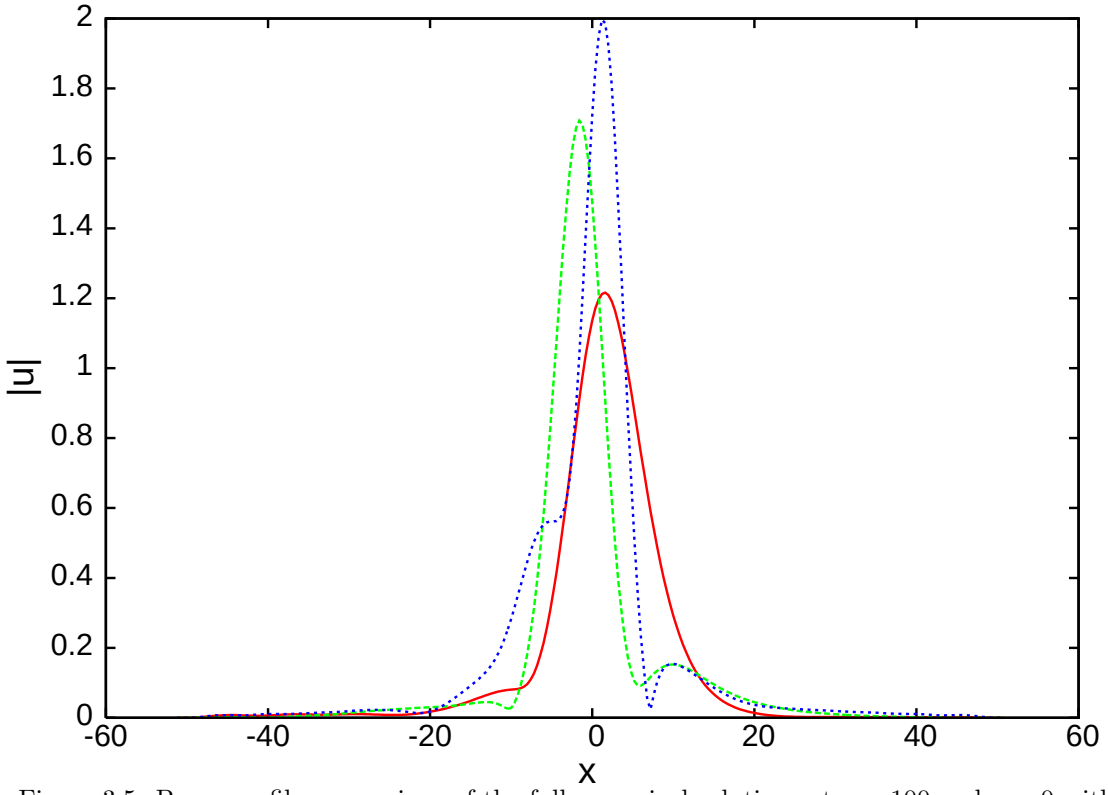

Figure 3.5: Beam profile comparison of the full numerical solutions at $z = 100$ and $y = 0$ with the initial values $a_u = a_v = 1.2$, $w_u = w_v = 4.0$, $\xi_u = 1.0$, $\xi_v = -1.0$, $V_u = 0.1$ with $q = 2$, $A_u = 1.0$, $A_v = 0.95$, $D_u = 1.0$, $D_v = 0.98$. Solution for $\nu = 1000$ (—)[red], solution for $\nu = 500$ (— — —)[green], solution for $\nu = 250$ (– – –)[blue].

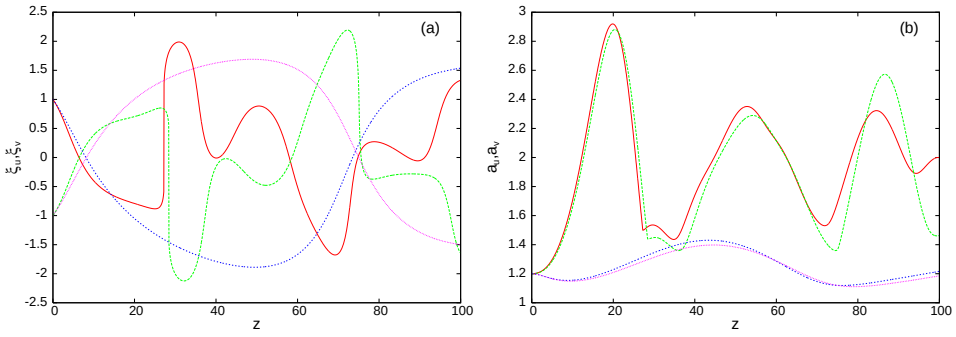

Figure 3.6: Comparisons for the initial values $a_u = a_v = 1.2$, $w_u = w_v = 4.0$, $\xi_u = 1.0$, $\xi_v = -1.0$, $V_{u0} = -0.1$, $V_{v0} = 0.1$ with $q = 2$, $A_u = 1.0$, $A_v = 0.95$, $D_u = 1.0$, $D_v = 0.98$. Full numerical solution for the u colour (—)[red] and v colour (— — —)[green] beams at $\nu = 250$; for the u colour (– – –)[blue] and v colour (- - -)[violet] beams at $\nu = 1000$. (a) Positions, (b) Amplitudes.

difference between the modulation solutions' mean momentum walk-off and that calculated from the momentum conservation equation (3.36). The maxima, minima and period of the position oscillations are also in very good agreement. In the local regime, as the beams approach a collision they experience a sudden acceleration accompanied by radiative losses, which result in a rapid reduction of peak position oscillations, as will be seen in Chapter 4. Nonlocal nematicon collisions do not involve such rapid accelerations because the beams interact at both distance, due to the nonlocality of the nematic, and upon collision. Consequently all interactions are relatively smooth in the nonlocal regime. However, this does not stop anharmonicity of the position oscillations for the full numerical solutions. As the beams experience a continual non-symmetric interaction the position of the beam peaks are perturbed by competing effects such as acceleration, attraction and distortion resulting in highly anharmonic position oscillations. The modulation solutions represent two beams of a fixed general shape that undergo perturbations of their parameters, which rules out the possibility of distorting the beams from their basic profiles and consequently the position oscillations are smooth. These differences between the modulation and full numerical solutions, however, do not effect the agreement in period, peak oscillations nor momentum walk-off.

In contrast to the position comparison, the amplitude comparison shown in Figure 3.4(b) is not as good. The modulation and full numerical solutions agree in the mean with the mean amplitude being the final steady state amplitude of the nematicon(s), but the damping of the oscillations of the modulation solution is larger than that of the full numerical solution. Mass and momentum losses are largely influenced by the acceleration of the beams. As acceleration does not play such a large part in beam evolution and interaction in the nonlocal regime, the inclusion of two radiative loss terms in the modulation equations slightly overestimates the effect that losses have. It is also clear from Figure 3.4 when comparing the modulation and full numerical solutions that, whilst position oscillations largely agree in period, amplitude oscillations do not. The modulation equations form a nonlinear oscillator. Accordingly the amplitude and period are linked, meaning that the lower amplitude of the modulation solutions results in the amplitude oscillation period being longer than the full numerical period [39]. This lower amplitude is caused by the overestimation of shed radiation.

Figure 3.5 shows the full numerical u colour solution profile at $z = 100$ and $y = 0$ for $\nu = 250$, $\nu = 500$ and $\nu = 1000$. As ν increases the deviation of the director angle θ decreases. Królikowski *et al* found that in similar media an increase in nonlocality ν for fixed amplitude causes the width of the resultant beam to increase [53], *"nonlocality smooths out the refractive index profile thereby leading to a broadening of the beam."* Here, as nonlocality increases a width increase is clearly seen, as is a marked decrease in the final amplitude as noted by Nikolov *et al* [54]. The effect of acceleration is shown by the asymmetry of the radiation shelves near the tails of the beams. It can be seen that symmetry increases as nonlocality grows, as discussed above. There is also a noticeable reduction in the peaks of the radiation shelves as ν increases. This figure confirms the conclusion that beam acceleration and radiative losses from the beams decrease as ν increases, the latter in agreement with experimental observations [24]. While the modulation solutions' positions reveal a harmonic oscillation over the full range of ν, the full numerical positions exhibit more complicated behaviour. As the degree of nonlocality is increased, from $\nu \sim 100$ to $\nu \sim 1000$, harmonicity of the full numerical position oscillation increases. Nematicons in the latter case experience a strong continual interaction with each other, but the profile shape change is much reduced. One reason for anharmonicity of the beam position oscillations is that beam distortions become amplified as accelerative and radiative effects take on a more significant role. These effects are more prevalent at lower values of ν. To highlight this further, a comparison of two full numerical solutions for different values of ν is shown in Figure 3.6. Clearly the evolution of position and amplitude is smooth and harmonic for the highly nonlocal regime ($\nu = 1000$), but warped and irregular for $\nu = 250$. Part of the reason for these large irregular changes in the latter case is that the initial conditions are quite far from stable vector nematicons and the beams are close to instability. Consequently the beam amplitudes grow until nonlocality eventually halts their progress and reverses the increase.

In the local limit the nematicons oscillate about each other for large z, with these oscillations gradually decreasing in amplitude until the two nematicons eventually have the same position [22]. In Figures 3.4(a) & 3.6(a) the decay of the position oscillations is much less obvious,

and it is not clear whether the beams eventually merge or continue oscillating as $z \to \infty$. Beam interactions for nonlocal nematicons are attractive. However in the local case these interactions can be repulsive if the two beams are out of phase [11, 43]. Similarly dipole nematicons, symmetric bound vector solitons in nonlocal NLC, have been shown to have stable positional oscillations when they are $\pi/2$ out of phase due to a balance between the soliton phase repulsion and the nonlocal nematic attraction [43, 55]. It was shown that for small initial separations, as here, beams of the same wavelength rapidly merged, regardless of their phase difference [43]. Two-colour nematicons with angular momentum have been investigated and found to form a bound state in which they spin around each other without merging [21, 24, 56]. Whilst this situation seems qualitatively similar to the case in the present work, the mechanism that stabilises spinning nematicons is a balance between an attractive potential and the centrifugal force, similar to the two-body problem of classical mechanics [24, 43]. The most likely explanation then of the apparently stable positional oscillations, or orbits, that the two nematicons form in the present work comes from the relationship that radiative losses have with nonlocality. As has been shown in numerous works [22, 30, 35, 39, 43, 57, 58], beams evolve to their steady state via decaying positional oscillations brought about by radiative losses. However, beams leak little radiation in the nonlocal regime. Single nematicons in the nonlocal regime were investigated by Minzoni *et al* and it was found that beam oscillations reduced over large z but the initial beams settle to steady nematicons over huge z values ($\gg 400$) [39]. The nonlocality parameter is $50\times$ larger in the present work than that investigated by Minzoni *et al* and consequently individual initial beams shed even less radiation. As a result, it is reasonable to conclude that two-colour beam initial conditions settle to steady two-colour bound vector nematicons over z distances that are too large for practical numerical simulations. Whilst the orbits appear stable it is the author's opinion that they are actually very slowly decaying to the fixed point at which the two beams finally merge.

The reduction of radiative losses with increased nonlocality can be explained as follows. The waveguides formed by the beams are much wider than the beams themselves in the nonlocal regime. Shed radiation then starts at the tails of the director beams rather than from the tails of the electric field beams. Consequently this shed radiation has lower amplitude than it would have if it were generated at the edges of the shelves. Since shelf height determines the rate at which radiative losses are shed [31], a reduction in the height of the shelves causes a reduction in the amount of radiation shed by the beams as they evolve. One particularly noticeable effect of reduced radiative losses is that the nonlocal momentum walk-off is well approximated by the conservation result (3.36), in contrast to the local case [22].

Due to the lack of strong damping of positional oscillations and the fact that full numerical solutions appear anharmonic, the mean momentum walk-off is found by taking a large final z and plotting the collision points of the u and v colour beams. Linear regression is then applied to obtain a value for the mean momentum walk-off of the two-colour vector nematicon. Figure 3.7 compares the mean momentum walk-off $\hat{\xi}'$ for the two beams as a function of the initial velocity of the v colour beam, V_{v0}, as given by the full numerical solution, the modulation solution and the momentum conservation result, which can be obtained from equation (3.36). As will be shown for the local case in Chapter 4, the agreement for momentum walk-off between the full numerical and modulation solutions is excellent. However in the nonlocal limit the momentum conservation result (3.36) is in much better agreement than in the local case, in fact the agreement is near perfect. This result is to be expected from the analysis of Figures 3.6(a) & (b).

Finally, beam profiles taken of full numerical u colour nematicon solutions at $z = 6$ and $z = 100$ are compared to fitted sech profiles in Figure 3.8. Early in the evolution, Figure 3.8(a), the beam generally conforms to a hyperbolic secant profile, but later in the evolution, Figure 3.8(b), the beam distorts. It is clear that profile distortions and accelerations continue for large z, although these distortions are not large in comparison to those in the local case. However, beam profile distortions do explain anharmonic position oscillations observed in Figures 3.4(a) & 3.6(a) which are not modelled by the modulation equations, as discussed earlier. As a consequence of large distortions in the beam position oscillations, amplitude oscillations also become distorted. This effect is most easily observed in Figure 3.6(b).

It is remarkable then that modulation equations, derived from simplified governing equations, neglecting beam accelerations with a beam profile that cannot account for large shape

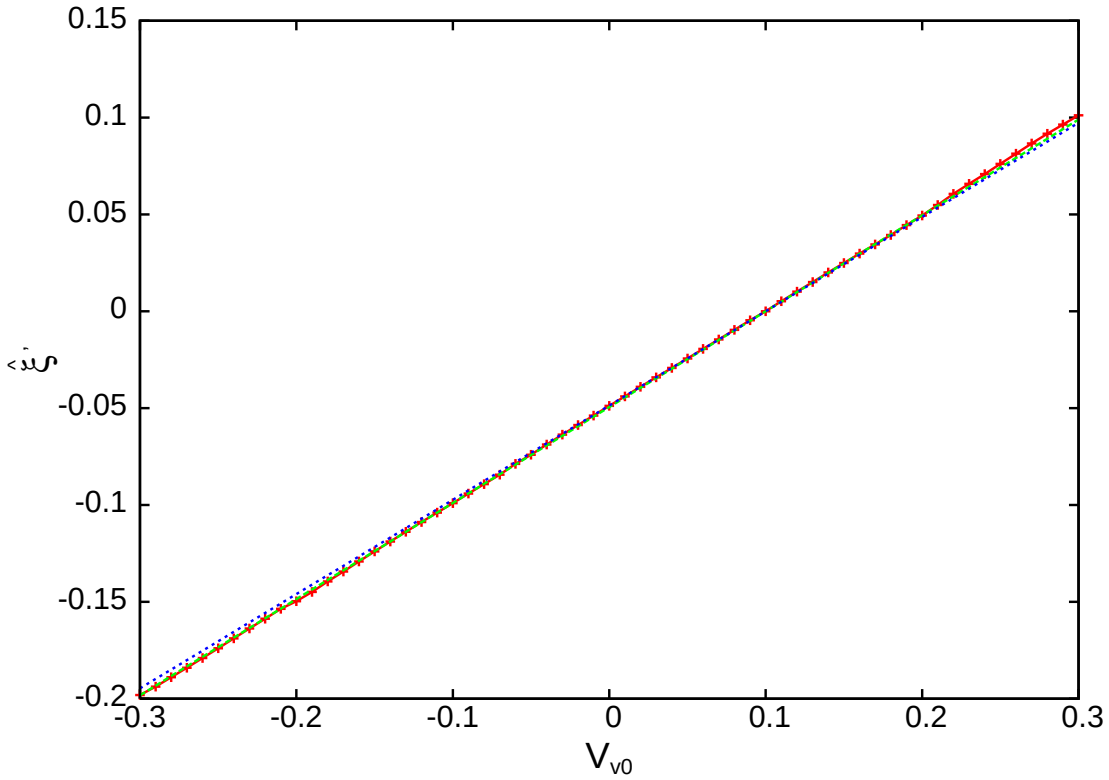

Figure 3.7: Steady value $\hat{\xi}'$ as a function of V_{v0} for the initial values $a_u = a_v = 1.8$, $w_u = w_v = 3.0$, $\xi_u = 1.0$, $\xi_v = -1.0$, $V_{u0} = 0.1$ with $\nu = 500$, $q = 2$, $A_u = 1.0$, $A_v = 0.95$, $D_u = 1.0$, $D_v = 0.98$. Full numerical solution (— + —)[red], solution of modulation equations (— — —)[green], momentum conservation result (– – –)[blue].

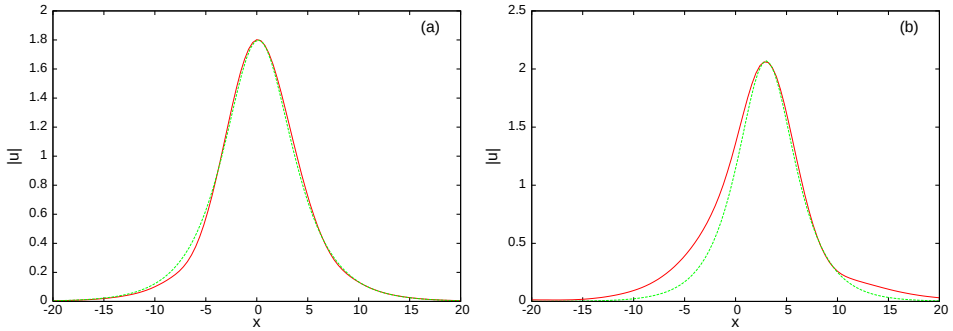

Figure 3.8: Comparisons for the initial values $a_u = a_v = 1.8$, $w_u = w_v = 3.0$, $\xi_u = 1.0$, $\xi_v = -1.0$, $V_{u0} = V_{v0} = 0.1$ with $\nu = 500$, $q = 2$, $A_u = 1.0$, $A_v = 0.95$, $D_u = 1.0$, $D_v = 0.98$. Full numerical solution of the u colour beam profile (—)[red]; fitted sech profile (— — —)[green] taken at (a) $z = 6$ and (b) $z = 100$.

changes, agree so well with numerical solutions of the full governing equations. Momentum loss due to acceleration cannot easily be incorporated into the present approximate method, since this would require the solution of a moving boundary value problem for which the boundary is unknown [32]. However, in the nonlocal limit qualitative and quantitative beam behaviour is clearly well approximated by the variational method employed, validating this approach for studying the evolution and interaction phenomena of two-colour nematicons in the nonlocal limit.

3.4 Discussion

The evolution and interaction of two-colour nematicons has been considered in the nonlocal regime for cases in which the two nematicon beams form a vector nematicon. A numerical method has been used to solve the nematicon governing equations exactly and these solutions have been used as a comparison to solutions of approximate modulation equations derived from simplified governing equations. The modulation equations were modified to include radiative losses caused by the beams evolution and interaction. Excellent agreement was found between full numerical solutions and solutions of the modulation equations for a variety of different properties. Agreement between position oscillation amplitude and period was remarkably good, and momentum walk-off was in near perfect agreement. Furthermore, the mean of the amplitude oscillations, representing the steady state amplitude of the final nematicon, was in very good agreement, although amplitude oscillation period and the maxima and minima of these oscillations was not in agreement due to an overestimation of radiative losses.

It was found that radiative losses and beam acceleration during collision decreased as the nonlocality of the nematic increased, in accord with experimental observations. Consequently, in the highly nonlocal regime investigated ($\nu = 500$), radiative losses had a small impact on beam propagation. However it is thought that this same shed radiation is the essential mechanism behind the eventual decay of the position oscillations of the two beams and their eventual merging.

Quite apart from the fact that the variational method is an intrinsically approximate method in itself that imposes a fixed shape on the beam profile and cannot account for beam acceleration effects, there have been several additional approximations made in the calculation of the modulation equations. Firstly, the original governing equations were simplified so that a relatively simple equivalent Lagrangian could be derived, then the resulting averaged Lagrangian required an equivalent Gaussian approximation of the trial function for certain integrals to be calculated. The inner shelves Λ_k under the beams were approximated by radiation shelves taken from the symmetric limit; these symmetric shelves being calculated via linearisation about the nematicons fixed points with the requirement that the frequencies of the shelves matched the respective fixed point nematicon frequencies. Finally the outer shelves $\tilde{\Lambda}_k$ were estimated from a particular numerical solution of a single nematicon beam [39]. What is surprising then is that, despite all of these assumptions and approximations, the solutions of the modulation equations are in excellent agreement with exact numerical solutions of the full governing equations.

A direct comparison with experimental two-colour vector nematicon results would have been useful to not only gauge the accuracy of the solutions of the approximate modulation equations but also to see how well the full nematicon governing equations model experiments. Yet several difficulties arise in attempting such a comparison. Firstly, to the authors knowledge, these two-colour nematicons have only been produced once experimentally in Ref. [17]. In this work, a pre-tilt of $\pi/6$ was induced via rubbing. Incorporating this pre-tilt via rubbing requires the incorporation of the boundary conditions at the cell walls because the optic axis response does not have a pulse shape, but extends to the cell walls in this case [48]. This greatly increases the complexity of the mathematical analysis. Secondly, the distances that nematicons have been observed to propagate are roughly $20\times$ their Rayleigh lengths [17]. Not long after this point experimental errors creep into the results due to scattering losses. Since the nematicon equations have been nondimensionalised by the Rayleigh lengths, and scattering losses have been shown to have a more prominent effect at larger z values, any comparison over large distances would be meaningless as scattering losses have not been incorporated into the mathematical analysis. Additionally, if the opposite approach were taken, and instead

experimental factors were incorporated into the theoretical model, the resulting variational equations would be rendered intractable. However, a pre-tilt of $\hat{\theta} \approx \pi/4$, achieved via an externally applied electric field, has been used in the formation of nematicons before [9, 12, 19, 59] and could theoretically be used for the formation of two-colour nematicons, as has been shown here.

One final note may be made on the initial conditions that were chosen for comparison. For all of the numerical solutions presented in this chapter and the following chapter, initial electric field amplitudes a_k and widths w_k and the shelf amplitudes g_k were chosen that were identical for the u and v colour beams. Symmetric values for the nematicon positions $\xi_u = -\xi_v$ were also taken. Clearly $g_u = g_v = 0$ initially and the symmetry of initial positions was just chosen for convenience, but there is no fundamental reason for choosing symmetric a_k and w_k. Numerical solutions with unequal initial conditions for these parameters were explored and it was found that the initial beams evolved to two-colour nematicons when the parameter values for the u and v beams were close to one another. When there were large differences between these initial values the beams could not form the vector nematicon fixed point and, after an initial collision, propagated as two separate single nematicons. For small differences between the initial amplitudes (or widths) it was found that these inequalities can affect beam evolution, interaction and momentum walk-off which could have lead to misinterpretation of the observed behaviour. Consequently equal amplitudes (and widths) were taken for the two beams so that a clear understanding of the effect that two nematicons of different wavelengths have on one another could be gained.

The next chapter completes the analysis of two-colour nematicons by considering the local nonlinear response regime.

Chapter 4

Two-Colour Nematicons in the Local Limit

4.1 Background

Essentially the equations governing two-colour nematicon propagation and interactions in the local and nonlocal regimes are identical, the value of the nonlocality parameter ν being the only obvious change. Yet this change is important and fundamental. By taking ν small, the interaction of the beams with the nematic is ruled by a completely different mechanism. The nematic medium responds only in the vicinity of the beams and consequently only affects them locally, resulting in an increase in radiation shed as they evolve. The interactions between the beams themselves are also far more local so that the influence that one beam has on the other is only significant when they are in close proximity. However, Chapter 3 and the work of Conti *et al* [27] have shown that nematicon propagation is stabilised by the *nonlocal* nature of the interaction of the beam with the nematic medium. It is of interest then to see if stable two-colour nematicon evolution can be achieved in the *local* regime and, if so, what the nature of this stability is and what differences can be observed between the dynamics of nematicons in the local and nonlocal regimes.

$(2+1)$-D soliton solutions of the nonlinear Schrödinger (NLS) equation, and consequently the coupled nonlinear Schrödinger (CNLS) equation, are unstable with eventual total collapse or infinite self-focusing, depending on an initial amplitude threshold, a certainty [5, 35]. The main reason for instability is that these solitons in $(2+1)$-D have more dimensions of freedom than needed for stable propagation, which leads to a greater likelihood that perturbations will lead to instabilities [11, 25]. However, by introducing an upper limit to the nonlinearity, the conventional NLS and CNLS equations with a modified nonlinear term admit stable soliton solutions, the resulting modified nonlinearity being termed a saturating nonlinearity. Saturation of the nonlinear response prevents the unlimited self-focusing or collapse seen in the standard $(2+1)$-D NLS equation. What is found in the case of a local nonlinear response of a nematic liquid crystal (NLC) is that nematicons are stabilised by this same saturation of the local nonlinearity.

Locality in a purely mathematical sense refers to a nonlinear refractive index change that is dependent on the intensity of the optical beam at that exact spatial point [60]. An example is the cubic Kerr response. However, in many physical situations there is some nonlocality in the medium response and some interaction between the medium and the beam in the close vicinity of the point under scrutiny. Experimentalists have defined locality more loosely. An effective local response is then one in which the refractive index change caused by the beams presence does not leak into the surrounding space over a significant fraction of the wavelength of the beam [60]. There are a number of different ways to achieve such a local nonlinear response in a NLC. Cooling the medium can reduce nonlocality. This has the effect of strengthening the bonds between nematic molecules, making it more difficult for molecular reorientation to occur. The stronger molecular bonding results in an upper limit on molecular reorientation and

therefore an upper limit on the nonlinear response. Another method is to introduce a pre-tilt of the nematic molecules by applying a static/low-frequency electric field to the bulk medium. In Chapter 3 for the nonlocal regime a pre-tilt was introduced which was close to $\pi/4$. This pre-tilt produces the optimum nonlocal response. However, a stronger static/low-frequency field can pre-tilt the molecules to such a degree that they almost align along the x axis, i.e. a pre-tilt close to $\pi/2$. An optical beam will increase the reorientation of the nematic molecules but the molecules have already been pre-tilted close to their maximum angle $\pi/2$. A stronger optical beam then cannot reorientate the nematic molecules any further and saturation once again prevents unlimited self-focusing.

Spatial optical solitons have been observed in many other media where a saturation of the perturbation to the refractive index of the medium is responsible for a local nonlinear response. However, many of these materials only admit solitons at very high beam intensities. In some instances the high intensities involved have lead experimentalists to pulse the beam to avoid material degradation [60]. Some examples of such local response media where solitons have been investigated include fused silica and similar related glasses, metal vapours such as Rubidium and crystals exhibiting a quadratic nonlinear response [60]. The most promising materials reported are the photorefractive crystals, such as Lithium Niobate and Barium Titanate. The propagation of a soliton in such materials can be modelled by a saturable NLS equation similar to the equation governing soliton propagation in a NLC [35]. There are two types of solitons that can be formed in photorefractives, namely screening solitons and photovoltaic solitons where an optically induced space-charge electric field and an externally applied static/low-frequency electric field are the means of achieving local nonlinear refractive index changes respectively. The fundamental difference between these photorefractive solitons and nematicons is that the waveguide formed by a photorefractive soliton will persist after the beam itself has been removed, whereas the waveguides formed in NLCs are transient [5]. Additionally the mechanism perturbing the refractive index is different.

Whilst there have been no experimental observations of two-colour nematicons in the local regime to the authors knowledge, the fact that theoretical and experimental investigations have proven the existence and stability of nonlocal two-colour nematicons, combined with the knowledge that a local response can be induced in a NLC, from which experimental observations of single nematicons have already been taken, suggests local two-colour nematicons could be produced. The main motivations then of investigating local two-colour nematicon dynamics are to determine the stability of these wave structures and to compare them to their nonlocal counterparts.

To this end, let us consider two copolarised, coherent light beams of two different wavelengths (colours) propagating through a cell filled with a NLC, as illustrated in Figure 4.1, and qualitatively identical to the model described in Chapter 3. The light initially propagates in the z direction, with the (x, y)-plane orthogonal to this. A static/low-frequency electric field is applied in the x direction so that in the absence of light the optical director is pre-tilted at an angle $\hat{\theta}$ to the z direction. Both input light beams are polarised with their electric fields in the x direction. Then let u and v be the electric field envelopes of the two light beams and θ be the perturbation of the optical director angle from its static value due to the light beams. The nematicon governing equations were derived in Chapter 3 from a combination of the two-colour equations found by Alberucci *et al* for two-colour nematicons with no external static/low-frequency electric pre-tilt field [17] and the director equation representing nonlinear refractive index perturbations in the presence of a pre-tilt field [18, 19]. These equations were derived and nondimensionalised in Chapter 3 and are presented again here

$$i\frac{\partial u}{\partial z} + \frac{1}{2}D_u\nabla^2 u + A_u u \sin 2\theta = 0, \tag{4.1}$$

$$i\frac{\partial v}{\partial z} + \frac{1}{2}D_v\nabla^2 v + A_v v \sin 2\theta = 0, \tag{4.2}$$

$$\nu\nabla^2\theta - q\sin 2\theta = -2\cos 2\theta\left(A_u|u|^2 + A_v|v|^2\right). \tag{4.3}$$

The Laplacian ∇^2 is taken with respect to the transverse coordinates, x and y. The coefficients D_u and D_v are the diffraction coefficients for the two colours and A_u and A_v are the coupling coefficients between the light and the nematic for the two colours. The parameter ν measures

the elasticity of the nematic and q is related to the energy of the static/low-frequency electric field which pre-tilts the nematic and is proportional to the square of the pre-tilt field.

4.2 Analysis

4.2.1 Modulation Equations

The usual operating regime for beam propagation in nematics has ν large, the so-called nonlocal regime, which was fully investigated in Chapter 3. However, by varying the operating temperature and/or the strength of the pre-tilt field (q), ν can be made to take a range of values from small (the local regime) to large (the nonlocal regime). A pre-tilt of $\pi/2$ represents the local regime and pre-tilts close to this, as high as $\hat{\theta} = 0.45\pi$, have been utilised to produce local stable nematicons and symmetric vector nematicons [12, 59]. In the present work, two-colour nematicon evolution will be considered in the local regime with ν small. In the limit of small ν the Laplacian term on the left hand side of the director equation (4.3) can be neglected. Rearrangement then leads to

$$\tan 2\theta = \frac{2}{q}\left(A_u|u|^2 + A_v|v|^2\right). \tag{4.4}$$

Utilising equation (4.4) for the director angle, the electric field equations (4.1) and (4.2) become the coupled system of saturating nonlinear Schrödinger equations

$$\begin{aligned} i\frac{\partial u}{\partial z} + \frac{1}{2}D_u\nabla^2 u + \frac{2A_u\left(A_u|u|^2 + A_v|v|^2\right)u}{\sqrt{q^2 + 4\left(A_u|u|^2 + A_v|v|^2\right)^2}} &= 0, \\ i\frac{\partial v}{\partial z} + \frac{1}{2}D_v\nabla^2 v + \frac{2A_v\left(A_u|u|^2 + A_v|v|^2\right)v}{\sqrt{q^2 + 4\left(A_u|u|^2 + A_v|v|^2\right)^2}} &= 0. \end{aligned} \tag{4.5}$$

The final terms in (4.5) are saturating nonlinearities. This expression shows that in the local regime the propagation of two-colour nematicons is closely approximated by a system of vector saturating nonlinear Schrödinger equations and that this saturation of the nonlinear response is responsible for the stability of nematicons.

The vector system (4.5) has the Lagrangian

$$\begin{aligned} L &= i(u^*u_z - uu_z^*) - D_u|\nabla u|^2 + i(v^*v_z - vv_z^*) \\ &\quad - D_v|\nabla v|^2 + \sqrt{q^2 + 4\left(A_u|u|^2 + A_v|v|^2\right)^2} - q, \end{aligned} \tag{4.6}$$

where the superscript * denotes the complex conjugate. Approximate solutions will now be sought by inserting appropriate trial functions in the averaged Lagrangian

$$\mathcal{L} = \int_{-\infty}^{\infty}\int_{-\infty}^{\infty} L\, dxdy. \tag{4.7}$$

The first trial functions to be used in the present chapter are identical to those of Chapter 3 and have been used in various different guises in other variational approximations for nematicon evolution [24, 30, 35, 39, 43, 57]. These trial functions for the electric field envelopes u and v are

$$\begin{aligned} u &= a_u \operatorname{sech}\frac{\chi_u}{w_u}\, e^{i\psi_u} + ig_u e^{i\psi_u}, \\ v &= a_v \operatorname{sech}\frac{\chi_v}{w_v}\, e^{i\psi_v} + ig_v e^{i\psi_v}, \end{aligned} \tag{4.8}$$

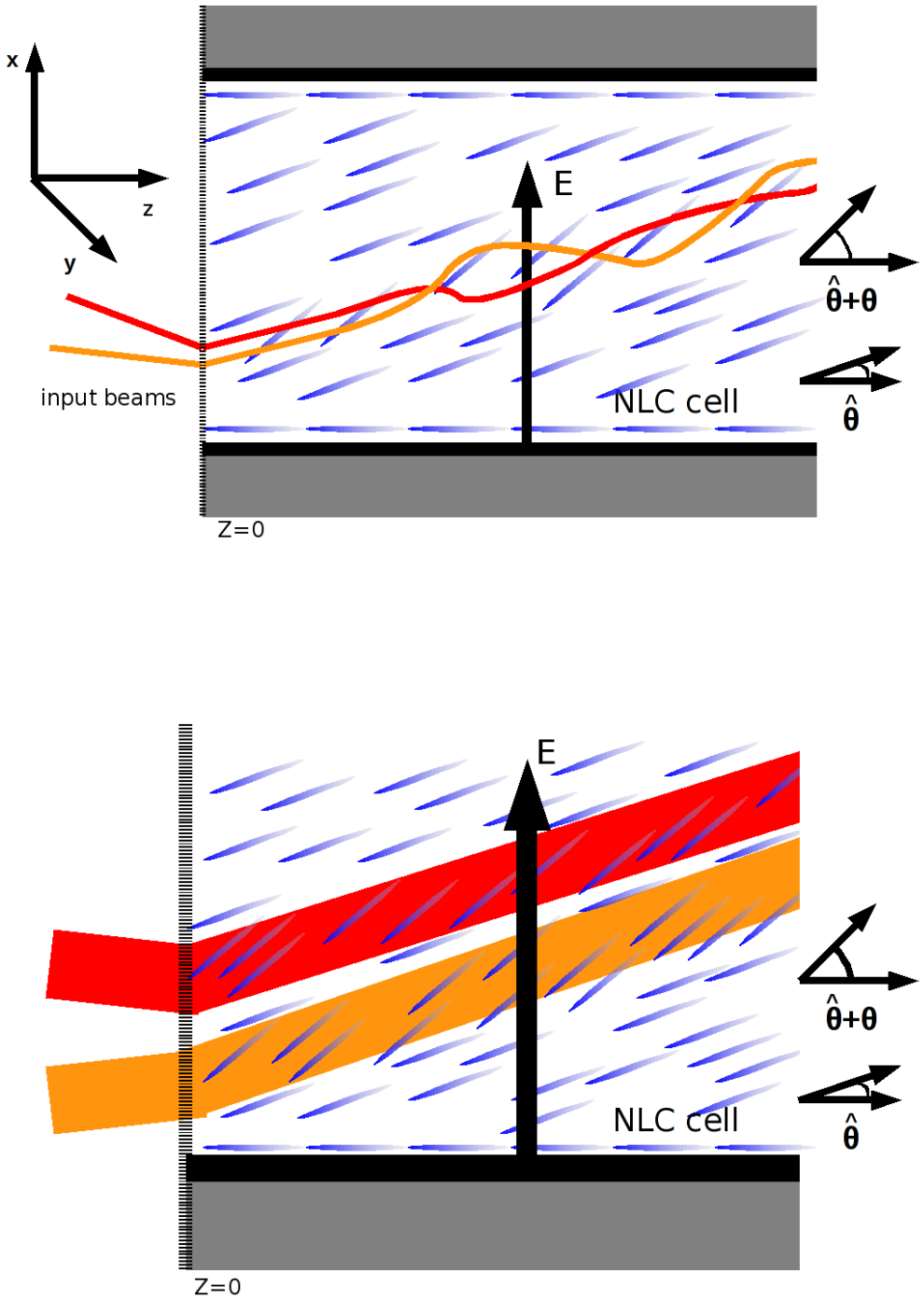

Figure 4.1: Schematic diagrams of a liquid crystal cell with two x-polarised light beams of different colours interacting. (a) the entire cell, (b) focus on the locality of the interaction between the beams and nematic molecules.

where

$$\chi_u = \sqrt{(x-\xi_u)^2 + y^2}, \qquad \chi_v = \sqrt{(x-\xi_v)^2 + y^2},$$
$$\psi_u = \sigma_u + V_u\,(x-\xi_u)\,, \qquad \psi_v = \sigma_v + V_v\,(x-\xi_v)\,. \tag{4.9}$$

The electric field amplitudes a_u, a_v, widths w_u, w_v, nematicon positions ξ_u, ξ_v, velocities V_u, V_v, phases σ_u, σ_v and shelf heights g_u, g_v are functions of z. The first terms in the trial functions (4.8) are varying solitary waves. The second terms represent the effect of the flat shelves of shed diffractive radiation which form under, and travel with, the evolving nematicons. It must be assumed that g_u (g_v) is non-zero in a disc $0 \le \sqrt{(x-\xi_u)^2+y^2} \le R_u$ ($0 \le \sqrt{(x-\xi_v)^2+y^2} \le R_v$) because if the flat shelves extended beyond the beam infinitely they would have infinite mass. In the case of the $(1+1)$-D NLS equation this shelf of low wavenumber radiation under the pulse, or in this case beam, can be justified using inverse scattering, which is also the justification for setting the shelf to be $\pi/2$ out of phase with the beam [31]. Whilst there are no inverse scattering solutions to prove the existence of a shelf for the current equations, the existence of a shelf travelling with $(2+1)$-D nematicons has been shown by numerical solutions of single nematicon equations [30, 35, 39] and was demonstrated in Chapter 3 for nonlocal two-colour nematicons.

The trial functions (4.8) are now substituted into the averaged Lagrangian (4.7), from which variational equations are obtained for the nematicon parameters. However, the integrals involving the nonlinear term in the Lagrangian (4.6) cannot be evaluated in closed form. To overcome this it is assumed, as in García-Reimbert *et al* [35], that the amplitudes of the two nematicons are small (or that q is large), so that the square root can be expanded in a Taylor series. The Lagrangian is then

$$\begin{aligned} L &= i(u^*u_z - uu_z^*) - D_u|\nabla u|^2 + i(v^*v_z - vv_z^*) - D_v|\nabla v|^2 \\ &\quad + \frac{2}{q}\left(A_u|u|^2 + A_v|v|^2\right)^2 - \frac{2}{q^3}\left(A_u|u|^2 + A_v|v|^2\right)^4, \end{aligned} \tag{4.10}$$

Whilst this then allows most of the integrals to be evaluated, four integrals involving products of u and v still cannot be evaluated. These cross integrals are of the form

$$\int_{-\infty}^{\infty}\int_{-\infty}^{\infty} |u|^s|v|^t\,dxdy, \tag{4.11}$$

where the powers (s,t) are $(2,2)$, $(2,6)$, $(4,4)$ and $(6,2)$. To evaluate the integrals (4.11) the idea of an 'equivalent' Gaussian is used, which was also used in Chapter 3 to evaluate integrals involving products of the director beam and the optical beam. The trial functions (4.8) are replaced by equivalent Gaussians

$$\operatorname{sech}\frac{\chi_u}{w_u} \to \alpha e^{-\chi_u^2/(\beta^2 w_u^2)}, \quad \operatorname{sech}\frac{\chi_v}{w_v} \to \alpha e^{-\chi_v^2/(\beta^2 w_v^2)}. \tag{4.12}$$

The scaling parameters α and β will be determined by matching the resulting averaged Lagrangian with the easily calculated averaged Lagrangian in the symmetric limit, $A_u = A_v$ and $D_u = D_v$ with $\xi_u = \xi_v$. Later in this section Gaussian trial functions will also be considered, for which the equivalent Gaussian substitution is obviously not needed.

One notable difference between the use of equivalent Gaussians here and their use in Chapter 3 is that they are required to evaluate integrals involving the two light beams u and v instead of integrals involving one of the light beams and the director beam θ. In Chapter 3 two different width corrections, A for the light beam width w_k and B for the director beam width β_k, were required to match the Gaussians to the hyperbolic secant trial functions in the problem integrals. Here, however, the equivalent Gaussians can be more accurately matched by including a width correction term β, as before, and allowing an amplitude correction α, since the widths of the two optical beams are very similar and separate width correction terms for each of the beams would be almost identical.

Using the small amplitude expansion and the equivalent Gaussian approximation the averaged Lagrangian (4.7) is calculated as

$$\begin{aligned}
\mathcal{L} &= -2\left(I_2 a_u^2 w_u^2 + \Lambda_u g_u^2\right)(\sigma_u' - V_u\xi_u') - 2I_1 a_u w_u^2 g_u' \\
&\quad + 2I_1 w_u^2 g_u a_u' + 4I_1 a_u w_u g_u w_u' - I D_u a_u^2 - D_u\left(I_2 a_u^2 w_u^2 + \Lambda_u g_u^2\right) V_u^2 \\
&\quad - 2\left(I_2 a_v^2 w_v^2 + \Lambda_v g_v^2\right)(\sigma_v' - V_v\xi_u') - 2I_1 a_v w_v^2 g_v' \\
&\quad + 2I_1 w_v^2 g_v a_v' + 4I_1 a_v w_v g_v w_v' - I D_v a_v^2 - D_v\left(I_2 a_v^2 w_v^2 + \Lambda_v g_v^2\right) V_v^2 \\
&\quad + \frac{2}{q}Q_1 - \frac{2}{q^3}Q_2,
\end{aligned} \tag{4.13}$$

where $'$ denotes differentiation with respect to z and

$$\begin{aligned}
Q_1 &= A_u^2 I_4 a_u^4 w_u^2 + A_v^2 I_4 a_v^4 w_v^2 \\
&\quad + \frac{A_u A_v}{2\left(w_u^2 + w_v^2\right)}\,\alpha^4\beta^2 a_u^2 a_v^2 w_u^2 w_v^2 e^{-2(\xi_u-\xi_v)^2/(\beta^2(w_u^2+w_v^2))},
\end{aligned} \tag{4.14}$$

$$\begin{aligned}
Q_2 &= A_u^4 I_8 a_u^8 w_u^2 + A_v^4 I_8 a_v^8 w_v^2 \\
&\quad + \frac{A_u^3 A_v}{\left(w_u^2 + 3w_v^2\right)}\,\alpha^8\beta^2 a_u^6 a_v^2 w_u^2 w_v^2\, e^{-6(\xi_u-\xi_v)^2/(\beta^2\left(w_u^2+3w_v^2\right))} \\
&\quad + \frac{3}{4}\frac{A_u^2 A_v^2}{\left(w_u^2 + w_v^2\right)}\,\alpha^8\beta^2 a_u^4 a_v^4 w_u^2 w_v^2 e^{-4(\xi_u-\xi_v)^2/(\beta^2\left(w_u^2+w_v^2\right))} \\
&\quad + \frac{A_u A_v^3}{\left(3w_u^2 + w_v^2\right)}\,\alpha^8\beta^2 a_u^2 a_v^6 w_u^2 w_v^2 e^{-6(\xi_u-\xi_v)^2/(\beta^2\left(3w_u^2+w_v^2\right))}.
\end{aligned}$$

Here, Λ_u and Λ_v are the shelf areas modulo 2π

$$\Lambda_u = \frac{1}{2}R_u^2 \quad \text{and} \quad \Lambda_v = \frac{1}{2}R_v^2. \tag{4.15}$$

The various integrals I and I_i resulting from the calculation of this averaged Lagrangian are

$$\begin{aligned}
I &= \int_0^\infty x\,\mathrm{sech}^2 x\,\tanh^2 x\,dx = \frac{1}{3}\log 2 + \frac{1}{6}, \\
I_1 &= \int_0^\infty x\,\mathrm{sech}\,x\,dx = 2C, \\
I_2 &= \int_0^\infty x\,\mathrm{sech}^2 x\,dx = \log 2, \\
I_4 &= \int_0^\infty x\,\mathrm{sech}^4 x\,dx = \frac{2}{3}\log 2 - \frac{1}{6}, \\
I_8 &= \int_0^\infty x\,\mathrm{sech}^8 x\,dx = \frac{16}{35}\log 2 - \frac{19}{105},
\end{aligned} \tag{4.16}$$

where C is the Catalan constant $C = 0.915965594\ldots$.

The scaling parameters α and β for the equivalent Gaussians (4.12) can now be determined by matching the calculated averaged Lagrangian for the current trial function, equation (4.13), with the averaged Lagrangian found by García-Reimbert *et al* [30], which is the same in the symmetric limit $A_u = A_v$, $D_u = D_v$, $a_u = a_v$, $w_u = w_v$, $g_u = g_v$, $V_u = V_v = 0$, $\xi_u = \xi_v$, $\sigma_u = \sigma_v$. The final result is

$$\alpha^4 = \frac{2I_8}{I_4} \quad \text{and} \quad \beta^2 = \frac{4I_4^2}{I_8}. \tag{4.17}$$

The scaling parameters are then $\alpha = 0.9794\ldots$ and $\beta = 1.6027\ldots$, so that the equivalent Gaussian has nearly the same amplitude as the original trial function, with the major change being a different width. It is noteworthy that this result justifies the approach taken in Chapter 3, where the equivalent Gaussians were assumed to have the same amplitude as hyperbolic

secants.

Taking variations of the averaged Lagrangian (4.13) with respect to the u colour nematicon parameters yields

$$\delta\sigma_u: \quad \frac{d}{dz}\left(a_u w_u^2 I_2 + \Lambda_u g_u^2\right) = 0, \tag{4.18}$$

$$\delta V_u: \quad 2\left(\frac{d\xi_u}{dz} - D_u V_u\right)\left(a_u^2 w_u^2 I_2 - \Lambda_u g_u^2\right) = 0, \tag{4.19}$$

$$\delta g_u: \quad \frac{d}{dz}\left(a_u w_u^2 I_1\right) - \Lambda_u g_u\left(\frac{d\sigma_u}{dz} - V_u\frac{d\xi}{dz} + \frac{1}{2}D_u V_u^2\right) = 0, \tag{4.20}$$

$$\begin{aligned}\delta a_u: \quad & -2I_2 a_u w_u^2\left(\frac{d\sigma_u}{dz} - V_u\frac{d\xi_u}{dz}\right) - I_1 w_u^2\frac{dg_u}{dz} - I_1\frac{d}{dz}\left(g_u w_u^2\right) + 2I_1 g_u w_u\frac{dw_u}{dz} \\ & - D_u I a_u - D_u I_2 a_u w_u^2 V_u^2 + \frac{2}{q}\left[2I_4 A_u^2 a_u^3 w_u^2 + \frac{A_u A_v \alpha^4\beta^2 a_u a_v^2 w_u^2 w_v^2}{2\left(w_u^2+w_v^2\right)} e^{-\frac{2(\xi_u-\xi_v)^2}{\beta^2\left(w_u^2+w_v^2\right)}}\right] \\ & - \frac{2}{q^3}\left[4I_8 a_u^4 a_u^7 w_u^2 + \frac{3A_u^3 A_v\alpha^8\beta^2 a_u^5 a_v^2 w_u^2 w_v^2}{w_u^2+3w_v^2} e^{-\frac{6(\xi_u-\xi_v)^2}{\beta^2\left(w_u^2+3w_v^2\right)}}\right. \\ & \left. + \frac{3A_u^2 A_v^2\alpha^8\beta^2 a_u^3 a_v^4 w_u^2 w_v^2}{2\left(w_u^2+w_v^2\right)} e^{-\frac{4(\xi_u-\xi_v)^2}{\beta^2\left(w_u^2+w_v^2\right)}} + \frac{A_u A_v^3\alpha^8\beta^2 a_u a_v^6 w_u^2 w_v^2}{3w_u^2+w_v^2} e^{-\frac{6(\xi_u-\xi_v)^2}{\beta^2\left(3w_u^2+w_v^2\right)}}\right] = 0,\end{aligned} \tag{4.21}$$

$$\begin{aligned}\delta w_u: \quad & -2I_2 a_u^2 w_u\left(\frac{d\sigma}{dz} - V_u\frac{d\xi}{dz}\right) - 4I_1 a_u w_u\frac{dg_u}{dz} - D_u I_2 a_u^2 w_u V_u^2 \\ & + \frac{2}{q}\left[A_u I_4 a_u^4 w_u + \frac{A_u A_v\alpha^4\beta^2 a_u^2 a_v^2 w_u w_v^2}{\left(w_u^2+w_v^2\right)^2}\left(\frac{w_v^2}{2} + \frac{\left(\xi_u-\xi_v\right)^2 w_u^2}{\beta^2\left(w_u^2+w_v^2\right)}\right) e^{-\frac{2(\xi_u-\xi_v)^2}{\beta^2\left(w_u^2+w_v^2\right)}}\right] \\ & - \frac{2}{q^3}\left[A_u^4 I_8 a_u^8 w_u + \frac{A_u^3 A_v\alpha^8\beta^2 a_u^6 a_v^2 w_u w_v^2}{\left(w_u^2+3w_v^2\right)^2}\left(3w_v^2 + \frac{6\left(\xi_u-\xi_v\right)^2 w_u^2}{\beta^2\left(w_u^2+3w_v^2\right)}\right) e^{-\frac{4(\xi_u-\xi_v)^2}{\beta^2\left(w_u^2+w_v^2\right)}}\right. \\ & + \frac{A_u^2 A_v^2\alpha^8\beta^2 a_u^4 a_v^4 w_u w_v^2}{\left(w_u^2+w_v^2\right)^2}\left(\frac{3w_v^2}{4} + \frac{3\left(\xi_u-\xi_v\right)^2 w_u^2}{\beta^2\left(w_u^2+w_v^2\right)} e^{-\frac{4(\xi_u-\xi_v)^2}{\beta^2\left(w_u^2+w_v^2\right)}}\right) \\ & \left. + \frac{A_u A_v^3\alpha^8\beta^2 a_u^2 a_v^6 w_u w_v^2}{\left(3w_u^2+w_v^2\right)^2}\left(w_v^2 + \frac{18\left(\xi_u-\xi_v\right)^2 w_u^2}{\beta^2\left(3w_u^2+w_v^2\right)}\right) e^{-\frac{6(\xi_u-\xi_v)^2}{\beta^2\left(3w_u^2+w_v^2\right)}}\right] = 0,\end{aligned} \tag{4.22}$$

$$\begin{aligned}\delta\xi_u: \quad & -\frac{d}{dz}\left(I_2 a_u^2 w_u^2 V_u + \Lambda_u g_u^2\right) - \frac{2}{q}\left[\frac{A_u A_v a_u^2 a_v^2 w_u^2 w_v^2\left(\xi_u-\xi_v\right)}{\left(w_u^2+w_v^2\right)^2} e^{-\frac{2(\xi_u-\xi_v)^2}{\beta^2\left(w_u^2+w_v^2\right)}}\right] \\ & + \frac{2}{q^3}\left[\frac{6A_u^3 A_v\alpha^8 a_u^6 a_v^2 w_u^2 w_v^2}{\left(w_u^2+3w_v^2\right)^2} e^{-\frac{6(\xi_u-\xi_v)^2}{\beta^2\left(w_u^2+3w_v^2\right)}} + \frac{3A_u^2 A_v^2\alpha^8 a_u^4 a_v^4 w_u^2 w_v^2\left(\xi_u-\xi_v\right)}{\left(w_u^2+w_v^2\right)^2} e^{-\frac{4(\xi_u-\xi_v)^2}{\beta^2\left(w_u^2+w_v^2\right)}}\right. \\ & \left. + \frac{6A_u A_v^3\alpha^8 a_u^2 a_v^6 w_u^2 w_v^2\left(\xi_u-\xi_v\right)}{\left(3w_u^2+w_v^2\right)^2} e^{-\frac{6(\xi_u-\xi_v)^2}{\beta^2\left(3w_u^2+w_v^2\right)}}\right] = 0.\end{aligned} \tag{4.23}$$

After some algebra these modulation equations can be reduced to the simpler modulation

equations for the u colour beam

$$\frac{d}{dz}\left(I_2 a_u^2 w_u^2 + \Lambda_u g_u^2\right) = 0, \tag{4.25}$$

$$\frac{d}{dz}\left(I_1 a_u w_u^2\right) = \Lambda_u g_u \left(\sigma_u' - V_u \xi_u' + \frac{1}{2} D_u V_u^2\right), \tag{4.26}$$

$$I_1 \frac{dg_u}{dz} = \frac{1}{2} D_u a_u w_u^{-2} - \frac{1}{2qa_u w_u^2}\left(a_u \frac{\partial Q_1}{\partial a_u} - w_u \frac{\partial Q_1}{\partial w_u}\right) + \frac{1}{2q^3 a_u w_u^2}\left(a_u \frac{\partial Q_2}{\partial a_u} - w_u \frac{\partial Q_2}{\partial w_u}\right), \tag{4.27}$$

$$I_2\left(\frac{d\sigma_u}{dz} - V_u \frac{d\xi_u}{dz}\right) = -ID_u w_u^{-2} - \frac{1}{2} D_u I_2 V_u^2 + \frac{1}{2qa_u^2 w_u^2}\left(2a_u \frac{\partial Q_1}{\partial a_u} - w_u \frac{\partial Q_1}{\partial w_u}\right) - \frac{1}{2q^3 a_u^2 w_u^2}\left(2a_u \frac{\partial Q_2}{\partial a_u} - w_u \frac{\partial Q_2}{\partial w_u}\right), \tag{4.28}$$

$$\frac{d}{dz}\left[\left(I_2 a_u^2 w_u^2 + \Lambda_u g_u^2\right) V_u\right] = \frac{1}{q}\frac{\partial Q_1}{\partial \xi_u} - \frac{1}{q^3}\frac{\partial Q_2}{\partial \xi_u}, \tag{4.29}$$

$$\frac{d\xi_u}{dz} = D_u V_u. \tag{4.30}$$

The v colour beam modulation equations require obvious symmetric substitutions of beam parameters and constants and so will not be repeated here.

In Chapters 2 & 3 the utility of conserved quantities in the analysis of beam dynamics was highlighted. The modulation equation (4.25) is the equation for conservation of mass and equation (4.29), when added to the symmetric equation in the v colour, is the equation for conservation of momentum, in the sense of invariances of the Lagrangian (4.10). Nöther's Theorem applied to the Lagrangian (4.10) shows that the local nematicon equations (4.5) also possess the energy conservation equation

$$\frac{dH}{dz} = \int_{-\infty}^{\infty}\int_{-\infty}^{\infty}\left[D_u|\nabla u|^2 + D_v|\nabla v|^2 - \sqrt{q^2 + 4\left(A_u|u|^2 + A_v|v|^2\right)^2}\right] dxdy = 0. \tag{4.31}$$

With the small amplitude assumption used for the evaluation of the averaged Lagrangian (4.7), the trial functions (4.8) can be inserted into equation (4.31), which then gives the total energy conservation equation for the two-colour nematicons

$$\frac{dH}{dz} = \frac{d}{dz}\left[ID_u a_u^2 + ID_v a_v^2 - \frac{2}{q}Q_1 + \frac{2}{q^3}Q_2\right] = 0, \tag{4.32}$$

on using the mass and momentum equations (4.25) and (4.29) and their v colour counterparts. Adding the momentum equation (4.29) in the u colour to its symmetric equation in the v colour gives the equation for total momentum conservation as

$$\frac{d}{dz}\left[\left(I_2 a_u^2 w_u^2 + \Lambda_u g_u^2\right) V_u + \left(I_2 a_v^2 w_v^2 + \Lambda_v g_v^2\right) V_v\right] = 0. \tag{4.33}$$

These conservation equations will be used to find various beam properties, including fixed point parameter values, momentum walk-off, shelf radii and radiative losses.

Much information about the evolution of the two-colour nematicons can be obtained by looking at the fixed points of the modulation equations (4.25)–(4.30). These modulation equations possess two types of fixed points, as did the nonlocal nematicons of Chapter 3. The two possible fixed points are: (i) a coupled vector nematicon with $\xi_u = \xi_v$ as $z \to \infty$ and (ii) separate nematicons, which become two single nematicons $|\xi_u - \xi_v| \to \infty$ as $z \to \infty$. As separate single nematicons in the local regime have been studied in detail before by García-Reimbert *et al* [35], it is of more interest to investigate the coupled vector nematicon fixed point. Let us denote fixed point values of the nematicon parameters by $\hat{}$ and boundary values at $z = 0$ by a 0 subscript. As the coupled vector nematicon boundary conditions which lead to a bound state of the two colours are the focus for this investigation, the asymptotic beam positions ξ_u,

ξ_v have the relation $\hat{\xi}_u = \hat{\xi}_v$ for these boundary conditions. On noting that $g_{u0} = g_{v0} = 0$ and $\hat{g}_u = \hat{g}_v = 0$, the mass and momentum conservation equations (4.25) and (4.33), plus the position relation (4.30), therefore give

$$\hat{\xi}'_u = \hat{\xi}'_v = \frac{D_u D_v M_0}{I_2 \left(D_v a_{u0}^2 w_{u0}^2 + D_u a_{v0}^2 w_{v0}^2\right)}, \tag{4.34}$$

where

$$M_0 = I_2 a_{u0}^2 w_{u0}^2 V_{u0} + I_2 a_{v0}^2 w_{v0}^2 V_{v0}, \tag{4.35}$$

is the total initial momentum from equation (4.33). The conservation expression (4.34) gives the mean momentum walk-off of the bound two-colour nematicon if radiative losses are neglected. These radiative losses will be discussed and calculated in the next section.

The final quantities to be determined before discussing radiative losses are the radii, R_u & R_v, of the radiation shelves travelling with the beams. In previous work involving the NLS equation and the single colour nematicon equations the shelf radius was determined by linearising the modulation equations about their fixed point, which resulted in a simple harmonic oscillator equation [30, 31, 32, 35, 39]. The frequency of this oscillator equation, which depends on the shelf width, was then matched to the soliton oscillation frequency, resulting in an expression for the shelf width. The same analysis could be performed for the present modulation equations but this would result in complicated expressions for R_u and R_v. Much simplified expressions for the shelf radii can be obtained in the same manner as that of Chapter 3, where the experiments of Alberucci *et al* on two-colour nematicons in the nonlocal limit were used to deduce that the diffraction and interaction coefficients for the two colours take very similar values. In a similar manner then it is reasonable to take values of D_u, D_v and A_u, A_v which are close to each other. The symmetric limit, where $D_u = D_v$ and $A_u = A_v$, has that the local nematicon equations (4.5) reduce to a coupled pair of local single nematicon equations of the type considered by García-Reimbert *et al* [30]. Making this approximation then, which is equivalent to taking the symmetric limit, allows the calculation of the shelf radii, which are

$$\Lambda_u = \frac{I I_1^2 D_u q^3}{384 I_2 I_8 A_u^4 \hat{a}_u^6} \quad \text{and} \quad \Lambda_v = \frac{I I_1^2 D_v q^3}{384 I_2 I_8 A_v^4 \hat{a}_v^6}, \tag{4.36}$$

with the fixed point amplitudes $\hat{a}_u$ and $\hat{a}_v$ defined as

$$\hat{a}_u^6 = -\frac{I_4 q^2 H}{16 I I_8 D_u A_u^2} \quad \text{and} \quad \hat{a}_v^6 = -\frac{I_4 q^2 H}{16 I I_8 D_v A_v^2}. \tag{4.37}$$

Here H is the (constant) energy given by equation (4.32). The calculation of expressions (4.36) and (4.37) is presented in full in Appendix B. These equations are the same as those found by García-Reimbert *et al* [30], except that here the diffraction and coupling coefficients for the two colours have been included, which preserves the symmetry.

The trial functions (4.8) have been assumed to have the same hyperbolic secant profile as the soliton solution of the NLS equation. Another possible choice for the trial functions is a Gaussian, particularly as this choice obviates the need for an equivalent function in order to explicitly calculate the various cross integrals (4.11) in the averaged Lagrangian. In this regard it was shown by Conti *et al* that a nematicon has a Gaussian profile near its peak and that its tail decays as the modified Bessel function of order zero, K_0, due to the circular symmetry [27]. A Gaussian trial function then gives a better representation of the nematicon near its peak, while the sech profile gives a better representation of its decay closer to the tail. To demonstrate this graphically, Figure 4.2 shows a solution of the single nematicon equations for which a steady single nematicon has formed. This solution is then compared with calculated Gaussian and sech profiles fitted closely to the numerical beam profile. It is clear that the Gaussian models the beam profile well near the peak, but decays far too quickly approaching the tail, whereas the sech profile is too steep near the peak, yet decays in a similar manner to the steady numerical beam profile.

To further understand the effect that the choice of trial function has on the final steady nematicon state, numerical solutions of the full two-colour nematicon governing equations will

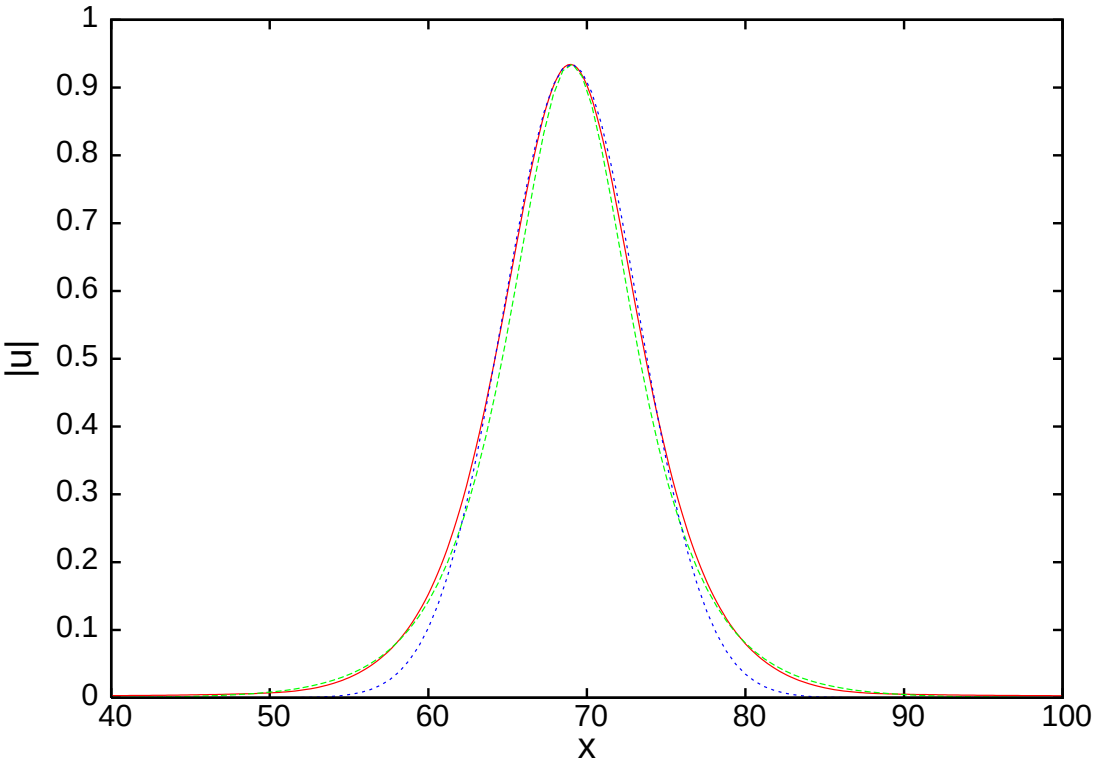

Figure 4.2: Numerical solution of the full governing equations showing the beam profile of a steady single nematicon (—)[red] taken from the results of Chapter 5 at $z = 90$; a fitted sech profile (— — —)[green]; a fitted Gaussian profile (– – –)[blue].

be sought, along with solutions of the corresponding modulation equations, for Gaussian trial functions. Appropriate Gaussian trial functions then include a Gaussian term representing the optical beam and a term representing the radiation shelf travelling with the beam, which is identical to the second term in the sech trial functions (4.8)

$$\begin{aligned} u &= a_u e^{-(\chi_u/w_u)^2}\, e^{i\psi_u} + i g_u e^{i\psi_u}, \\ v &= a_v e^{-(\chi_v/w_v)^2}\, e^{i\psi_v} + i g_v e^{i\psi_v}. \end{aligned} \tag{4.38}$$

No new calculations are required for these new trial functions. All that is required is to replace the integrals (4.16) by

$$\begin{aligned} I &= \int_0^\infty x\left(-2xe^{-x^2}\right)^2 dx = \frac{1}{2}, \\ I_1 &= \int_0^\infty xe^{-x^2}\, dx = \frac{1}{2}, \\ I_2 &= \int_0^\infty xe^{-2x^2}\, dx = \frac{1}{4}, \\ I_4 &= \int_0^\infty xe^{-4x^2}\, dx = \frac{1}{8}, \\ I_8 &= \int_0^\infty xe^{-8x^2}\, dx = \frac{1}{16}. \end{aligned} \tag{4.39}$$

With these replacements for the integrals I and I_i the averaged Lagrangian and the modulation equations for the Gaussian trial functions are identical to equations (4.13) and (4.25)–(4.30) respectively. Clearly, as there is no call for an equivalent Gaussian when the trial functions are Gaussians themselves, the scaling parameters are $\alpha = 1.0$ and $\beta = 1.0$, which can also

be verified by substituting the integrals (4.39) into equations (4.17). It should be noted that the averaged Lagrangian (4.13) and the modulation equations (4.25)–(4.30) hold for any self-similar trial functions of u and v. All that is needed is that the integrals I and I_i of (4.16) are replaced by the equivalent first order moments of powers of this trial function and its first derivative. This suggests that the trial function is relatively unimportant. However, a trial function that diverges from the nematicon steady state profile by too large a degree will not admit modulation equations whose solutions are in good agreement with numerical solutions. In addition, numerical solutions of the governing equations where the initial conditions are significantly different from the steady nematicon profile would show large profile changes as the initial beams attempt to settle to steady nematicon solutions. Such large profile changes would be impossible to replicate with trial functions with fixed profiles. Initial conditions and trial functions that are close to the steady nematicon profile are then desirable for the solutions of the resulting modulation equations to have good agreement with numerical solutions.

4.2.2 Radiation Calculation

To complete the modulation equations the effect of the diffractive radiation shed by the nematicons as they evolve must be included in the modulation equations (4.25)–(4.30). Numerical solutions show that the shed radiation has small amplitude relative to the nematicons. Hence this radiation is governed by the linearised Schrödinger equations

$$\begin{aligned} i\frac{\partial u}{\partial z} + \frac{1}{2r}D_u\frac{\partial}{\partial r}\left(r\frac{\partial u}{\partial r}\right) &= 0, \\ i\frac{\partial v}{\partial z} + \frac{1}{2r}D_v\frac{\partial}{\partial r}\left(r\frac{\partial v}{\partial r}\right) &= 0. \end{aligned} \tag{4.40}$$

Solving these equations yields the form of the diffractive radiation shed as the beams evolve. This radiation problem has already been studied by García-Reimbert *et al* [35] and has also been presented in Chapters 2 & 3 for local single nematicons and nonlocal two-colour nematicons, respectively. It is clear that the radiation calculation differs little from that presented before since nonlinear coupling is neglected. Solely for completeness then, the final result of the radiation calculation is that two modulation equations, the mass equation (4.25) and the equation for the radiation shelf height g_u (4.27), plus their v colour beam equivalents, are modified to include losses

$$\frac{d}{dz}\left(I_2 a_u^2 w_u^2 + \Lambda_u g_u^2\right) = -2D_u\delta_u\Lambda_u\kappa_u^2, \tag{4.41}$$

$$\begin{aligned} I_1\frac{dg_u}{dz} = {} & \frac{1}{2}D_u a_u w_u^{-2} - \frac{1}{2qa_u w_u^2}\left(a_u\frac{\partial Q_1}{\partial a_u} - w_u\frac{\partial Q_1}{\partial w_u}\right) \\ & + \frac{1}{2q^3 a_u w_u^2}\left(a_u\frac{\partial Q_2}{\partial a_u} - w_u\frac{\partial Q_2}{\partial w_u}\right) - 2D_u\delta_u g_u, \end{aligned} \tag{4.42}$$

where the loss coefficient δ_u is

$$\delta_u = -\frac{\sqrt{2\pi}I_1}{2e\kappa_u\Lambda_u}\int_0^z \frac{\pi\kappa_u(z')\log((z-z')/\Lambda_u)}{\left[\left\{\left[\frac{1}{2}\log((z-z')/\Lambda_u)\right]^2 + \frac{3\pi^2}{4}\right\}^2 + \pi^2\left[\log((z-z')/\Lambda_u)\right]^2\right]}\frac{dz'}{(z-z')}, \tag{4.43}$$

and

$$\kappa_u^2 = \frac{1}{\Lambda_u}\left[I_2 a_u^2 w_u^2 - I_2\hat{a}_u^2\hat{w}_u^2 + \Lambda_u g_u^2\right]. \tag{4.44}$$

The variable κ_u measures the difference between the mass of the u colour at z and its mass at the fixed point. Notice that the radiation calculation is simplified here from the nonlocal case in that there is only one shelf radius required, since the director and optical beams have the same width. Consequently there is no need to split the radiation shelf into inner and outer components. The loss coefficient and the modified equations for the v colour beam are obtained

by obvious symmetric substitutions.

With the inclusion of diffractive radiation, the modulation equations for the two-colour nematicons are complete.

4.2.3 Adjustments to Numerical Methods

The numerical schemes used to solve the modulation equations [(4.26), (4.28)–(4.30), (4.41) and (4.42) plus the equivalent modulation equations for the v colour beam] and the full governing equations [(4.1)–(4.3)] are based on the schemes presented in Sections 2.2.4 and 2.3 respectively. These numerical schemes have been adjusted for the local two-colour nematicon problem in an identical manner as that described in Chapter 3 for two-colour nematicons in the nonlocal regime.

4.3 Results

In this section numerical solutions of the modulation equations will be compared with numerical solutions of the full two-colour nematicon governing equations. For brevity numerical solutions of the modulation equations will be named 'modulation solutions' and the numerical solutions of the full governing equations will be referred to as 'full numerical solutions.'

As for the full numerical solutions in the nonlocal limit, step sizes of $\Delta x = \Delta y = 0.4$ and $\Delta z = 0.005$ were taken, with spatial intervals of 102.4 in the x and y directions. Similarly, the step size chosen for the numerical scheme used to solve the modulation equations was $\Delta z = 0.005$. Coupling and diffraction coefficients were chosen that reflect the dimensionalised differences in these values in experimental studies. Equal initial values of amplitude (and width) were taken to prevent ambiguity when investigating the sources of different dynamical behaviours. A value of $\nu = 0.01$ was chosen to calculate the full numerical solutions. This value corresponds to highly local behaviour. It was found that for this value of ν numerical solutions of the full equations (4.1)–(4.3) agreed to graphical accuracy with numerical solutions of the saturable CNLS equations (4.5), from which the modulation equations were derived. This agreement was found by García-Reimbert *et al* [35] when investigating single, large amplitude local nematicons. Such agreement validates the comparison between the full two-colour nematicon equations and the modulation equations derived from the local saturable equations.

Figure 4.3(a) shows a comparison of the momentum walk-off $\hat{\xi}' = \hat{\xi}'_u = \hat{\xi}'_v$, as given by the full numerical solutions, the modulation solutions and the momentum conservation result, as a function of V_{v0} for sech initial conditions (4.8) which result in the formation of a vector nematicon (where V_{v0} is the initial value of V_v). The full numerical and modulation solutions do not settle to the steady state until large values of z are reached. This slow evolution to the steady state is typical of nematicon evolution. To enable a large number of numerical runs to be made in a reasonable time, the full numerical solutions were run until the oscillations of the positions of the nematicons about the final steady state were small and then an average was taken of these oscillations to determine $\hat{\xi}'$. It can be seen that there is near perfect agreement between the full numerical and modulation solutions for momentum walk-off. The momentum conservation result (4.34) was derived on the assumption that the nematicons do not shed mass and momentum. It is therefore apparent that the inclusion of the mass and momentum shed by the nematicons as they evolve is vital in order to obtain good agreement with full numerical solutions, which is in stark contrast to the momentum walk-off comparison for nonlocal two-colour nematicons for which radiative losses were shown to play a relatively insignificant role. A physical reason for the radiation loss difference between the local and nonlocal limits is that the wide response of the nematic in the nonlocal case forms a wide potential well from which little radiation can escape. In contrast, the narrow response of the nematic in the local limit allows large amounts of diffractive radiation to escape.

Figure 4.3(b) shows a similar comparison to Figure 4.3(a) for momentum walk-off, except that here Gaussian initial conditions (4.38) were used. The results are similar to those for the hyperbolic secant profile, with near perfect agreement between full numerical and modulation solutions. Again the inclusion of shed mass and momentum in the modulation equations is shown to be vital to obtain good agreement with full numerical solutions. Inspection of Figures

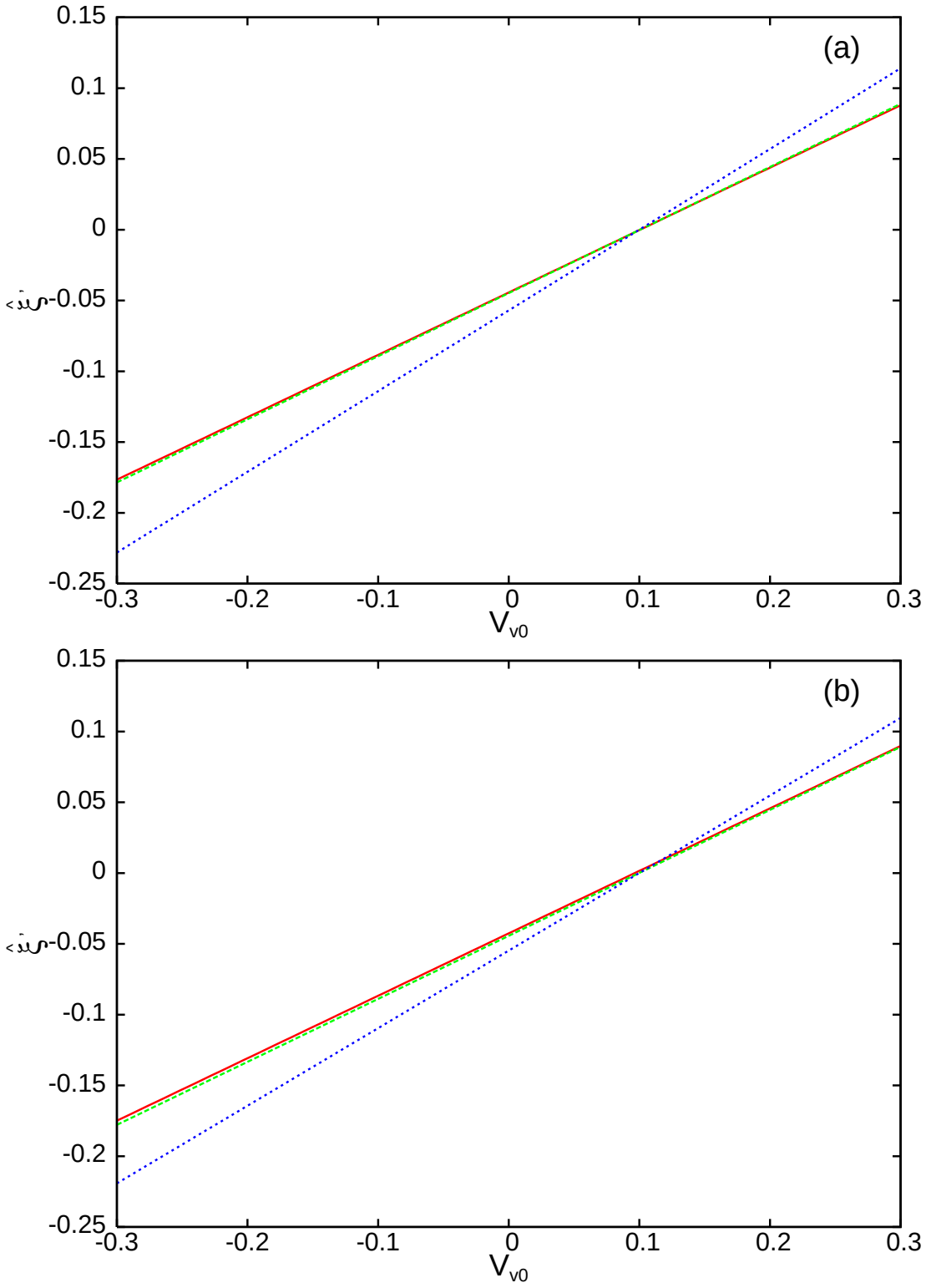

Figure 4.3: Steady value $\hat{\xi}' = \hat{\xi}'_u = \hat{\xi}'_v$ as a function of V_{v0} for the initial conditions $a_u = 0.35$, $a_v = 0.35$, $w_u = 3.0$, $w_v = 3.0$, $V_{u0} = -0.1$, $\xi_u = 1.0$ and $\xi_v = -1.0$ with $D_u = 1.0$, $D_v = 0.8$, $A_u = 1.0$ and $A_v = 0.9$ for (a) the sech initial condition (4.8) and (b) the Gaussian initial condition (4.38). Full numerical solution (—)[red], solution of modulation equations (— — —)[green], momentum conservation result (4.34) (– – –)[blue].

4.3(a) and 4.3(b) show that there is little difference when comparing the full numerical solutions for the sech and Gaussian trial functions. From the discussion of the use of a Gaussian trial function in Section 4.2.1 this may have been expected since the sech and Gaussian profiles are good approximations to the actual nematicon solution in different regions of the steady nematicon profile. The vital point with the use of various trial functions is that as long as the equations for certain basic gross quantities, such as mass, momentum and energy, are satisfied, then enough constraints are placed on the approximate equations to give good agreement with full numerical solutions. In contrast to the case for the nonlocal nematicon, the tail of a local nematicon is not extended. Nonlocal nematicons interact at distance due to overlap of these extended tails, whereas local nematicons interact only in close proximity to one another. As there is less interaction solely in the tails of the beams, the tail shape becomes less important, and consequently Gaussian trial functions seem to perform just as well as hyperbolic secants in this local regime. This will be investigated further later in the chapter.

A comparison for the evolution of the beams between a full numerical solution and a modulation solution is shown in Figure 4.4. The sech trial function (4.8) is used for a case leading to a vector nematicon shown in Figure 4.3(a). Figure 4.4(a) compares the positions ξ_u and ξ_v of the maxima of the beams as they propagate over z. Figure 4.4(b) is an equivalent plot for the amplitudes a_u and a_v. As expected from Figure 4.3(a) the agreement for the position evolution of the two solutions is excellent in the mean, which is equivalently the momentum walk-off of the two-colour vector nematicon. However the modulation solution peak positional separation of the two beams about this mean is greater than that of the full numerical solution. Additionally, for the latter solution, the two beams experience a stronger attraction initially and cross over one another much earlier in the z evolution than for the modulation solution. As for the position comparison, the means of the amplitude oscillations are in good agreement in Figure 4.4(b). However the peak amplitudes as given by the modulation equations are about 7% higher than the full numerical peak amplitudes. As the modulation equations are equivalent to those for a nonlinear oscillator, this amplitude difference causes a period difference in the oscillations, which accounts for the increasing difference in the peak amplitude positions of the full numerical and modulation solutions. The more rapid decay of the numerical solution to the steady state is due to the diffractive radiation analysis slightly underestimating this shed radiation.

A direct comparison of the beam dynamics between Figures 4.4 in the local limit and Figures 3.4 in the nonlocal limit is useful (these Figures having the same initial conditions for beam widths, beam separations and velocities), but such a comparison is to be carried out with caution as the mass of the nonlocal nematicons is roughly $30\times$ that of the local nematicons. When comparable initial conditions to those of Chapter 3 are taken here, extreme self-focusing occurs, so much so that it leads to large numerical errors. Some observations can, however, be made. One noticeable difference between these local results and results obtained for nonlocal two-colour nematicons is that a clear decay of position and amplitude oscillations is observed in the local limit. As radiation leaks more easily from the beams into the far field in this regime, the two-colour vector nematicon steady state is reached far more rapidly. Position oscillations decay so rapidly that anharmonicity is not observed in this regime, in contrast to the results of Chapter 3 where increased locality caused an increase in anharmonicity for the full numerical solutions. The large anharmonic, distorted position oscillations of beams propagating in moderately nonlocal media ($\nu \approx 250$) caused corresponding anharmonicity in the amplitude oscillations. Since the position oscillations die away very rapidly in the local limit they do not have such an effect on the amplitude oscillations, which are consequently smooth and harmonic in this regime.

Although the initial amplitudes are low ($a_k = 0.35$), as the beams evolve the amplitudes reach peaks of $a_k \approx 0.9$ before they begin to decay to the steady state. This large increase can be explained in relation to the standard $(2+1)$-D NLS and CNLS equations. Solitons obeying these equations are inherently unstable and a critical amplitude threshold dictates how the instability manifests itself. Below this threshold total decay is certain, whereas above the threshold infinite self-focusing will occur. The rapid amplitude increases seen in Figure 4.4(b) then are a result of the initial amplitudes being above this threshold value. Nonlinear self-focusing causes a rapid growth, but the effect is curtailed by the saturation of this nonlinearity and the beams stabilise, as noted by García-Reimbert *et al* for a single nematicon [35].

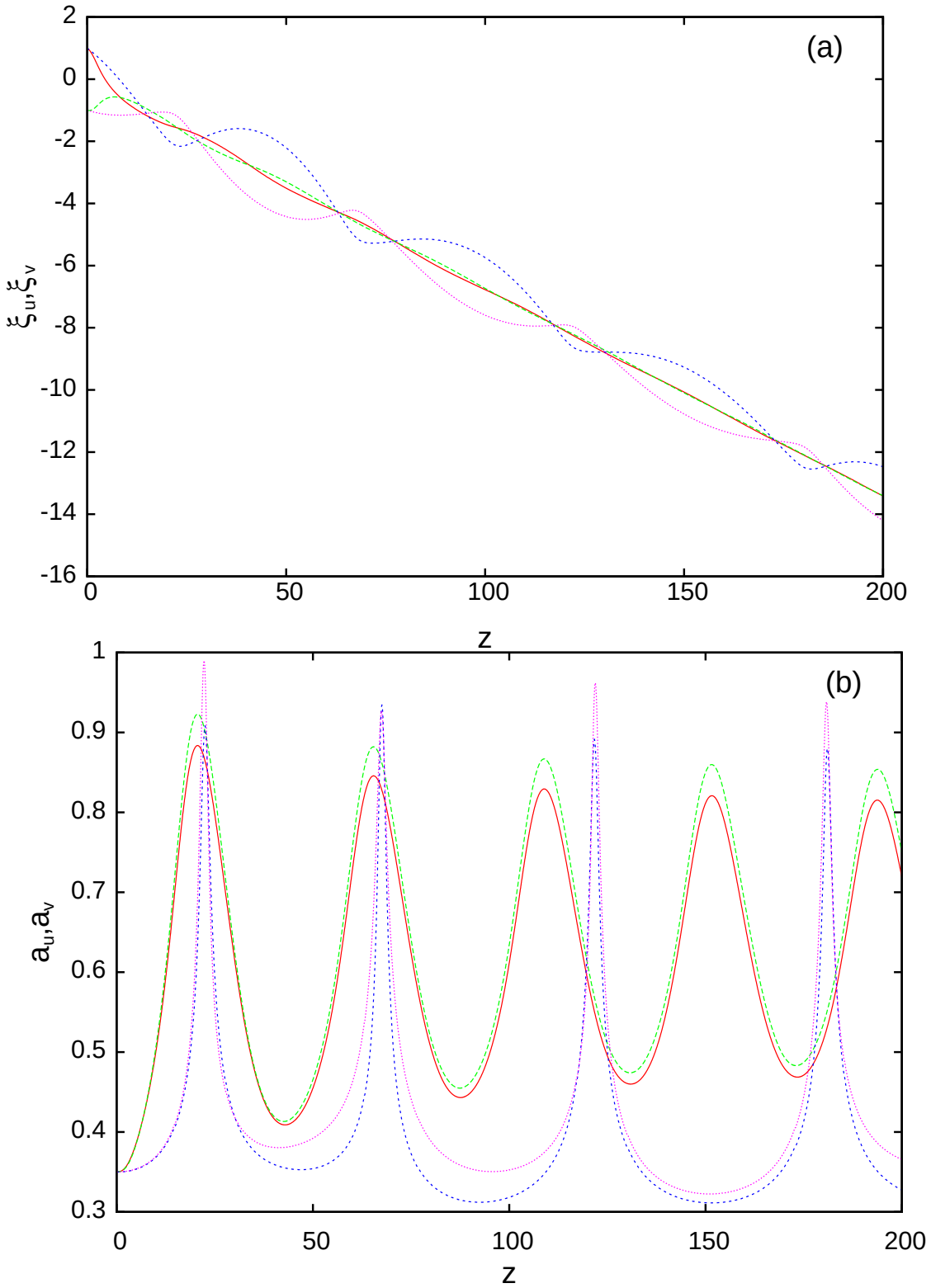

Figure 4.4: Solution of two-colour nematicon equations for an initial sech profile beam (4.8) with the initial conditions $a_u = 0.35$, $a_v = 0.35$, $w_u = 3.0$, $w_v = 3.0$, $V_{u0} = -0.1$, $V_{v0} = -0.05$, $\xi_u = 1.0$ and $\xi_v = -1.0$ with $D_u = 1.0$, $D_v = 0.8$, $A_u = 1.0$ and $A_v = 0.9$. Full numerical solution for the u colour (—)[red] and v colour (— — —)[green] beams; solution of modulation equations for the u colour (– – –)[blue] and v colour (- - -)[violet] beams. (a) Positions, (b) Amplitudes.

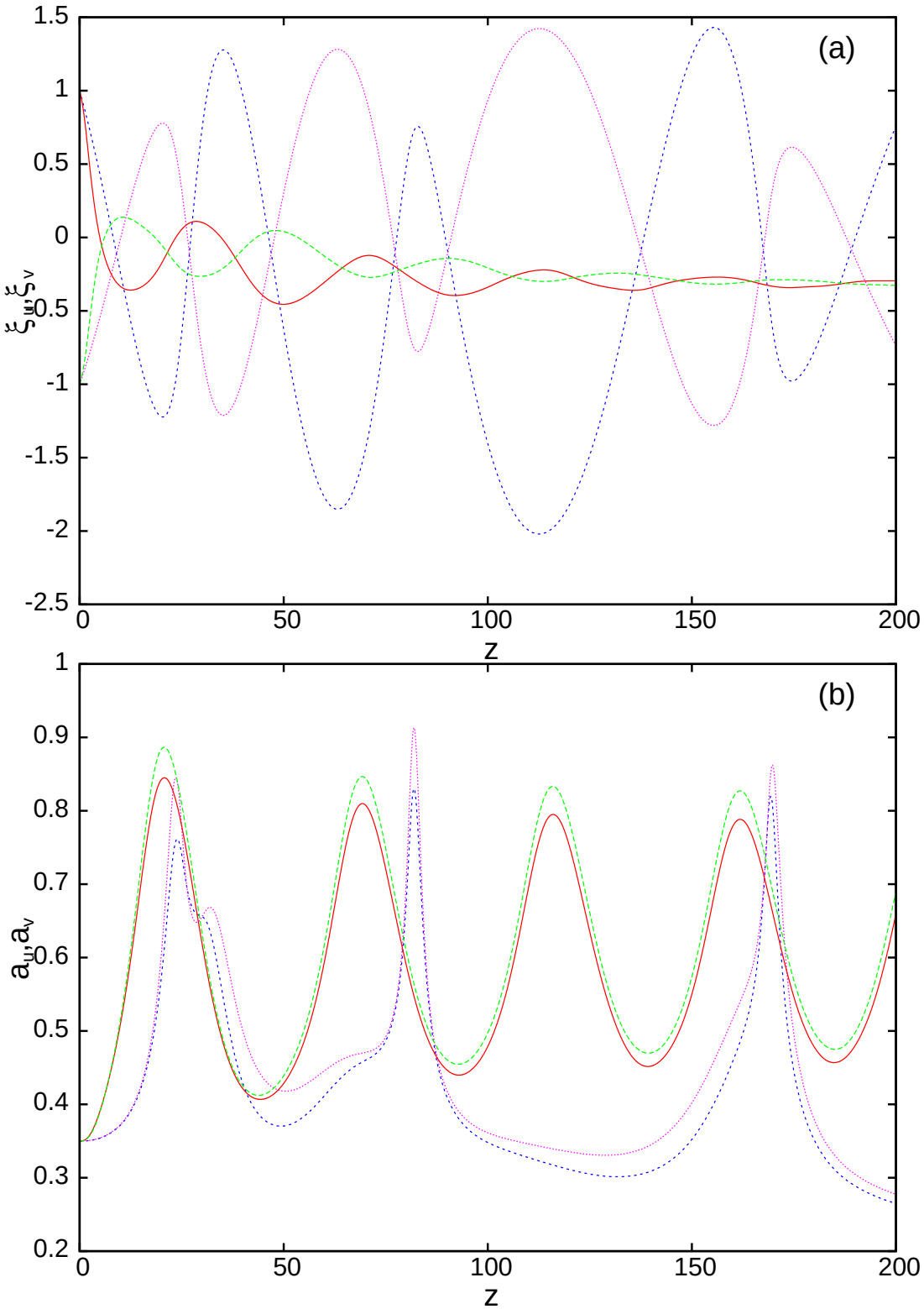

Figure 4.5: Solution of two-colour nematicon equations for an initial sech profile beam (4.8) with the initial conditions $a_u = 0.35$, $a_v = 0.35$, $w_u = 3.0$, $w_v = 3.0$, $V_{u0} = -0.1$, $V_{v0} = 0.1$, $\xi_u = 1.0$ and $\xi_v = -1.0$ with $D_u = 1.0$, $D_v = 0.8$, $A_u = 1.0$ and $A_v = 0.9$. Full numerical solution for the u colour (—)[red] and v colour (— — —)[green] beams; solution of modulation equations for the u colour (– – –)[blue] and v colour (- - -)[violet] beams. (a) Positions, (b) Amplitudes.

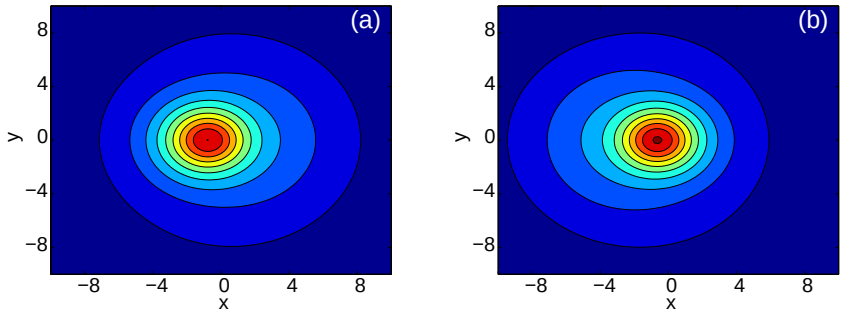

Figure 4.6: Numerical solution of the two-colour nematicon equations for the sech trial function (4.8) with initial conditions $a_u = 0.35$, $a_v = 0.35$, $w_u = 3.0$, $w_v = 3.0$, $V_{u0} = -0.1$, $V_{v0} = -0.05$, $\xi_u = 1.0$ and $\xi_v = -1.0$ with $D_u = 1.0$, $D_v = 0.8$, $A_u = 1.0$ and $A_v = 0.9$. (a) contour plot of numerical solution for $|u|$ at $z = 10$, (b) contour plot of numerical solution for $|v|$ at $z = 10$.

A similar comparison to Figure 4.4 is shown in Figure 4.5 for different initial values. Here the stark differences between full numerical solutions and the modulation solutions are far clearer. The amplitude and position oscillations do not agree in their peak separations nor in their periodicity, as for Figures 4.4, but there are additional observations that can be made here. The amplitude oscillations in Figure 4.5(b) no longer agree in the mean, which is equivalent to the modulation solution and the full numerical solution settling to two different steady states. Additionally these oscillations are anharmonic for the modulation solution, which is an effect clearly not present in the full numerical solution. When comparing the position oscillations and the amplitude oscillations it is clear that the large oscillations of the one affects the oscillations of the other. The largest oscillation in position, beginning around $z = 90$, corresponds to a long dip in amplitude which only begins to correct itself as the beams approach another collision.

There are a number of reasons for these various differences between the full numerical and modulation solutions. Early small differences with respect to radiative losses will grow over z. In addition the radiation calculation which is included in the modulation equations involves an asymptotic approximation of the Bessel function K_0 which is valid for large z [35]. The initial approximation to the radiation loss can therefore differ significantly from the actual loss. The importance of this difference depends on the relative weights of the initial and large z radiation losses. To some extent this accounts for the difference in the first collision point of the nematicons in Figures 4.4(a) & 4.5(a) and the difference in the first peak amplitudes of Figure 4.4(b). These early differences compound as the beams evolve over large z. There are, however, other factors that cause discrepancies between the full numerical and modulation solutions. The first can be seen from the full numerical solutions for $|u|$ and $|v|$ at $z = 10$, shown in Figures 4.6(a) & 4.6(b). These solutions are at a value of z just after the point at which the two colours first collide. It can be seen that the two nematicons have become distorted by their collision. This distortion is, of course, not accounted for in the variational approximation since the symmetric shapes of the two nematicons are fixed by the trial functions (4.8). Distortions will make a difference to the subsequent evolution of the nematicons. It is also notable that more mass is concentrated on one side of each of these beams. For example, Figure 4.6(a) has that the centre of mass is to the right of the beam (positive x). This corresponds to an acceleration of the beam in the opposite direction to the side of greater mass. These two beams are accelerating away from one another. As discussed by Smyth & Kath [32], the radiation calculation of Section 4.2.2 does not take acceleration into account. The inclusion of accelerative effects on radiation loss in the terms representing mass and momentum loss in the modulation equations is a nontrivial calculation as it involves solving a moving boundary value problem with an unknown boundary.

As the initial velocity difference between the nematicons increases, the nematicons become more distorted upon collision and interaction. This results in the difference in the position oscillations about the mean (i.e. momentum walk-off) as given by the full numerical and modulation solutions becoming greater, as seen in Figure 4.5(a). Also for large velocity differences

the approximate amplitude oscillations gain a second frequency due to an interaction with the large position oscillations which oscillate at a different frequency. This second frequency generation is most conspicuous in Figure 4.5(b) at $z \approx 35$. The full numerical solution does not have this second frequency as the acceleration and distortion of the nematicons upon collision, and the consequent losses to radiation, result in a rapid damping of the position oscillations about the mean momentum walk-off. However the various dynamical differences between the modulation and full numerical solutions for the various initial conditions does not change the excellent agreement for the momentum walk-off.

When comparing full numerical and modulation solutions in the limit of large velocity differences it was found that the Gaussian trial functions (4.38) gave slightly better agreement for the amplitude evolution, while there was little difference between the Gaussian and sech trial functions for the position evolution. For a small velocity difference between the two beams a sech trial function gave a slightly improved agreement in the position evolution and the agreement with respect to the amplitude evolution was very similar for the two trial functions. A comparison of the positions ξ_u and ξ_v between the sech trial functions and the Gaussian trial functions is given in Figure 4.7. Whilst there is almost no difference in the momentum walk-off value and both full numerical solutions settle to the steady state quickly in an almost identical fashion, it is interesting to note that the modulation solution with the Gaussian trial functions settles to the steady vector nematicon over larger z distances than for the sech trial function. This result suggests that a sech trial function is slightly better in this particular case for modelling nematicon evolution. Evidence from Chapter 3 on nonlocal two-colour nematicons gives further support to this conclusion.

4.4 Discussion

Two-colour vector nematicon evolution in the local regime has been considered. The full nematicon governing equations were simplified to approximate nematicons travelling in a local response NLC medium and the mechanism that allowed the stability of two-colour vector nematicons was found to be a saturation of the nonlinear term in the resulting approximated equations, which was a CNLS equation with a saturable nonlinearity. The simplified governing equations were reformulated as a Lagrangian and the variational approximate method was then used to derive modulation equations for the beam parameters. Radiative losses were later calculated and combined with these equations. Solutions of the modulation equations were compared with numerical solutions of the full governing equations. Excellent agreement was found between full numerical and modulation solutions, particularly when considering the momentum walk-off. The radiative losses included in the modulation equations were found to be essential for good agreement with respect to momentum walk-off. Whilst the agreement between the modulation and full numerical solutions for the period and peak separation of the u & v beam positions was not as good as for the nonlocal two-colour nematicons of Chapter 3, there was qualitative agreement in the sense that the oscillations were damped over large z, revealing considerable evolution to the final steady state. The conclusion of Chapter 3 that radiative losses increase as locality increases is given further weight here as damping in the amplitude and position oscillations was found to be much increased over that for the nonlocal limit of the previous Chapter. However it is clear that the radiation calculation underestimates radiation losses in this local regime, since accelerative effects cannot be included in the approximation and acceleration was found to increase loss.

Whilst the results presented here do not make it entirely clear whether a hyperbolic secant trial function is more appropriate than a Gaussian for modelling nematicon evolution, or indeed two-colour vector nematicon evolution, what is clear is that a sech is on average no worse than a Gaussian. There are, however, several reasons for preferring the use of a sech trial function, based on previous investigations. Results of Minzoni *et al* [39] and García-Reimbert *et al* [35] on single nematicon evolution in both local and nonlocal NLCs have suggested that a Gaussian initial condition is more likely to split into multiple beams at moderate initial amplitudes above a certain threshold. García-Reimbert *et al* even identified the source of beam splitting as the large difference in width between an initial Gaussian beam and a nematicon [35]. Their results and those of Chapter 5 also lead to the conclusion that a hyperbolic secant trial function has a

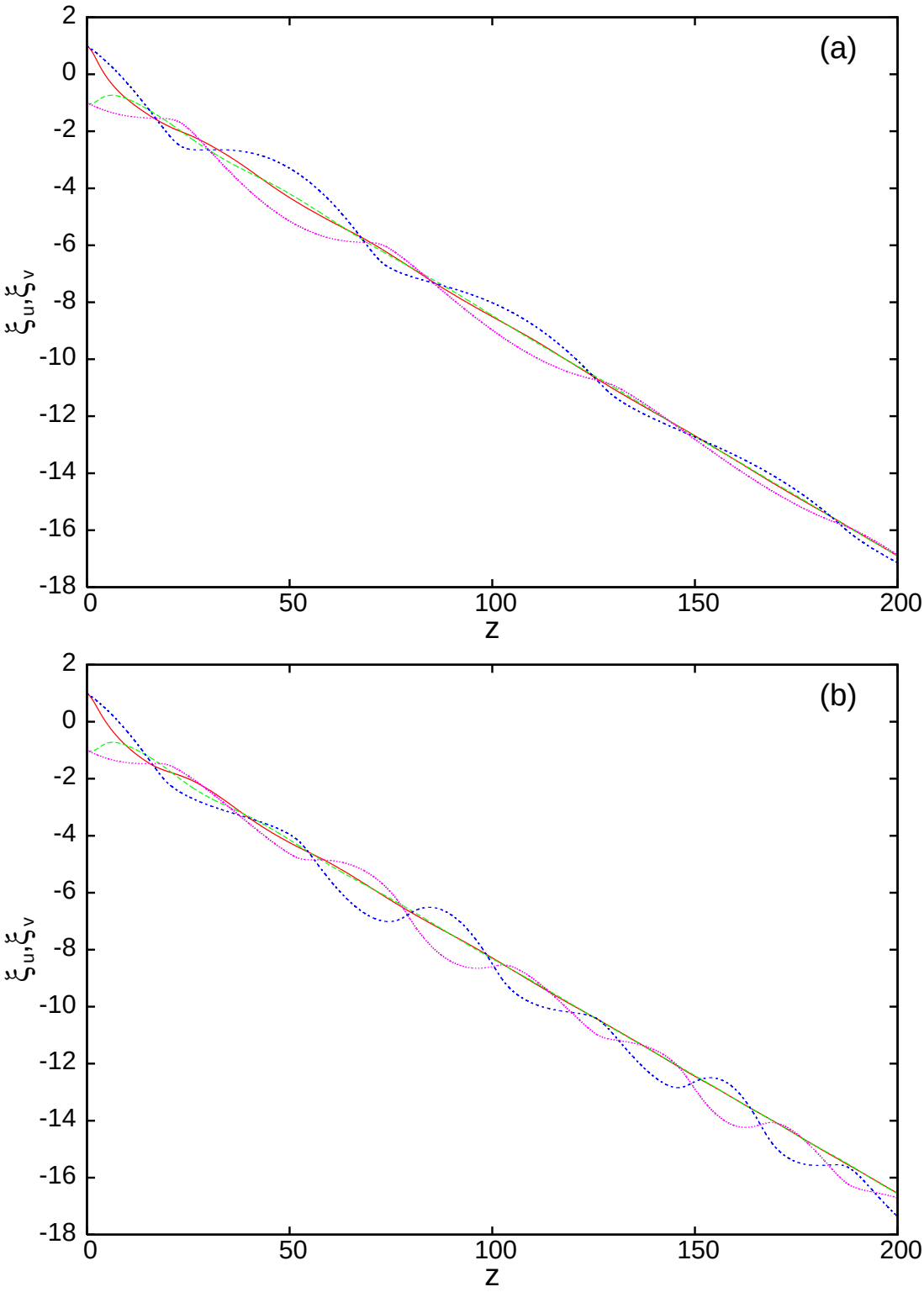

Figure 4.7: Positions given by the solutions of the two-colour nematicon equations for (a) the sech profile (4.8) and (b) the Gaussian profile (4.38) with the initial conditions $a_u = 0.35$, $a_v = 0.35$, $w_u = 3.0$, $w_v = 3.0$, $V_{u0} = -0.1$, $V_{v0} = -0.09$, $\xi_u = 1.0$ and $\xi_v = -1.0$ with $D_u = 1.0$, $D_v = 0.8$, $A_u = 1.0$ and $A_v = 0.9$. Full numerical solution for the u colour (—)[red] and v colour (— — —)[green] beams; solution of modulation equations for the u colour (– – –)[blue] and v colour (- - -)[violet] beams.

far wider range of initial amplitude and width values that can be taken in order that the beam evolves into a single nematicon.

Experiments have not been conducted on two-colour nematicons in the local regime, but the ease with which a local response of the nematic can be induced suggests that it would not be difficult to realise such an experiment. Furthermore, local responses have been found to be far faster than nonlocal responses because of the reduced reliance on a slow diffusion of molecular reorientation due to the optical beam(s) [60]. As multiple soliton interactions have been a topic of interest recently for their potential in optoelectronics, the author suggests that such an experiment is worthy of investigation.

In the next chapter, the methods developed for local and nonlocal two-colour nematicons will be applied to a very different experimental regime. The link between the different regimes is that each one provides a different method for steering nematicons. In the regimes presented in Chapter 3 and this chapter the coupled nematicon waveguides steer each other and the momentum walk-off can be adjusted by the initial separations and initial velocities. Although not explored here, these vector nematicons can also be steered by choosing unequal initial values of amplitude or width for the u and v colour beams. The following chapter will reveal a completely different way of steering nematicons that does not require the mutual interaction of two or more nematicons.

Chapter 5

Optical Steering in DD-NLCs

5.1 Background

Nematicons form due to a balance between linear beam diffraction and the self-focusing of an input beam, an effect brought about by the thermal and/or molecular reorientational nonlinear response of the material to the beam, fully described in Chapter 1. Although this balance is delicate, once created nematicons are stable and robust, allowing nematicon survival through defects in the medium [16]. One common method of introducing a defect into a nematic liquid crystal (NLC) is to alter the molecular reorientational response of the NLC medium to light by introducing a small amount ($\sim 1\%$) of photosensitive dye compound, a process known as doping. Dye molecules can be excited to induce a guest-host effect between the dye and nematic molecules, leading to reorientation.

A pre-tilt of the nematic molecules in a dye-doped nematic liquid crystal (DD-NLC) with appropriate anchoring at the boundaries can be induced by the various different methods outlined in Section 1.3. If an external beam (control beam) of a wavelength appropriate for dye molecule photon absorption is shone into the DD-NLC, the dye compound molecules adsorbed onto the surface of the nematic cell are excited and further adsorption and/or desorption occurs [61]. This changes the boundary anchoring conditions of the nematic molecules according to the guest-host effect; whereby adsorption/desorption of dye molecules at the boundary is directly related to surface charge adsorption/desorption, and changes to the surface charge density modify the anchoring conditions [62]. Essentially the initial molecular orientation at the boundaries in the region of the external beam is perturbed. Due to the elasticity of the NLC medium a perturbation of the molecular alignment at the boundary will, in turn, perturb the molecular orientation through the bulk cell, leading to a change from the original pre-tilt. The new pre-tilt will be observed in the direction in which the control beam is shone [61]. The resultant reorientation of the pre-tilt field in the bulk medium is then a nonlinear effect induced by the molecular reaction to the control beam at the boundary and is not directly caused by a molecular reaction in the bulk NLC. The main effect that the inclusion of dye molecules has in the bulk is to cause an increase in the Fréedericksz transition threshold due to the charge-screening effect. This means that a stronger static/low-frequency electric field is required to induce an initial pre-tilt in the nematic molecules. However, this is only of concern to experimentalists [63]. Any other effects that the control beam or dye molecules have on molecular alignment in the bulk can be assumed to be negligible.

A general prevalence of dye adsorption or desorption at the NLC surface when the control beam illuminates the interface is fundamentally responsible for an increase or decrease in the refractive index of the bulk DD-NLC in the illuminated region [63], as illustrated in the sketch of Figure 5.1 where additional adsorption of dye molecules at the boundary leads to a reduced director angle orientation in the bulk. This adsorption/desorption prevalence can be controlled by the polarisation and/or intensity of the control beam [63, 64]. Consequently, the nonlinear response, and by association the refractive index, of the DD-NLC in the illuminated region can be indirectly optically tuned. The control beam illumination subjects an area of the DD-NLC to what will be termed a refractive index defect. Such an index defect was placed in the path of

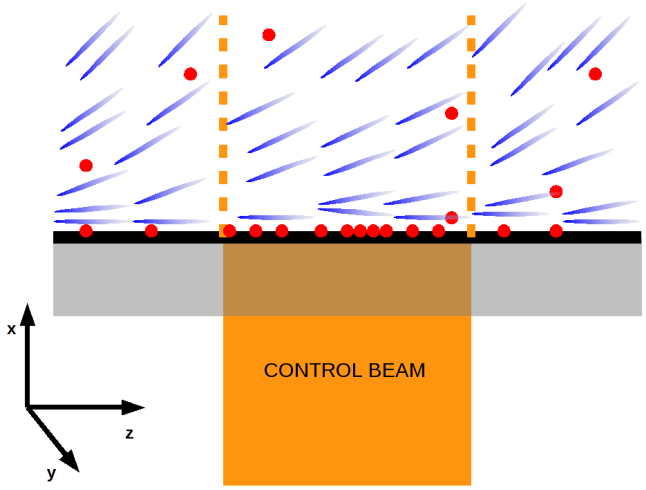

Figure 5.1: Sketch of adsorption of dye molecules (red circles) at the surface of the interface causing a change in orientation of nematic molecules (blue cigar-shapes) through the bulk cell.

nematicons propagating through a DD-NLC in experiments conducted by Piccardi *et al* [16]. In this work the inherent stability of nematicons, once formed, was verified by nematicon survival through the index defect. Furthermore, nematicon large angle refraction and total internal reflection (TIR) were observed, induced by the perturbation of the refractive index in the defect. Since this index perturbation can be optically tuned by the control beam parameters, the angle of refraction or reflection was also tunable, resulting in the ability to steer nematicons in a desired direction. In addition, copolarised weak beams were introduced and were observed being confined by the nematicon and steered in the direction that the nematicon took.

A pre-tilt of the nematic molecules of $\pi/4$ was achieved via rubbing at one of the interfaces in these experiments [16]. Whilst this ensured the desired pre-tilt in the bulk and planar anchoring conditions at the boundary, a static/low-frequency electric field applied across the thickness x can be used to control and vary the initial pre-tilt of the bulk nematic and thus control the nonlocality of the medium. Investigations conducted by Simoni *et al* [63] and Lucchetti *et al* [62] revealed that a low-frequency electric field applied to the DD-NLC cell creates a large controllable nonlinear response of the medium to light beams entering the cell. It is anticipated then that nematicons may be formed in the manner of Piccardi *et al* [16], but with the advantage of control of the pre-tilt outside of the illuminated region, dictated by an applied electric field such as that employed by Simoni *et al* and Lucchetti *et al* [62, 63].

The present work theoretically addresses the steering of nematicons passing through an index defect in a DD-NLC with an initial pre-tilt dictated by an applied static/low-frequency electric field. Before considering nematicon propagation, the index defect in the DD-NLC must first be defined. Let θ_b be the reorientation of the director angle from the initial pre-tilt value $\hat{\theta}$ caused by the control beam. This reorientation can be in the same direction as that of the optical beam reorientation θ_a (discussed below) or can be in the opposite direction, depending on the polarisation and/or intensity of the illumination [16]. If E represents the electric field of the control beam, the equation governing the effect of the index defect on the reorientation of the nematic molecules through z is given by

$$q \sin 2\theta_b + 2p|E|^2 \cos 2\theta_b = \nu \frac{\partial^2 \theta_b}{\partial z^2}, \tag{5.1}$$

where $p = \pm 1$, the sign being determined by the direction of the refractive index reorientation. Assuming small deviation from the pre-tilt $\hat{\theta}$, this equation can be approximated by

$$2q\theta_b + 2p|E|^2 = \nu \frac{\partial^2 \theta_b}{\partial z^2}. \tag{5.2}$$

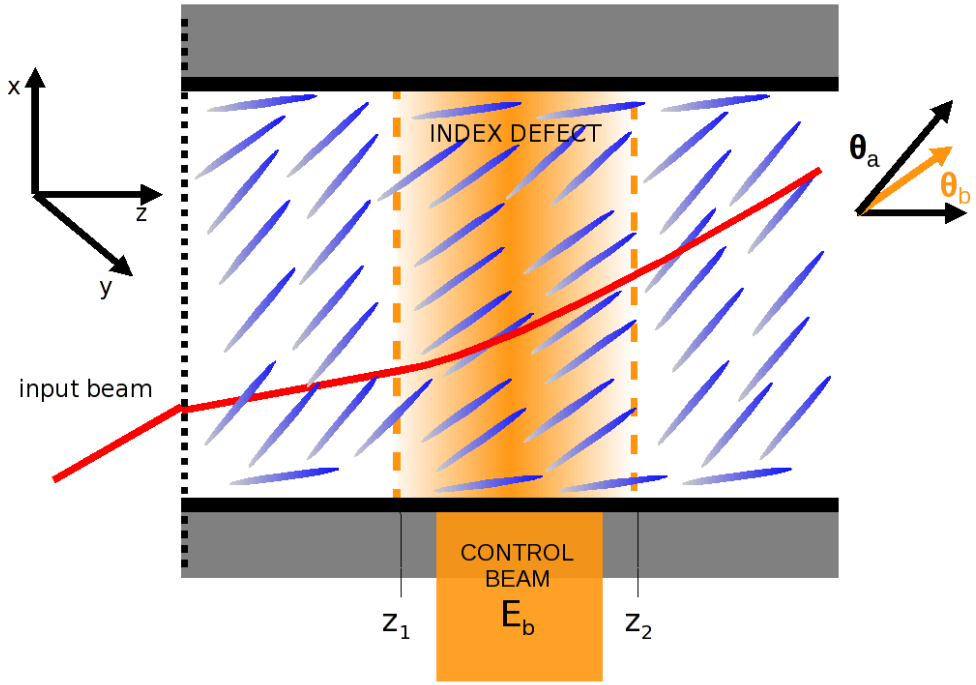

Figure 5.2: Schematic diagram of a dye-doped nematic liquid crystal cell with an optically rarer index defect. An x-polarised beam is propagating through the cell.

Let us assume that a stripe-shaped control beam in the (x, z)-plane is shone into the DD-NLC from the cell boundary between $z = z_1$ and $z = z_2$. Neglecting any beam spreading, the electric field of the control beam is defined as

$$E = \begin{cases} E_b, & \text{if} \quad z_1 < z < z_2 \\ 0, & \text{otherwise} \end{cases} . \tag{5.3}$$

Solving equation (5.2) with the boundary condition (5.3), the director distribution within the index defect is given by

$$\theta_b = pF(z)e^{-\gamma x} = \begin{cases} pA_1 e^{\sqrt{\frac{2q}{\nu}}z} e^{-\gamma x}, & z < z_1, \\ p\left(A_2 e^{-\sqrt{\frac{2q}{\nu}}z} + A_3 e^{\sqrt{\frac{2q}{\nu}}z} - \frac{|E_b|^2}{q}\right) e^{-\gamma x}, & z_1 < z < z_2, \\ pA_4 e^{-\sqrt{\frac{2q}{\nu}}z} e^{-\gamma x}, & z > z_2, \end{cases} \tag{5.4}$$

where

$$\begin{aligned} A_1 &= \frac{|E_b|^2}{2q}\left(-e^{-\sqrt{\frac{2q}{\nu}}z_1} + e^{-\sqrt{\frac{2q}{\nu}}z_2}\right), \\ A_2 &= \frac{|E_b|^2}{2q} e^{\sqrt{\frac{2q}{\nu}}z_1}, \\ A_3 &= \frac{|E_b|^2}{2q} e^{-\sqrt{\frac{2q}{\nu}}z_2}, \\ A_4 &= \frac{|E_b|^2}{2q}\left(e^{\sqrt{\frac{2q}{\nu}}z_1} - e^{\sqrt{\frac{2q}{\nu}}z_2}\right). \end{aligned} \tag{5.5}$$

The exponential decay in x, with decay rate γ, has been introduced to account for the observed decay of the beam intensity due to scattering losses [64]. When the index defect causes a negative

refractive index change, corresponding to an optically rarer region, the director distribution is $\theta_b = F(z)\exp(-\gamma x)$, and for an optically denser region the director distribution is $\theta_b = -F(z)\exp(-\gamma x)$.

With the index defect now defined, the equations governing nematicon propagation can be derived. Consider an x-polarised, coherent light beam propagating through a cell filled with a nematic liquid crystal and mixed with a small amount of dye-dopant, as illustrated in Figure 5.2. The transverse coordinates (x, y) are orthogonal to the z direction. The input beam is launched and initially propagates at an arbitrary angle with respect to the z direction. Let θ_a be the perturbation of the optical director angle due to the light beam (nematicon) from the initial pre-tilt $\hat{\theta}$ determined by the external bias and θ_b be the perturbation of the director from the initial pre-tilt induced by the index defect due to the control beam. If u represents the slowly-varying electric field envelope of the light beam, the governing equations of the nematicon in the bulk DD-NLC are

$$i\frac{\partial u}{\partial z} + \frac{1}{2}\nabla^2 u + u\sin 2\left(\theta_a + \theta_b\right) = 0, \tag{5.6}$$

$$q\sin 2\theta_a - 2|u|^2\cos 2\theta_a = \nu\nabla^2\theta_a, \tag{5.7}$$

where the Laplacian ∇^2 is in the (x, y)-plane. q is determined from the square of the static/low-frequency electric field and is related to the pre-tilt of the nematic. ν is a measure of the elastic response, or nonlocality, of the nematic, with a local response corresponding to ν small. The DD-NLC must be assumed to possess a nonlocal response if the indirect optical perturbation of the pre-tilt by the control beam is to be achieved for the index defect in the bulk DD-NLC [61]. Hence the ν large limit must be taken.

The index defects, represented by equation (5.4), are much simplified approximations to the defects introduced by Piccardi *et al*, which were induced by an elliptical control beam with a Gaussian profile that introduced a graded-index perturbation [16] into the cell. Such a perturbation naturally spreads and decays through the thickness of the cell due to diffraction and scattering losses. Giving a Gaussian profile to the control beam E_b would yield very complicated, and possibly intractable, modulation equations. Additionally, if a simple control beam was modelled by the modulation equations and solutions compared with full numerical solutions for which the control beam was modelled as a Gaussian, the comparison would be unreasonable since the modulation equations would be approximating a completely different index defect. The best compromise then has been to simplify the control beam profile to a one-dimensional stripe. Decay in x due to scattering losses is accounted for by the factor $\exp(-\gamma x)$. The director perturbation outside of the region illuminated by the control beam due to the nonlocal response of the nematic is included by the terms $\exp(\lambda z)$ for $z < z_1$ and $\exp(-\lambda z)$ for $z > z_2$, where $\lambda = \sqrt{2q/\nu}$, but diffractive spreading of the perturbation as x increases is not included in the approximation. Additionally, spreading in the (y, z)-plane has been neglected to simplify the analysis. A typical resulting extraordinary refractive index n_e is shown in Figure 5.3.

As a final note, in Chapters 3 & 4 birefringent Poynting vector walk-off was factored out of the two-colour nematicon equations by a phase factor. This was allowed because walk-off was constant throughout the medium. Strictly speaking here, however, the Poynting vector walk-off cannot be treated in the same fashion because it was shown experimentally to be variable due to the index defect deviating the nematicon path [16]. To keep the analysis reasonably simple an approximation is made whereby it is assumed that Poynting vector walk-off is not affected by the index perturbation. With this approximation nematicon evolution in a DD-NLC with a simple index defect can be modelled by equations (5.6), (5.7) and (5.4).

5.2 Analysis

5.2.1 Modulation Equations

If a large pre-tilt of the nematic molecules is induced, which is close to and above the optimum pre-tilt of $\pi/4$ with respect to the direction of propagation of the beam [16, 19], it can be seen

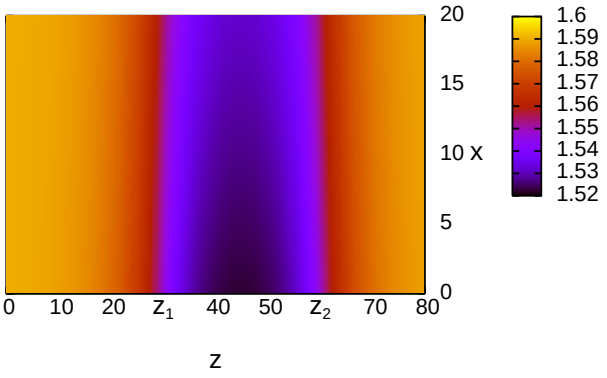

Figure 5.3: Typical refractive index profile n_e produced by a control beam causing a negative reorientation of the director.

from the director equation (5.7) that θ_a, the optically induced deviation of the director angle from the pre-tilt value outside the illuminated region, is small at low input beam powers. In this $|\theta_a|$ small limit the governing equations (5.6) and (5.7) may be approximated by

$$i\frac{\partial u}{\partial z} + \frac{1}{2}\nabla^2 u + 2u\left(\theta_a + \theta_b\right) = 0, \tag{5.8}$$

$$2q\theta_a - 2|u|^2 = \nu\nabla^2\theta_a, \tag{5.9}$$

where θ_b is defined by equation (5.4), found by taking a similar small deviation assumption. Equations (5.8) and (5.9) have the corresponding Lagrangian formulation

$$L = i\left(u^* u_z - u u_z^*\right) - |\nabla u|^2 + 4\left(\theta_a + \theta_b\right)|u|^2 - \nu|\nabla\theta_a|^2 - 2q\theta_a^2, \tag{5.10}$$

where the superscript * denotes the complex conjugate. To obtain approximate modulation equations for the beam parameters trial functions are now inserted into the averaged Lagrangian given by

$$\mathcal{L} = \int_{-\infty}^{\infty}\int_{-\infty}^{\infty} L\, dxdy. \tag{5.11}$$

Appropriate trial functions for the electric field of the light beam u and the director angle θ_a respectively are

$$u = a\,\mathrm{sech}\,\frac{\chi}{w}\,e^{i\psi} + ige^{i\psi}, \qquad \theta_a = \alpha\,\mathrm{sech}^2\,\frac{\chi}{\beta}, \tag{5.12}$$

where

$$\chi = \sqrt{(x-\xi)^2 + y^2}, \qquad \psi = \sigma + V\left(x - \xi\right). \tag{5.13}$$

The electric field amplitude a, width w, nematicon position ξ, velocity V, phase σ and shelf amplitude g are functions of z. The first term in the trial function for u is a solitary wave with variable parameters. The second term represents the out of phase interaction of the nematicon

with a flat shelf of low-amplitude diffractive radiation which develops under the evolving beam and travels with it. These trial functions are identical to those used in Chapter 3 and for a variety of different nematicon regimes. If the shelf were assumed to have non-zero amplitude throughout the bulk medium the mass of the shelf would be infinite. Hence the shelf is assigned a radius $0 \leq \chi \leq R$ within which it is non-zero [30, 31, 65].

The first step to deriving the modulation equations for these trial functions is to insert the trial functions (5.12) into the averaged Lagrangian (5.11). All of the averaged Lagrangian integrals can be evaluated exactly except the cross integral

$$\int_{-\infty}^{\infty}\int_{-\infty}^{\infty} |u|^2\theta_b dxdy. \tag{5.14}$$

To calculate this integral 'equivalent' Gaussians are once again utilised whereby sech terms in the integral are replaced by Gaussians, $\text{sech}^2(\chi/w) \to \exp\left(-\chi^2/(B^2w^2)\right)$, $\text{sech}^2(\chi/\beta) \to \exp\left(-\chi^2/(A^2\beta^2)\right)$, with width correction coefficients A and B. These equivalent Gaussians are the same as those used in Chapter 3 and were chosen because the cross integral involves two structures with distinct widths, where $w \ll \beta$ due to the high nonlocality of the nematic response. A and B are calculated by matching the Taylor series of the original integral using sech trial functions in the limit $w \ll \beta$ to the equivalent Gaussian result [39], yielding

$$A = \frac{I_2\sqrt{2}}{\sqrt{I_{32}}}, \quad \text{and} \quad B = \sqrt{2I_2}. \tag{5.15}$$

The final averaged Lagrangian for these trial functions is

$$\begin{aligned}\mathcal{L} = &-2\left(a^2w^2I_2 + \Lambda g^2\right)(\sigma' - V\xi') - 2I_1aw^2g' + 2I_1gw^2a' \\ &+4I_1awgw' - a^2I_{22} - \left(a^2w^2I_2 + \Lambda g^2\right)V^2 - 4\nu I_{42}\alpha^2 \\ &-2qI_4\alpha^2\beta^2 + \frac{2A^2B^2\alpha a^2\beta^2w^2}{A^2\beta^2 + B^2w^2} + 2F(z)a^2B^2w^2e^{-\gamma\xi+\gamma^2B^2w^2/4},\end{aligned} \tag{5.16}$$

where $'$ denotes differentiation with respect to z. The insertion of the trial functions (5.12) into the averaged Lagrangian (5.11) allows variations of the beam parameters to be taken. For simplicity we set $\theta_b = F(z)e^{-\gamma x}$, where $F(z)$ is defined by equation (5.4), and $\Lambda = \frac{1}{2}\ell^2$. The modulation equations of the nematicon are given by

$$\delta\sigma: \quad \frac{d}{dz}\left(I_2a^2w^2 + \Lambda g^2\right) = 0, \tag{5.17}$$

$$\delta V: \quad 2\left(\frac{d\xi}{dz} - V\right)\left(a^2w^2I_2 - \Lambda g^2\right) = 0, \tag{5.18}$$

$$\delta g: \quad \frac{d}{dz}\left(aw^2I_1\right) - \Lambda g\left(\frac{d\sigma}{dz} - V\frac{d\xi}{dz} + \frac{1}{2}V^2\right) = 0, \tag{5.19}$$

$$\delta a: \quad -2aw^2I_2\left(\frac{d\sigma}{dz} - V\frac{d\xi}{dz}\right) - I_1w^2\frac{dg}{dz} - I_1\frac{d}{dz}\left(gw^2\right) + 2I_1wg\frac{dw}{dz} \tag{5.20}$$

$$-aI_{22} - aw^2I_2V^2 + \frac{2A^2B^2a\alpha w^2\beta^2}{A^2\beta^2 + B^2w^2} + 2F(z)B^2aw^2e^{-\gamma\xi+\frac{1}{4}\gamma^2B^2w^2} = 0, \tag{5.21}$$

$$\delta w: \quad -2a^2wI_2\left(\frac{d\sigma}{dz} - V\frac{d\xi}{dz}\right) - 4I_1aw\frac{dg}{dz} - I_2a^2wV^2 + \frac{2A^4B^2a^2\alpha w\beta^4}{\left(A^2\beta^2 + B^2w^2\right)^2} \tag{5.22}$$

$$+2F(z)B^2a^2we^{-\gamma\xi+\frac{1}{4}\gamma^2B^2w^2} + \frac{1}{2}F(z)B^2\gamma^2a^2w^3e^{-\gamma\xi+\frac{1}{4}\gamma^2B^2w^2} = 0, \tag{5.23}$$

$$\delta\xi: \quad \frac{d}{dz}\left[2\left(a^2w^2I_2 + \Lambda g^2\right)V\right] + 2F(z)B^2\gamma a^2w^2e^{-\gamma\xi+\frac{1}{4}\gamma^2B^2w^2} = 0, \tag{5.24}$$

with the algebraic equations

$$\delta\alpha: \quad -4\nu I_{42}\alpha - 2qI_4\alpha\beta^2 + \frac{A^2B^2a^2w^2\beta^2}{A^2\beta^2 + B^2w^2} = 0, \tag{5.25}$$

$$\delta\beta: \quad -qI_4\alpha^2\beta + \frac{A^2B^4a^2\alpha w^4\beta}{\left(A^2\beta^2 + B^2w^2\right)^2} = 0. \tag{5.26}$$

Modulation equations (5.17)–(5.26) can then be rearranged to the simpler form

$$\frac{d}{dz}\left(I_2a^2w^2 + \Lambda g^2\right) = 0, \tag{5.27}$$

$$\frac{d}{dz}\left(I_1aw^2\right) = \left(\frac{d\sigma}{dz} - V\frac{d\xi}{dz} + \frac{1}{2}V^2\right), \tag{5.28}$$

$$I_1\frac{dg}{dz} = \frac{I_{22}a}{2w^2} - \frac{A^2B^4aw^2\alpha\beta^2}{\left(A^2\beta^2 + B^2w^2\right)^2} + \frac{1}{4}F(z)\gamma^2B^4aw^2e^{-\gamma\xi + \frac{1}{4}\gamma^2B^2w^2}, \tag{5.29}$$

$$I_2\left(\frac{d\sigma}{dz} - V\frac{d\xi}{dz}\right) = -\frac{I_{22}}{w^2} - \frac{1}{2}I_2V^2 + \frac{A^2B^2\alpha\beta^2\left(A^2\beta^2 + 2B^2w^2\right)}{\left(A^2\beta^2 + B^2w^2\right)^2}$$
$$+F(z)B^2\left(1 - \frac{\gamma^2B^2w^2}{4}\right)e^{-\gamma\xi + \frac{1}{4}\gamma^2B^2w^2}, \tag{5.30}$$

$$\frac{d}{dz}\left[V\left(I_2a^2w^2 + \Lambda g^2\right)\right] = -F(z)\gamma a^2B^2w^2e^{-\gamma\xi + \frac{1}{4}\gamma^2B^2w^2}, \tag{5.31}$$

$$\frac{d\xi}{dz} = V, \tag{5.32}$$

where

$$\alpha = \frac{A^2B^4a^2w^4}{qI_4\left(A^2\beta^2 + B^2w^2\right)^2} \quad \text{and} \quad \alpha = \frac{A^2B^2a^2\beta^2w^2}{\left(A^2\beta^2 + B^2w^2\right)\left(4\nu I_{42} + 2qI_4\beta^2\right)}. \tag{5.33}$$

The definite integrals I_i and I_{ij} resulting from the averaged Lagrangian calculation are

$$\begin{aligned}
I_1 &= \int_0^\infty x\,\mathrm{sech}\,x\,dx = 2C,\\
I_2 &= \int_0^\infty x\,\mathrm{sech}^2\,x\,dx = \ln 2,\\
I_4 &= \int_0^\infty x\,\mathrm{sech}^4\,x\,dx = \frac{2}{3}\ln 2 - \frac{1}{6},\\
I_{22} &= \int_0^\infty x\,\mathrm{sech}^2\,x\tanh^2 x\,dx = \frac{1}{3}\ln 2 + \frac{1}{6},\\
I_{32} &= \int_0^\infty x^3\,\mathrm{sech}^2\,x\,dx = 1.3523145016\ldots,\\
I_{42} &= \frac{1}{4}\int_0^\infty x\left[\frac{d}{dx}\,\mathrm{sech}^2\,x\right]^2 dx = \frac{2}{15}\ln 2 + \frac{1}{60},
\end{aligned} \tag{5.34}$$

where C is the Catalan constant $C = 0.915965594\ldots$. Mass conservation is ruled by equation (5.27) and equation (5.31) is the equation of momentum conservation. Some disparities between these modulation equations and those of Chapter 3 are immediately noticeable. Equations (5.29)–(5.31) include terms relating to the index defect. The momentum conservation equation (5.31) is no longer homogeneous, with the rate of change of momentum of the beam now being proportional to γ, the decay rate in x of the boundary-driven reorientational effect of the index defect. Consequently for non-negligible values of γ, the beam will be expected to experience a rate of change of momentum, or force, in the x direction due to the small differences in molecular orientation on either side of the beam.

The energy equation can be derived by applying Nöther's Theorem to the Lagrangian which

shows that the nematicon equations possess the energy conservation equation

$$\frac{dH}{dz} = \frac{d}{dz}\int_{-\infty}^{\infty}\int_{-\infty}^{\infty}\left[|\nabla u|^2 - 4\theta_a|u|^2 - 4\theta_b|u|^2 + \nu|\nabla\theta_a|^2 + 2q\theta_a^2\right]\,dxdy = 0. \tag{5.35}$$

Inserting the trial functions into (5.35) and using the mass, momentum and ξ variational equations appropriately results in the total energy conservation equation

$$\frac{d}{dz}[a^2 I_{22} + 4\nu I_{42}\alpha^2 + 2qI_4\alpha^2\beta^2 - \frac{2A^2B^2\alpha\beta^2a^2w^2}{A^2\beta^2 + B^2w^2} - 2F(z)a^2B^2w^2e^{-\gamma\xi+\frac{1}{4}\gamma^2B^2w^2}] = 0. \tag{5.36}$$

Since energy is conserved, this equation can be used to predict the final steady state of the nematicon from the input beam. But the decay onto the steady nematicon state has not been modelled by the modulation equations yet. The mechanism behind this decay is loss to diffractive radiation.

5.2.2 Radiation Calculation

García-Reimbert *et al* calculated the diffractive radiation shed by a nematicon as it evolves and included the effect of this shed radiation in the modulation equations for nematicon evolution in the local limit [30]. Radiative losses in the current regime are governed by the same linearised field equations, which are solved using Laplace transforms. As for the radiation calculation of Chapter 3, there is an additional component to the radiation shelf here resulting from the nonlocality of the nematic reaction to the beam. The director beam is extended, which in turn extends the tail of the radiation shelf travelling with the beam. To account for this extension, the radiation shelf is split into two components; the radiation shelf with radius R relates to the component travelling and interacting with the beam; the radius ρ relates to the shelf's interaction with the director, with $\rho \gg R$. Minzoni *et al* estimated the value of ρ from numerical solutions [39]. Denoting the half-width of the optical disturbance by $\beta_{1/2}$, and introducing the relation $\tilde{\Lambda} = \rho^2/2$, ρ is approximated by

$$\tilde{\Lambda} = \frac{1}{2}\rho^2 = \left(7\beta_{1/2}\right)^2. \tag{5.37}$$

Mass shed from the beam forms the major contribution to the radiation shed as it propagates. The mass flux lost to dispersive radiation from the beam is found by integrating the mass equation from the edge of the shelf $r = \rho$ to infinity

$$\frac{d}{dz}\int_{\rho}^{\infty} r|u|^2dr = \mathrm{Im}\left(ru^*u_r\right)|_{r=\rho} + O[\rho(z)]. \tag{5.38}$$

To find this mass flux, the shed radiation must be matched to the shelf under the beam at the boundary between them. The final result is similar to that shown in Section 3.2.2 in that equation (5.29) for the radiation shelf height g and the mass conservation equation (5.27) gain a loss term δ

$$I_1\frac{dg}{dz} = \frac{I_{22}a}{2w^2} - \frac{A^2B^4aw^2\alpha\beta^2}{\left(A^2\beta^2 + B^2w^2\right)^2} + \frac{1}{4}F(z)\gamma^2B^4aw^2e^{-\gamma\xi+\frac{1}{4}\gamma^2B^2w^2} - 2\delta g, \tag{5.39}$$

$$\frac{d}{dz}\left(I_2a^2w^2 + \Lambda g^2\right) = -2\delta\tilde{\Lambda}\kappa^2, \tag{5.40}$$

where the loss coefficient δ is

$$\begin{aligned}\delta \;=\; & -\frac{\sqrt{2\pi}I_1}{2e\kappa\tilde{\Lambda}}\int_0^z \pi\kappa(z')\ln((z-z')/\tilde{\Lambda})\left[\left\{\left[\frac{1}{2}\ln((z-z')/\tilde{\Lambda})\right]^2 + \frac{3\pi^2}{4}\right\}^2\right. \\ & \left.+\pi^2\left[\ln((z-z')/\tilde{\Lambda})\right]^2\right]^{-1}\frac{dz'}{(z-z')}.\end{aligned} \tag{5.41}$$

Finally

$$\kappa^2 = \frac{1}{\tilde{\Lambda}} \left[I_2 a^2 w^2 - I_2 \hat{a}^2 \hat{w}^2 + \tilde{\Lambda} g^2 \right]. \tag{5.42}$$

Equations (5.28), (5.30)–(5.32), (5.39) and (5.40) form the full set of modulation equations for the evolution of a nematicon in a DD-NLC with an index defect.

5.2.3 Adjustments to Numerical Methods

The modulation equations were solved using the standard fourth order Runge-Kutta scheme. The full nematicon electric field equation (5.6) was solved using a pseudo-spectral method based on that of Fornberg & Whitham [42], with θ_b defined by equation (5.4). The main difference from the scheme created by Fornberg & Whitham is that the stepping in the z direction is performed in Fourier space using a fourth order Runge-Kutta method, rather than in physical space using a second order scheme. The director equation (5.7) was solved using fast Fourier transforms (FFTs) in the x direction, followed by a standard Picard iteration of the resultant two-point boundary value problem in y. These methods are summarised in detail in Chapter 2.

5.3 Results

In this section solutions of the modulation equations (5.28), (5.30)–(5.32), (5.39) and (5.40) will be compared with numerical solutions of the full nematicon equations (5.6)–(5.7). The full governing equations have been numerically solved using step sizes $\Delta x = \Delta y = 0.2$ and $\Delta z = 0.005$, with spatial intervals 409.6 and 204.8 in the x and y directions respectively. The computational domain has been increased and step sizes have been reduced from those values used to solve two-colour nematicon equations in Chapters 3 & 4. This is because there are only two governing equations to be solved, and thus computational speed increases for equal step sizes and domains. Whilst there is an almost negligible graphical difference when comparing the solutions given here with those using the stepping and intervals used to solve the two-colour nematicon equations, it will be shown that some notable comparisons can be made between the full numerical solutions and the solutions of the modulation equations from small differences between the two. Consequently a higher accuracy has been sought for both full numerical and modulation solutions so as to measure these differences accurately. With this in mind, the stepping in z for the solution of the approximate modulation equations has also been reduced to $\Delta z = 0.002$. A value of E_b has been taken which closely matches physical values obtained by Piccardi *et al* [16] and the reorientational decay factor γ has been chosen so that significant decay of the reorientational effect of the defect in x can be observed. Nonlocality has been given the value $\nu = 200$, which is experimentally realistic. For example, the nonlocality of the DD-NLC medium in the experiments conducted by Piccardi *et al* was $\nu \approx 144$ [16, 66, 67]. Once again the numerical solutions of the modulation equations will be named 'modulation solutions' and the numerical solutions of the full governing equations will be referred to as 'full numerical solutions.'

A comparison between a full numerical solution and a modulation solution for (a) the beam peak position and (b) beam amplitude is presented in Figure 5.4 for a DD-NLC with an optically rarer index defect, i.e. the defect causes a decrease in refractive index. There is near perfect agreement in the position of the maximum of the nematicon and very good agreement for the amplitude. A beam with an initial trajectory of $V = 0$ would be expected to propagate straight parallel to the z axis with no deviation of its course. This is not the case here, as there is a clear refraction of the beam trajectory within and near the boundaries of the illuminated region. The cause of the observed beam refraction is the non-uniform index distribution through the bulk which is ruled by γ, the decay in strength of the reorientational effect in the index defect through the bulk medium in the x direction. A beam propagating through the index defect experiences γ decay as a force which deviates it in the direction of increased molecular reorientation θ_b. From the modulation equations the cause of this beam refraction can easily be verified. The momentum equation (5.32) shows that the rate of change of momentum, or the force, exerted on the beam is proportional to γ. It can then be shown that γ refraction is ruled by a completely different refraction mechanism to that found by Piccardi *et al*, where refraction was a Poynting

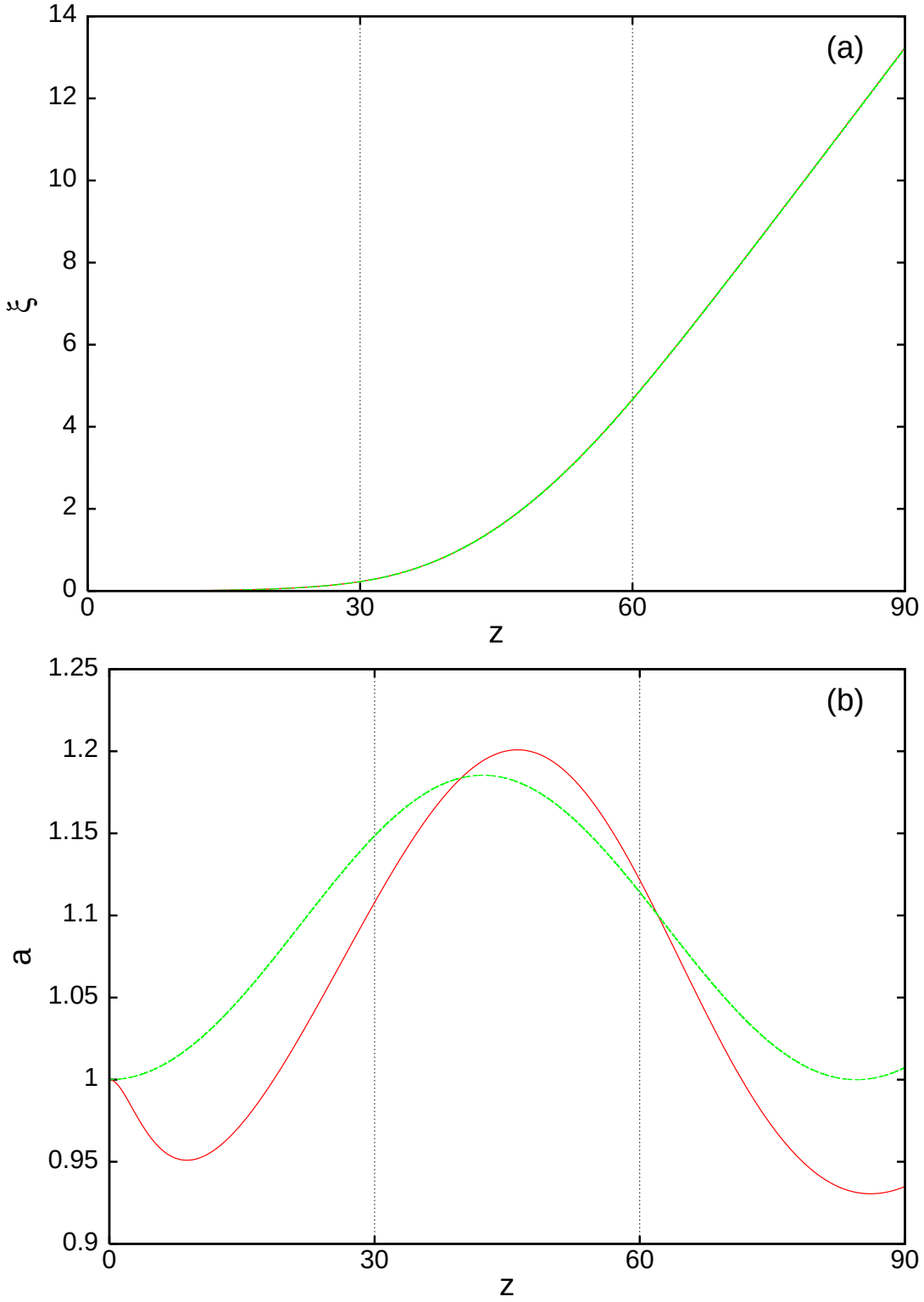

Figure 5.4: Comparisons in a DD-NLC with an optically rarer index defect for the initial conditions $a = 1.0$, $w = 3.5$, $V_0 = 0.0$, $\xi = 0.0$, $E_b = 1.0$, $\gamma = 0.01$, $\nu = 200$ and $q = 2$ with $z_1 = 30$ and $z_2 = 60$. Full numerical solution (—)[red]; solution of modulation equations (— — —)[green]. (a) Positions, (b) Amplitudes.

vector walk-off effect brought about by a complicated interaction between a variety of properties of the medium and beam [16]. Another notable observation is that refraction begins before the beam reaches the illuminated region. The reorientational effect, induced by the control beam illumination in $30 < z < 60$, extends beyond the region itself due to the effect of nonlocality, as can be seen from equation (5.4) for θ_b, and this is clearly the reason for the observed refraction early in the evolution. What is remarkable is that the approximate momentum equation models the dynamical behaviour of the beam as given by the full governing equations so accurately.

Figure 5.5 is the symmetric equivalent of Figure 5.4 but here the DD-NLC contains an optically denser index defect. An optically denser index defect is created when dye molecule desorption prevails over adsorption at the boundary of the DD-NLC. The beam refracts by roughly the same amount in the opposite direction due to an increase of the refractive index within the defect. Once again the agreement between the full numerical solutions and the modulation solutions is very good, with most features of the dynamical evolution modelled well by the approximation.

One point of interest can be found in the difference between the large z amplitude evolution when comparing the full numerical solutions for optically rarer (Figure 5.4) and denser (Figure 5.5) index defects. The optically rarer index defect example displays a smooth amplitude oscillation throughout the evolution, whereas the amplitude oscillations for the optically denser example gain a perturbation at $z \approx 80$ which is almost undetectable for the solution presented in Figure 5.5. A further example exhibiting a perturbation is given in Figure 5.6 to highlight this behaviour. Perturbations are shown to increase when the intensity of the control beam is increased. In this example the control beam electric field has been increased from $E_b = 1.0$ to $E_b = 1.5$. It is also worth noting that $V = 0$ has been chosen to show that the effect is not brought about by a large initial velocity. Perturbed oscillations begin when the beam exits the index defect and returns to a region of lower refractive index. Figure 5.6 shows that the beam becomes destabilised by the amplitude oscillation perturbations and eventually forms multiple nematicons. This effect is most clear in Figure 5.6(a) where the beam maximum position can be seen to discontinuously jolt from one of the two newly formed beams to the other near $z = 80$. An even more extreme perturbation can be induced when a nematicon is given a high initial velocity and passes through an index defect induced by a high intensity control beam, as shown in Figure 5.7. In this figure the beam has split into two nematicons and the director beam has also split along similar lines. These profiles have diverged from the steady nematicon profile which resembles sech and Gaussian profiles closely. Consequently, a combination of high nematicon beam velocity and high control beam intensity cannot be modelled by a fixed ansatz approach, limiting the range of the approximate method. A control beam intensity of $E_b = 1.5$ is physically unrealistic, therefore this result is only of theoretical interest.

Figure 5.8 highlights the fundamental role that the decay factor γ plays for nematicon evolution in the current regime. The comparisons of peak position and amplitude, respectively, are for two nematicons with sech trial functions and equal initial conditions other than the value of γ, where the decay is 10 times stronger for the dashed green-coloured beam. The stronger decay causes abrupt changes in the amplitude of the nematicon very early in its propagation. Momentum dependence on γ means that there is then a larger refraction of the beam for larger γ which affects amplitude & width oscillations. This result is in accord with the results obtained for two-colour nematicons in Chapters 3 & 4 which showed that position & velocity oscillations were largely independent of amplitude & width oscillations, but if one of these oscillations grows significantly then the other oscillation is influenced. Unfortunately a comparison with modulation solutions is impossible here since the decay is too strong for any modulation solutions to be found. For $\gamma > 0.025$ there are no modulation solutions, whereas full numerical solutions exist for $0 \leqslant \gamma < 0.2$. It is clear that the full numerical solution experiences extreme amplitude changes and corresponding changes in position as γ increases. Such behaviour suggests that the solution diverges wildly from the initial sech beam profile. These changes cannot be modelled by the modulation equations. Whilst it is interesting that the range of modulation solutions is limited in comparison with full numerical solutions, values of γ beyond $\gamma \approx 0.02$ are not experimentally realistic. The decay rate of $\gamma = 0.01$, which has been chosen for most of the results presented, is a physically reasonable one. For this value the modulation solutions are remarkably accurate, particularly in relation to refraction, as shown in Figure 5.4. It is encouraging to note that both full numerical solutions and modulation

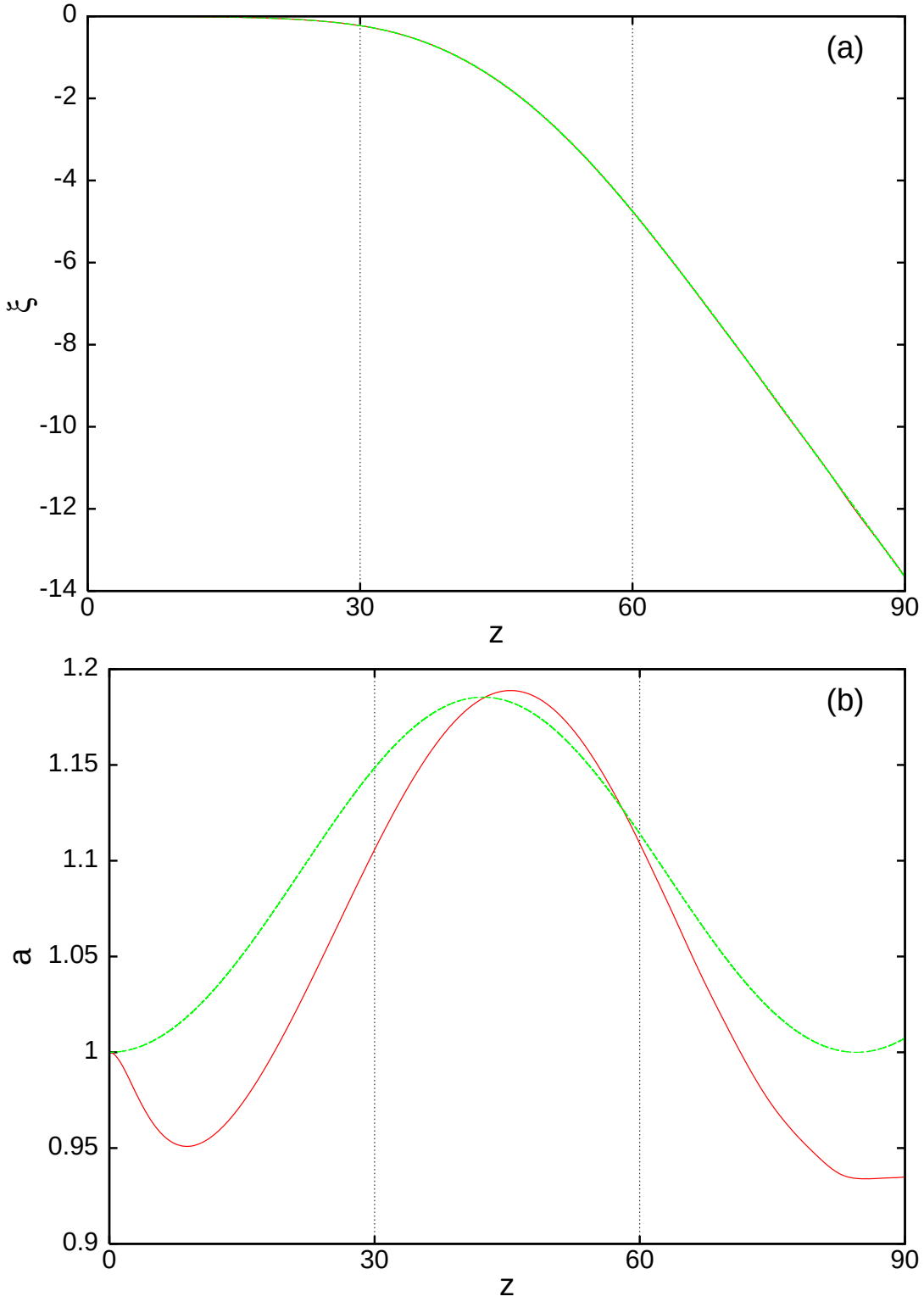

Figure 5.5: Comparisons in a DD-NLC with an optically denser index defect for the initial conditions $a = 1.0$, $w = 3.5$, $V_0 = 0.0$, $\xi = 0.0$, $E_b = 1.0$, $\gamma = 0.01$, $\nu = 200$ and $q = 2$ with $z_1 = 30$ and $z_2 = 60$. Full numerical solution (—)[red]; solution of modulation equations (— — —)[green]. (a) Positions, (b) Amplitudes.

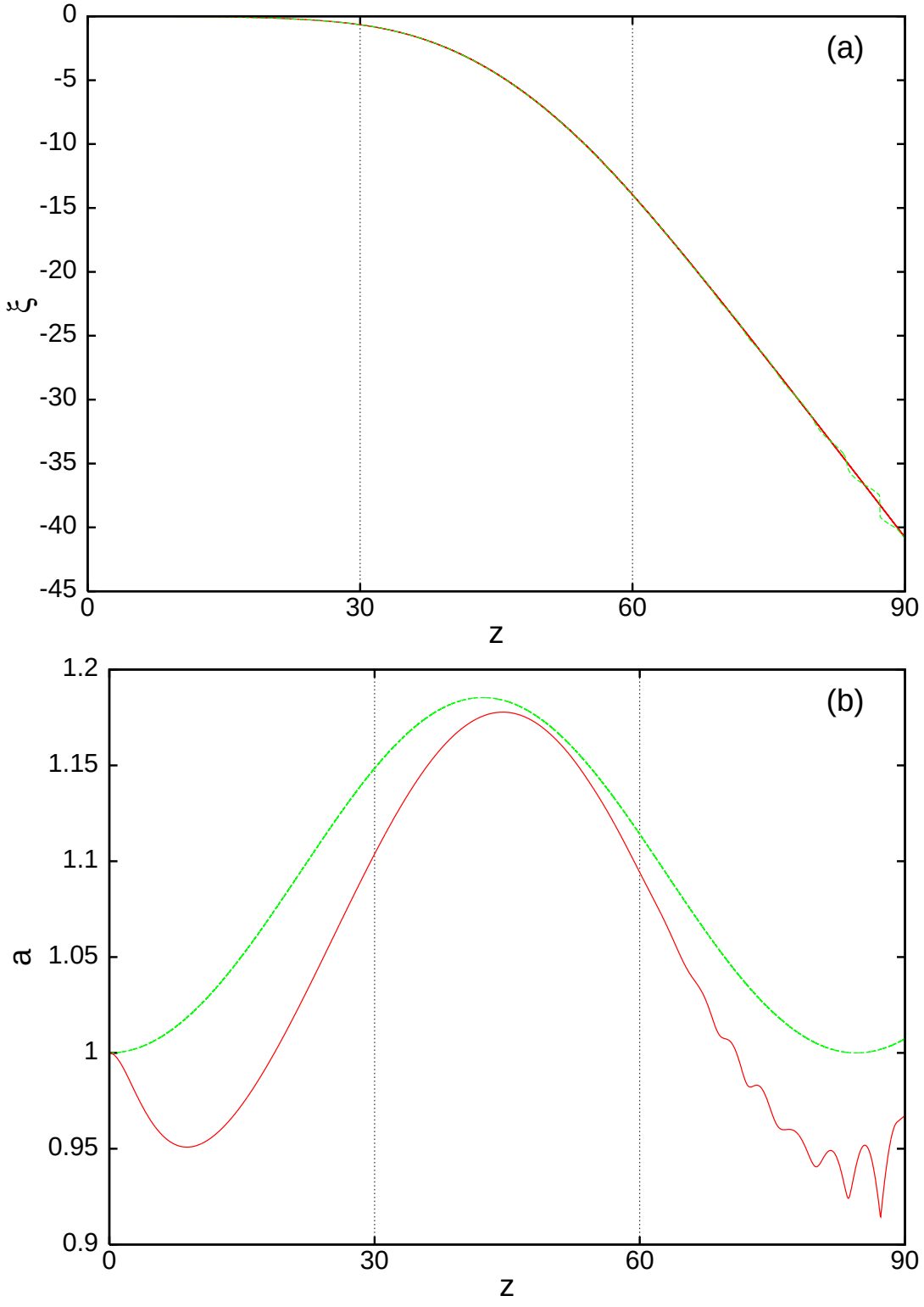

Figure 5.6: Comparisons for the initial values $a = 1.0$, $w = 3.5$, $V_0 = 0.0$, $\xi = 0.0$, $E_b = 1.5$, $\gamma = 0.01$, $\nu = 200$ and $q = 2$ where $z_1 = 30$ and $z_2 = 60$ with a sech initial profile. Full numerical solution (—)[red]; solution of modulation equations (— — —)[green]. (a) Positions, (b) Amplitudes.

solutions exist for physically realistic constants and initial conditions. It is also promising that no solutions exist outside of this physically realistic range. Both of these results justify the approach and the governing equations chosen.

The accuracy of the modulation solutions with respect to beam refraction for different initial V values is revealed in Figure 5.9. It is clear that the modulation theory is highly accurate for all values of V_0 presented, particularly for values close to 0. Figure 5.9(b) shows that differences begin to appear between the modulation and full numerical solutions for large negative V_0 values. One possible reason for this is that the beam begins to experience large profile changes at these higher velocities which cannot be modelled by the approximation with its fixed trial function.

Two-colour nematicons were steered by changing the initial velocity V_0 of one or both of the beams and nematicons travelling through a DD-NLC with an index defect can be steered in this way as well. But steering can also be achieved in the current regime by choosing different electric field strengths of the control beam E_b. Figure 5.10(a) shows the refraction angle as given by the modulation solutions and full numerical solutions for a nematicon where the initial velocity is set at $V_0 = 0$ and the control beam field strength is varied from $E_b = 0$ to $E_b = 2.0$. It is immediately clear that this steering technique allows a very large range of refraction angles to be achieved, although a negative refraction angle (refraction in the opposite direction in x) can only be achieved by varying V_0. Figure 5.9(b) showed that the modulation solution is highly accurate for $V_0 = 0.0$, $E_b = 1.0$ so it is not surprising that modulations solutions are highly accurate across the range of E_b in Figure 5.10(b), for which velocity has been chosen such that $V_0 = 0.0$.

Piccardi *et al* reported their observation of total internal reflection at the index defect for appropriate initial conditions [16]. Here, TIR cannot occur as the index defect has been chosen to be orthogonal to the z direction. A beam reflecting from the index defect would thus be required to propagate in the negative z direction. In other words, TIR is not possible within the current paraxial nonlinear Schrödinger-like (NLS-like) equation (5.6) model because z has been chosen as a time-like forward propagating coordinate. To account for TIR the NLS-like equation (5.6) must be replaced by one in 'ray' coordinates, for which the time-like variable z is replaced by the arc length s along the nematicon trajectory (ray) [18]. As the arc length increases monotonically, there is no 'backwards' propagation in the time-like variable when total internal reflection occurs. This approach leads to further complications in the analysis. Fortunately what has been found here are indications of where the beam would have reflected had the modelling approach allowed for TIR. Solutions were sought for increasingly large E_b and it was found that no modulation solutions exist for values $E_b > 2.4$ and no full numerical solutions exist for $E_b > 3.5$. This suggests that the higher refractive index perturbation caused by the increase in the control beam field grows to a value large enough to induce TIR. Similar trials were conducted for increasingly large $|V_0|$ and it was found that solutions could not be obtained for values of $|V_0| > 0.5$. Such a result reveals qualitative agreement with the experimental results of Piccardi *et al* who showed that, for appropriate initial conditions, beams reflect when incident upon an index defect at acute angles [16].

Figure 5.11 is analogous to Figure 5.9 comparing the refraction angles found for full numerical and modulations solutions, but here the comparison is made for nematicons propagating in a DD-NLC with an optically denser index defect. Once again the modulation solutions show excellent agreement with the full numerical results with respect to refraction. There is one noticeable difference, however, with the results obtained for an optically rarer index defect. The accuracy of the modulation solutions is lost when $E_b \to 2.0$ since the beam approaches and reaches an instability which cannot be modelled by the ansatz approach. This instability is caused by the beam passing from an optically denser region to an optically rarer region as it exits the right hand side of the index defect. For higher values of E_b this change is pronounced and abrupt, and causes a destabilisation of the nematicon. In the optically rarer index defect regime nematicons experience TIR for high values of E_b. TIR is not occurring here because it is clear from Figure 5.6 that the beams have split. Some general comments can be made, however. Despite the impossibility of modelling beam splitting in the modulation equations, due to the fixed trial function, the average beam path of the multi-nematicons formed is still modelled well by the modulation theory. Furthermore, full numerical and modulation solutions cannot be found beyond the same control beam intensity of $E_b \approx 1.9$, showing that the most

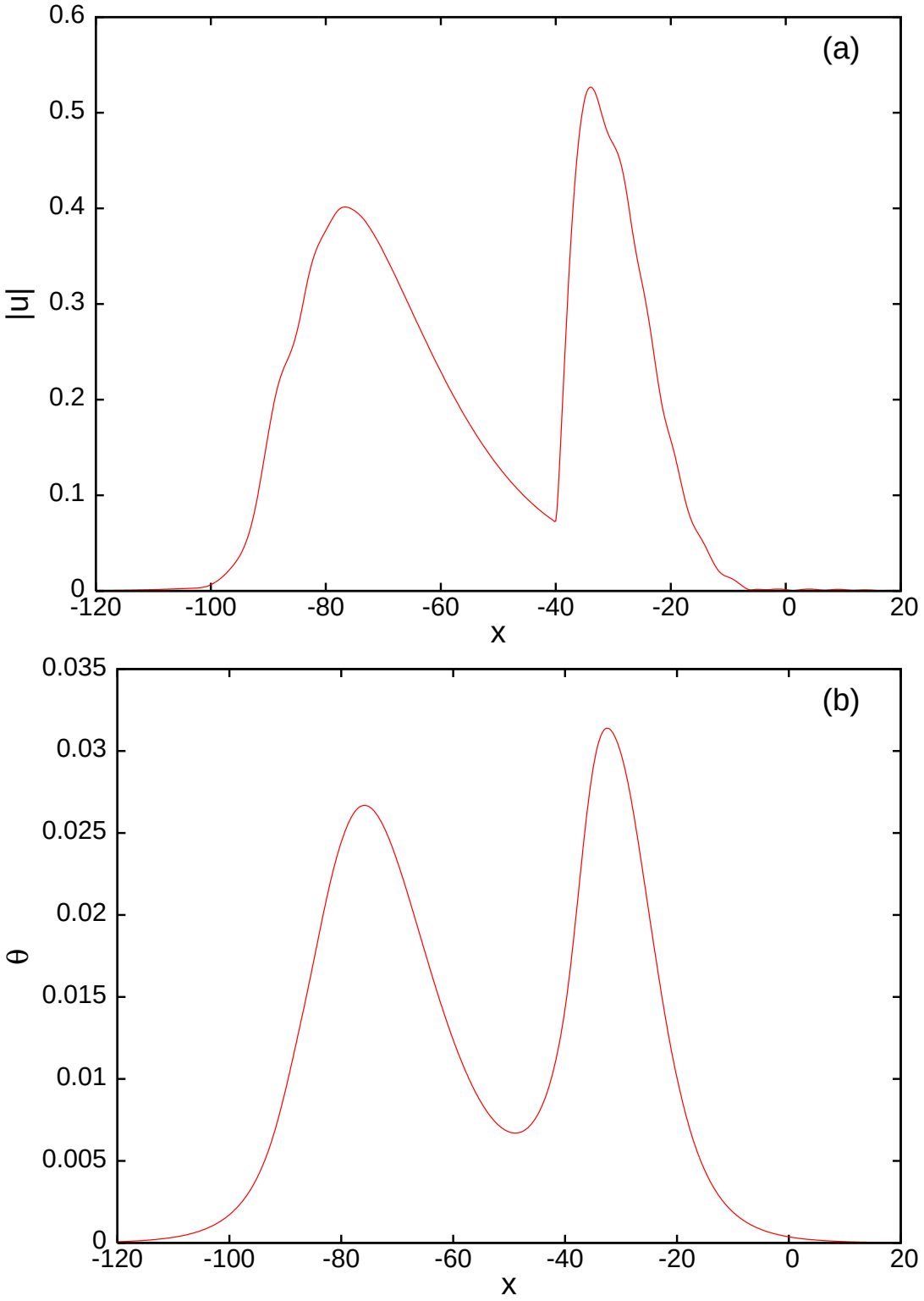

Figure 5.7: Full numerical solution for a sech initial profile at $z = 57$ with initial values $a = 1.0$, $w = 3.5$, $V_0 = -1.0$, $\xi = 0.0$, $E_b = 1.5$, $\gamma = 0.01$, $\nu = 200$ and $q = 2$ where $z_1 = 30$ and $z_2 = 60$. (a) Solution for $|u|$, (b) Solution for θ.

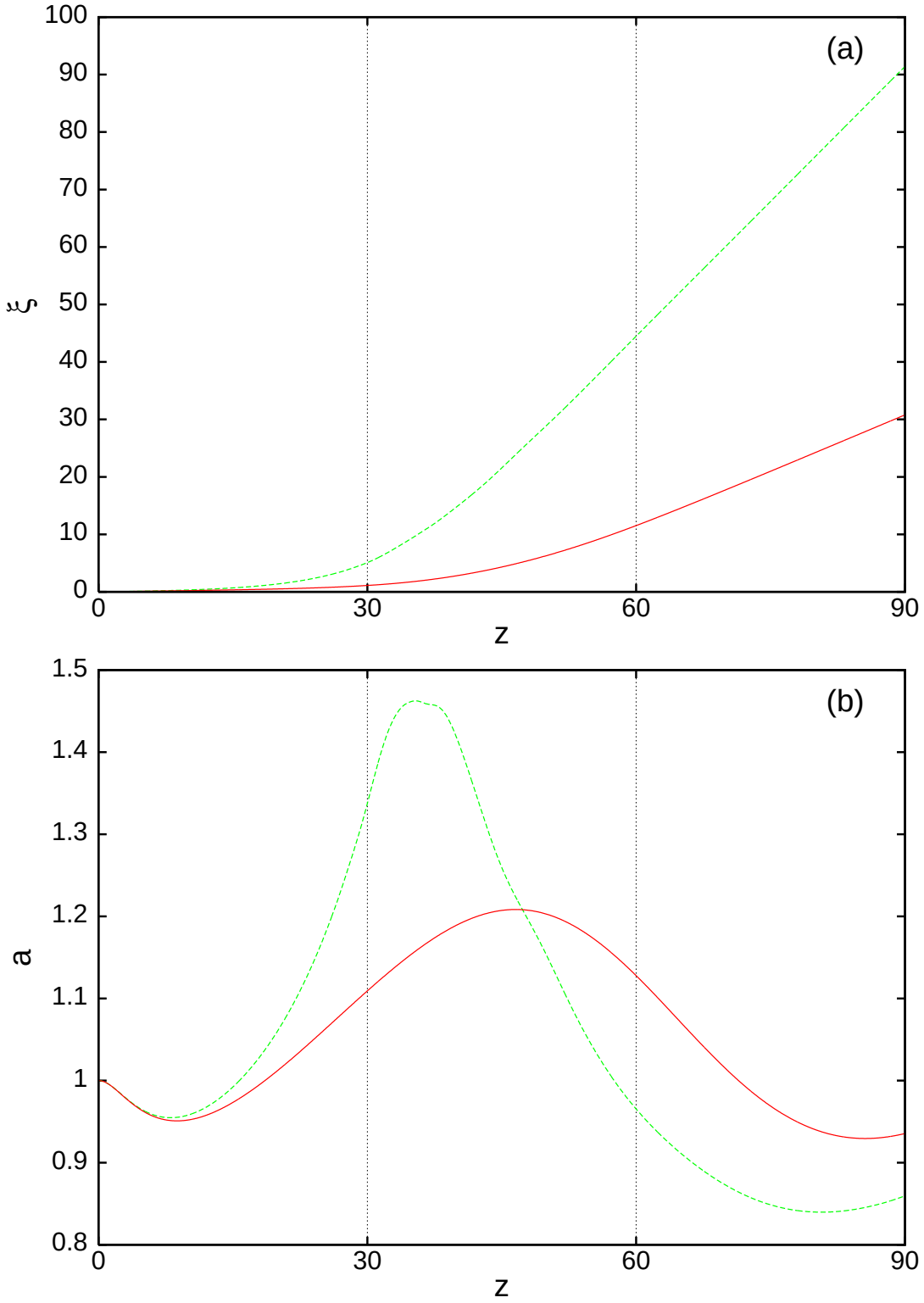

Figure 5.8: Full numerical solutions for initial values $a = 1.0$, $w = 3.5$, $V_0 = 0.02$, $\xi = 0.0$, $E_b = 1.5$, $\nu = 200$ and $q = 2$ where $z_1 = 30$ and $z_2 = 60$ with a sech initial profile where $\gamma = 0.01$ (—)[red]; $\gamma = 0.1$ (– – –)[green]. (a) Positions, (b) Amplitudes.

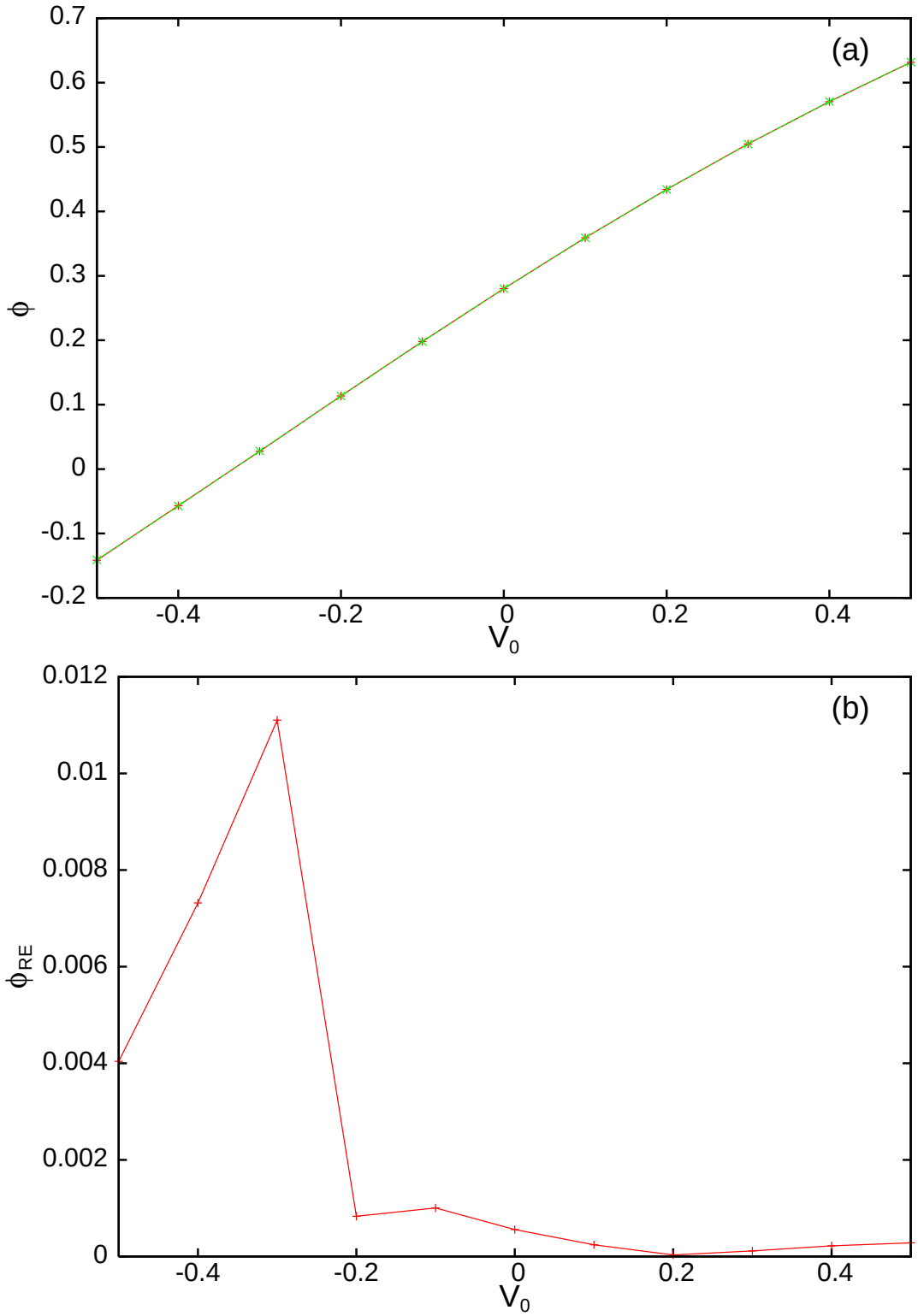

Figure 5.9: (a) Refraction angle ϕ as given by the full numerical solutions (— + —)[red] and the modulation solutions (– – × – –)[green]; (b) Refraction angle relative error ϕ_{RE} (— + —)[red] through an optically rarer index defect as given by the modulation solutions relative to the numerical solutions, as a function of V_0 with initial values $a = 1.0$, $w = 3.5$, $\xi = 0.0$, $E_b = 1.0$, $\gamma = 0.01$, $\nu = 200$, $q = 2$ where $z_1 = 30$, $z_2 = 60$.

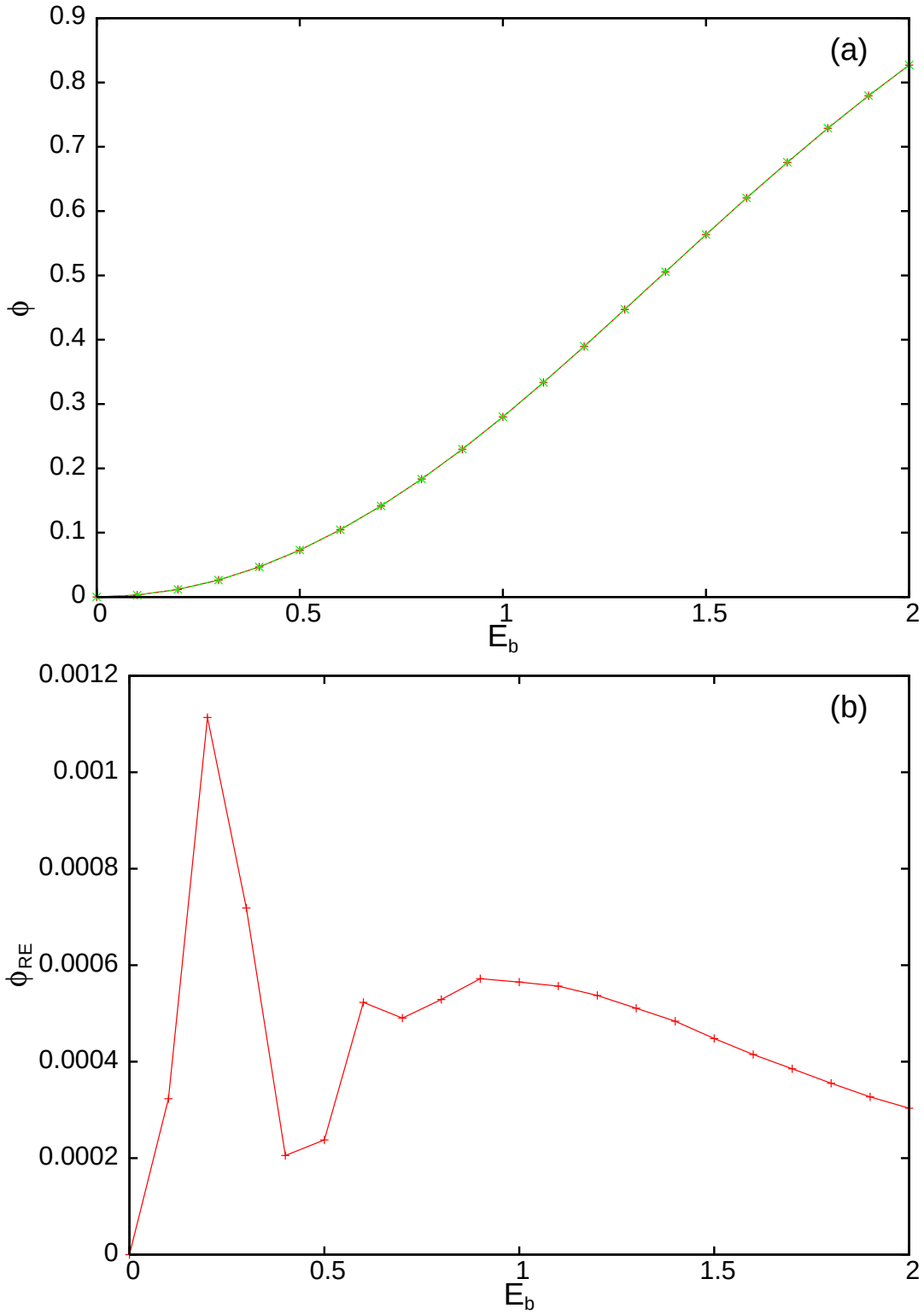

Figure 5.10: (a) Refraction angle ϕ as given by the full numerical solutions (— + —)[red] and the modulation solutions (– – × – –)[green]; (b) Refraction angle relative error ϕ_{RE} (— + —)[red] through an optically rarer index defect as given by the modulation solutions relative to the numerical solutions, as a function of E_b with initial values $a = 1.0$, $w = 3.5$, $\xi = 0.0$, $V_0 = 0.0$, $\gamma = 0.01$, $\nu = 200$, $q = 2$ where $z_1 = 30$, $z_2 = 60$.

important features of nematicon behaviour are modelled well by the modulation equations.

The effects of changes to the initial velocity of the nematicon are even more sensitive in this optically denser index defect regime. Whilst modulation solutions have been obtained for the same range of V_0 values as were obtained for nematicons in the optically rarer index defect regime, only a small range of V_0 allow sensible full numerical solutions. Outside of this smaller range the beams experience huge profile changes. Violent reactions at the right hand interface between the defect and the unaltered DD-NLC are observed. These large interactions are impossible to approximately model and so have been omitted from this analysis.

Figure 5.12 shows the influence that radiation has on the accuracy of the modulation solutions. Clearly, over the relatively short z range chosen for most of the results presented ($z \in [0, 90]$), radiation has little effect on nematicon evolution. However, over large z, radiation allows the initial beam to settle to the steady state nematicon solution. The early decay of the initial beam to the steady state can be seen in Figure 5.12(b), where the amplitude oscillations clearly begin to decay for the solution including radiation loss. Solutions excluding radiation show no oscillatory decay. It is found that removing radiation loss from the modulation equations does not affect the beam position propagation significantly, as can be seen in Figure 5.12(a). This is because the approximation is almost identical whether including or excluding radiation loss near the index defect, when the index defect is placed relatively early in the z evolution. Placing the defect further into the z evolution allows significant parameter differences to manifest between the beams including and excluding radiation loss and therefore markedly affects the refraction angle.

Figure 5.13 is a similar comparison of beam peak position and amplitude to Figure 5.5, but here the comparison is made between two full numerical solutions. A solution with a sech trial function, whose initial conditions are $a = 1.0$ and $w = 3.5$, is compared to a solution with a Gaussian trial function with initial conditions $a = 1.5$ and $w = 5.0$. Initial conditions for the Gaussian equal to those of the sech trial function were impossible because Gaussian initial conditions require more mass to form nematicons as they decay faster. A direct comparison of amplitude, for instance, is not possible due to the higher initial amplitude of the Gaussian initial beam. But it is immediately apparent that a comparison of position reveals that refraction has little to no dependence on initial beam profile, nor initial mass, since the agreement is once again near perfect. This is a surprising result since momentum walk-off observed in Chapters 3 & 4 was shown to be highly dependent on initial mass. Moreover Gaussian initial conditions did not admit nematicon solutions at all in the nonlocal regime until unphysically large nonlocality values were taken ($\nu \sim 2000$). Beam refraction observed by Piccardi *et al* was found to be highly dependent on the initial beam profile [16]. Additionally, previous results obtained by García-Reimbert *et al*, Minzoni *et al* and others whilst analysing nematicon dynamics have shown a strong dependence of beam evolution on beam initial conditions [30, 39]. Interestingly, when solutions of the *approximate equations* with Gaussian and sech trial functions, represented in Figure 5.14, are compared to the full numerical results of Figure 5.13 it is found that there is excellent agreement for the modulation solution with a hyperbolic secant trial function, but little agreement when a Gaussian trial function is used. This implies that a Gaussian initial condition undergoes significant profile changes as it evolves.

The solution of the modulation equations for a Gaussian trial function in Figure 5.14 has a very high amplitude oscillation periodicity when compared to all of the other modulation solutions presented here. Also, the amplitude more than doubles for the modulation solution, in contrast to the full numerical solution shown in Figure 5.13. This large increase in amplitude is indicative of the initial conditions being close to instability, as observed for the local two-colour nematicons of Chapter 4, for which the initial beam rapidly self-focused followed by a reversal caused by the nature of the nonlinearity. Modulation solutions are not expected to agree with numerical solutions near these regions of instability. But this does not explain the excellent agreement that the Gaussian full numerical solution has with the results obtained for the hyperbolic secant trial function. The discrepancy then is due to the regime and initial conditions being more suited to a hyperbolic secant trial function, i.e. the hyperbolic secant profile is closer to that of the steady state nematicon profile than the Gaussian profile. Since the full numerical solution allows the beam profile to change, a Gaussian initial condition may evolve to a shape more akin to a sech profile. But this option is not available when solving the modulation equations, for which the Gaussian initial profile remains a Gaussian and the beam

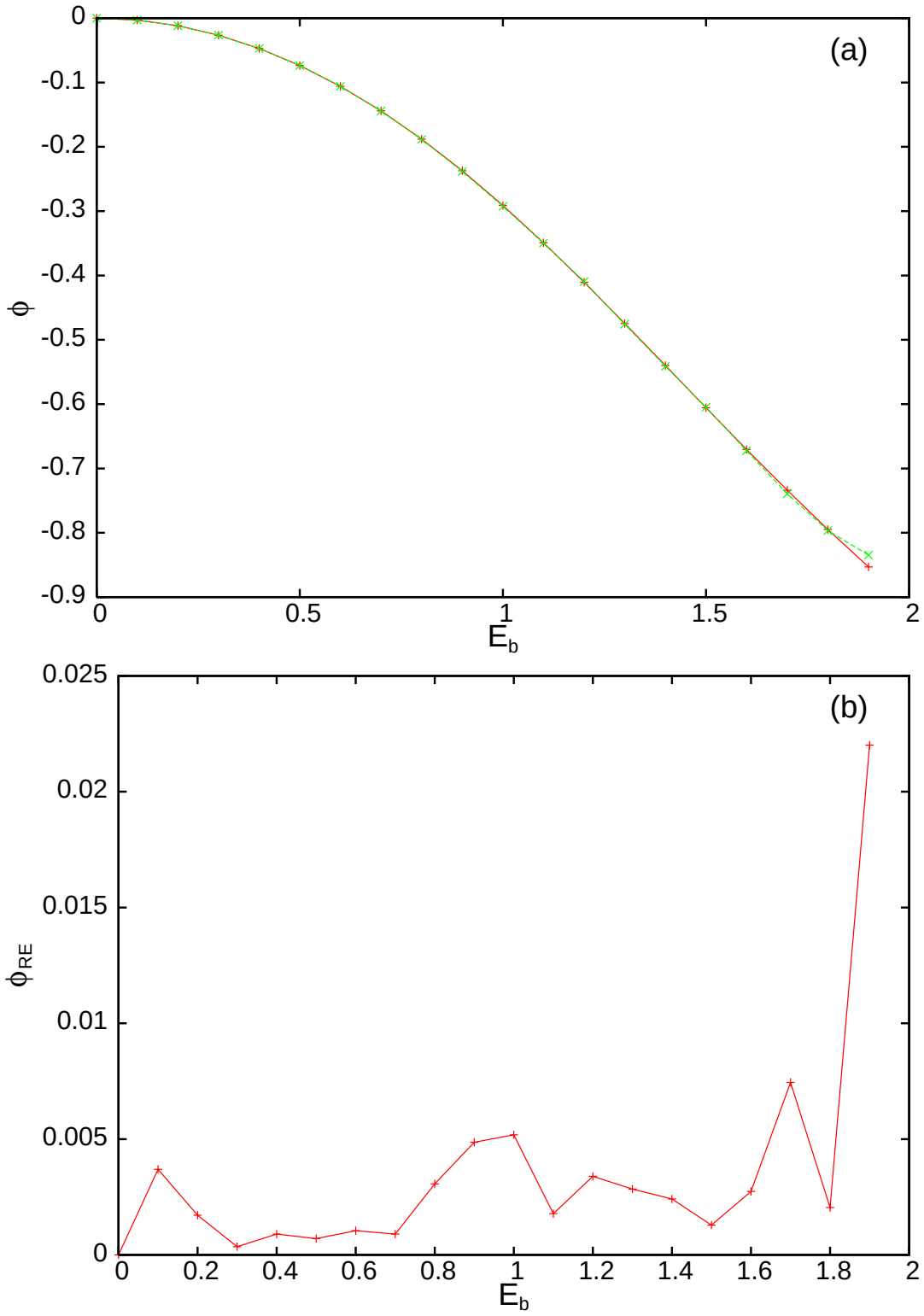

Figure 5.11: (a) Refraction angle ϕ as given by the full numerical solutions (— + —)[red] and the modulation solutions (– – × – –)[green]; (b) Refraction angle relative error ϕ_{RE} (— + —)[red] through an optically denser index defect as given by the modulation solutions relative to the numerical solutions, as a function of E_b with initial values $a = 1.0$, $w = 3.5$, $\xi = 0.0$, $V_0 = 0.0$, $\gamma = 0.01$, $\nu = 200$, $q = 2$ where $z_1 = 30$, $z_2 = 60$.

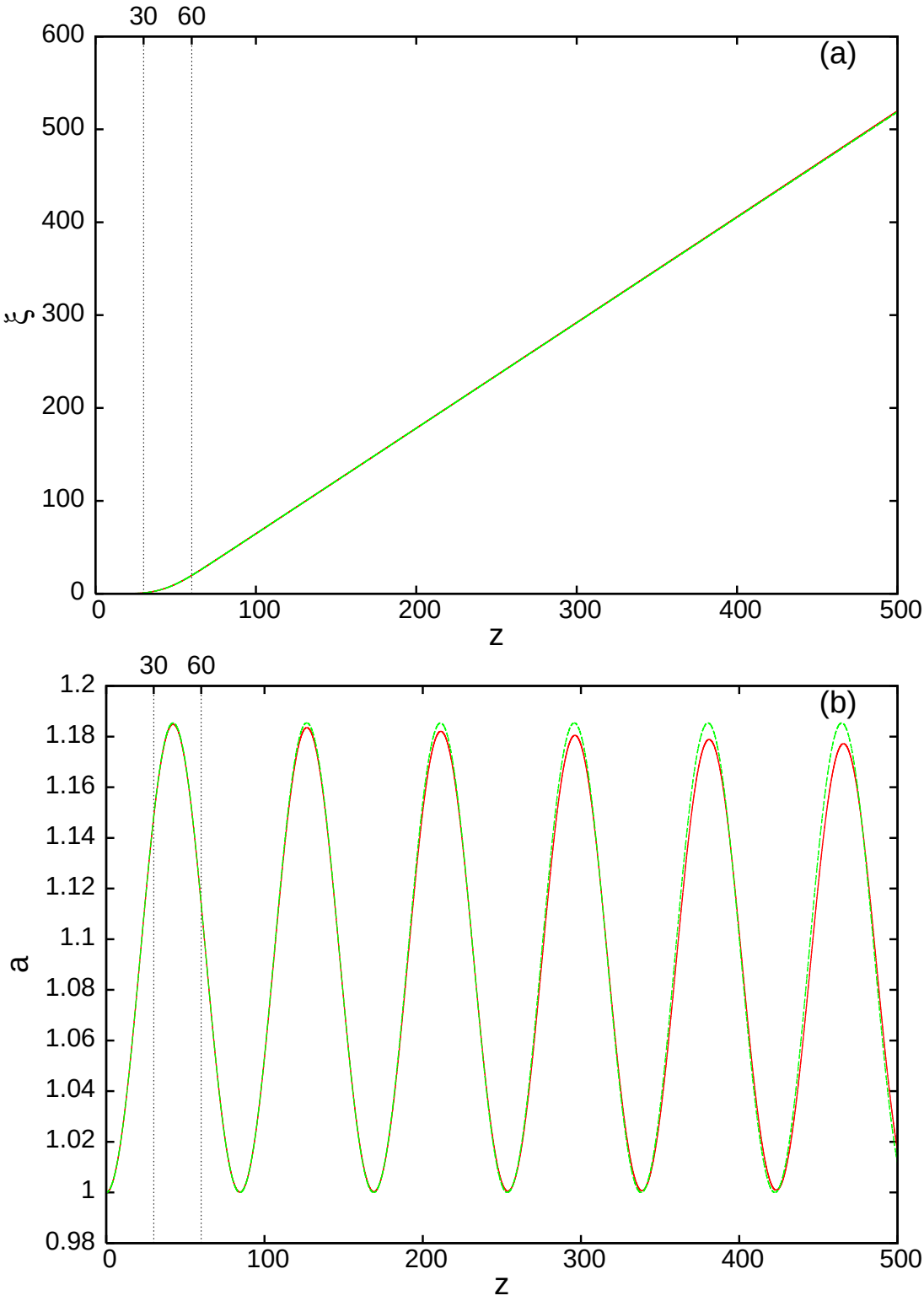

Figure 5.12: Comparisons in a DD-NLC with an optically rarer index defect for the initial conditions $a = 1.0$, $w = 3.5$, $V_0 = 0.0$, $\xi = 0.0$, $E_b = 1.5$, $\gamma = 0.02$, $\nu = 200$ and $q = 2$ with $z_1 = 30$ and $z_2 = 60$. Modulation solution including radiation loss (—)[red]; modulation solution excluding radiation loss (— — —)[green]. (a) Positions, (b) Amplitudes.

evolves to a separate steady state. A comparison of solutions obtained with sech and Gaussian trial functions in Chapter 4 revealed that the agreement between the modulation solutions and the full numerical solutions depended on the regime in question and the quantity under investigation. The results of Chapter 3 also showed that agreement improved dramatically for a Gaussian initial condition when higher values of nonlocality ($\nu \approx 2000$) were taken. However, the most interesting point about the comparison between solutions obtained with Gaussian and sech trial functions is not that the modulation solutions and full numerical solutions do not match well, nor is it that the Gaussian full numerical solution compares so well to solutions obtained with a sech trial function. It is that the Gaussian gives such good agreement for position with a completely different initial mass. Further investigation has revealed that changing the amplitude and/or width, and hence the mass, of the initial beam has little effect on the trajectory of the beam. This result is remarkable because the combined momentum walk-off found in Chapters 3 & 4 was found to be highly dependent on the initial mass of the beam.

The reason for the independence of the beam trajectory on the beam profile and its initial amplitude and width can be seen from the momentum equation (5.31). Noting that $B^2 = 2I_2$ and neglecting the radiation shelf term Λg^2 on the left hand side of the momentum equation, the terms $I_2 a^2 w^2$ and $a^2 w^2 B^2/2$ cancel out on both sides of the momentum equation, with the term $\gamma^2 B^2 w^2/4$ in the exponential on the right hand side being negligible for small γ. All of the terms in the momentum equation containing the profile of the beam then fall out and the beam trajectory is independent of the beam profile and its mass. The numerical observation that the beam trajectory is independent of the beam profile and its mass shows that the beam is shedding little diffractive radiation as it evolves, in accord with Figure 5.12. Index defect refraction then bears no relation to Poynting vector walk-off, nor the momentum walk-off found in Chapters 3 & 4.

5.4 Discussion

The evolution of a nematicon in a DD-NLC with an optical index defect has been considered. Solutions obtained in optically rarer and denser index defect regimes have been compared and contrasted. Numerical solutions of the full governing equations have been compared with solutions of approximate modulation equations, which were found in a similar manner to the approximate equations in Chapters 3 & 4. Initial velocity and the strength of the control beam electric field were varied to all-optically steer the nematicon beams. It was found that approximate solutions were in excellent agreement with full numerical solutions when considering the evolution of a variety of beam parameters. Interestingly, modulation solutions obtained for nematicons travelling in a DD-NLC with an optically rarer index defect displayed better agreement with full numerical solutions than those found for nematicons passing through an optically denser defect. Additionally, it was found that varying the initial velocity of nematicons travelling through an optically denser index defect could cause beams to split, whereas doing so in the optically rarer index defect regime could allow TIR. Finally, it was shown that initial beam mass and profile has little influence on refraction angle, and that refraction in this regime is governed by a completely different mechanism to Poynting vector walk-off and momentum walk-off observed for the two-colour nematicons in Chapters 3 & 4

It has been shown that control of nematicon beam paths can be achieved by varying the beam's initial velocity and the control beam field. The results suggest that varying both the velocity and the control beam field strength allows large nematicon refraction angles to be achieved.

The results obtained are experimentally realistic, yet a direct comparison could not be made between these results and those obtained by Piccardi *et al* experimentally [16] for a variety of reasons. In the work of Chapters 3 & 4 Poynting vector walk-off was accounted for by a phase factor transformation. Here, the same technique was used. However, the transformation is not fully justified since Poynting vector walk-off varies through the index defect. Another difficulty was found in modelling the index defect itself. The defect created in the experiments of Piccardi *et al* was too complex to be incorporated into a variational approximation due to the spreading of the control beam [16]. As a consequence, a simplified index defect model was chosen. Whilst these significant simplifications render direct comparisons with experimental results impossible,

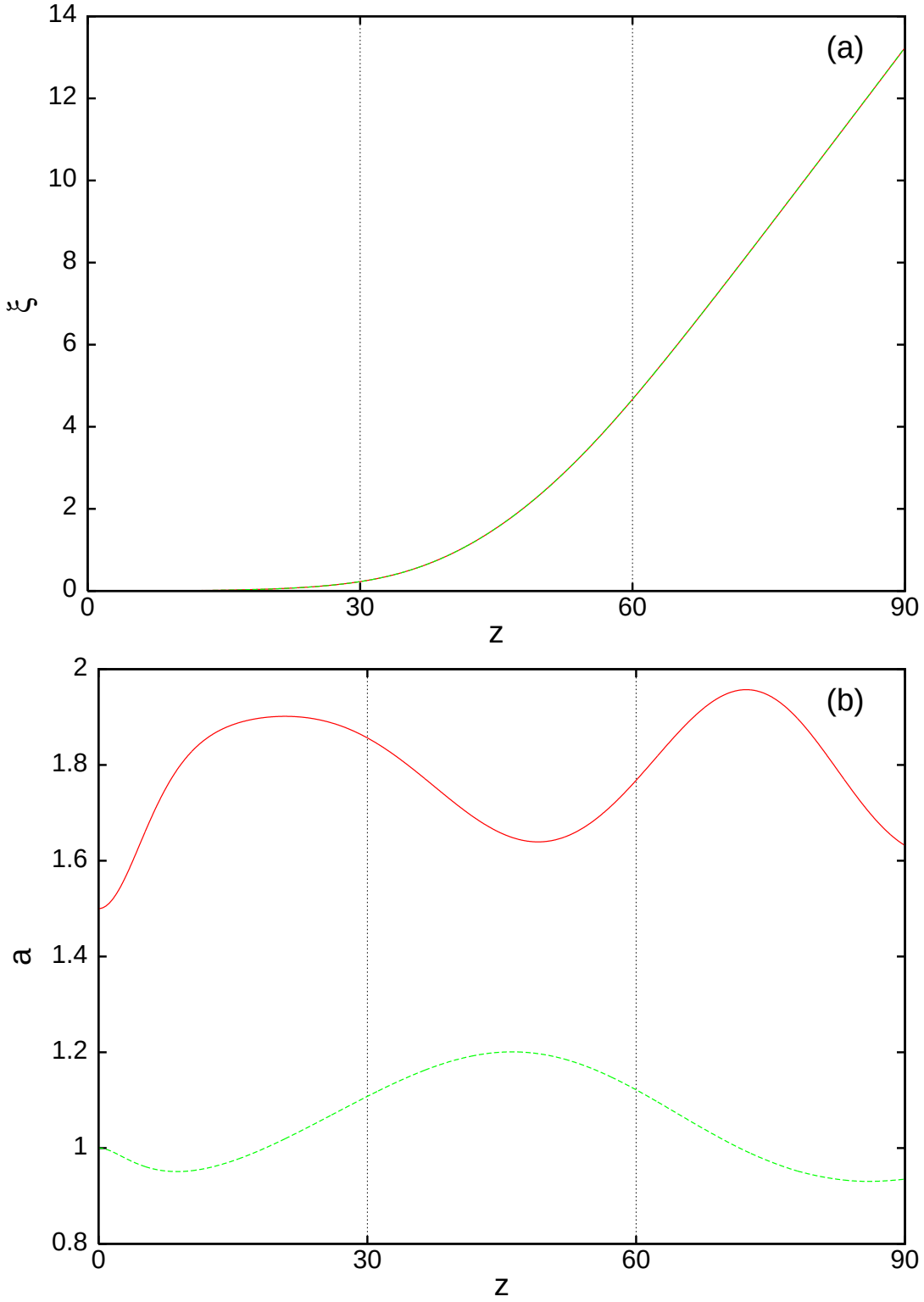

Figure 5.13: Full numerical solutions with initial values $V_0 = 0.02$, $\xi = 0.0$, $E_b = 1.5$, $\gamma = 0.01$, $\nu = 200$ and $q = 2$ with $z_1 = 30$ and $z_2 = 60$; with a sech initial profile where $a = 1.0$, $w = 3.5$ (—)[red]; with a Gaussian initial profile where $a = 1.5$, $w = 5$ (— — —)[green]. (a) Positions, (b) Amplitudes.

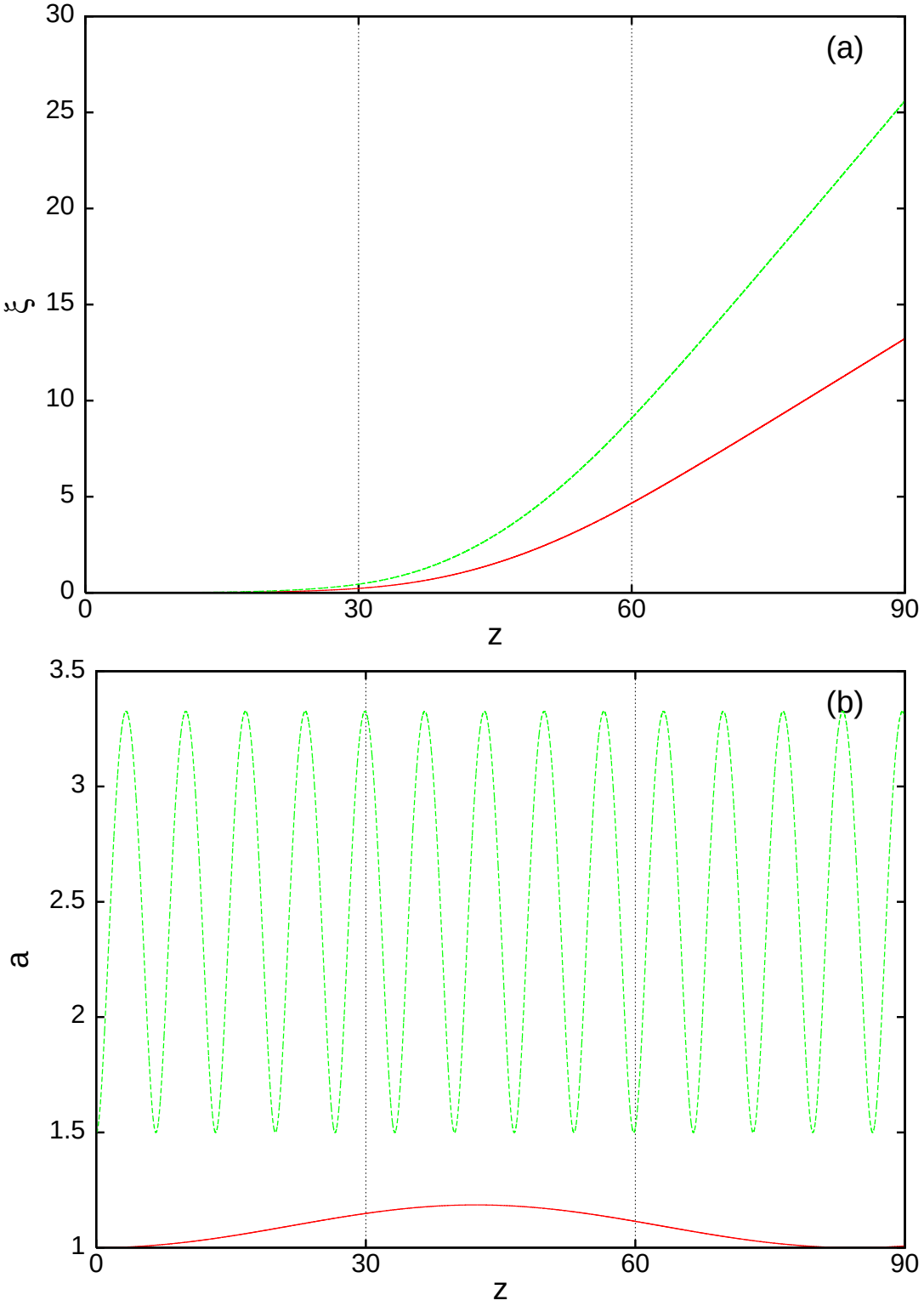

Figure 5.14: Modulation solutions with initial values $V_0 = 0.0$, $\xi = 0.0$, $E_b = 1.5$, $\gamma = 0.01$, $\nu = 200$ and $q = 2$ with $z_1 = 30$ and $z_2 = 60$; with a sech initial profile where $a = 1.0$, $w = 3.5$ (—)[red]; with a Gaussian initial profile where $a = 1.5$, $w = 5$ (— — —)[green]. (a) Positions, (b) Amplitudes.

many interesting results and conclusions have been made from such a simplified model.

Similar difficulties to those found in earlier chapters were found when calculating approximate modulation equations here. Equivalent Gaussians were used to calculate otherwise intractable integrals, an asymptotic approximation of radiation loss was made and the radiation shelf was once again modelled as being flat with an approximately calculated radius. With all of these approximations needed to calculate the modulation equations, it is remarkable that so many properties of the approximate solutions matched those of the full numerical solutions almost perfectly.

Chapter 6

Conclusions

6.1 Summary of Research

The field of liquid crystal research is now a vast and varied multi-disciplinary area with investment from industry funding investigations focusing on numerous technological applications. Nematics are just one of a large array of liquid crystals which have been utilised for their nonlinear optical properties. The nematic liquid crystal (NLC) nonlinear response to light is highly nonlocal, a result of molecular reorientation. This response is of particular interest due to its exceptional controllability. Consequently much research has been devoted to exploring and harnessing it. Introducing a beam with appropriate initial conditions into a NLC, experimental researchers have managed to balance the nonlocal nonlinear response, which causes the beam to self-focus, against natural local beam diffraction, in essence self-localising the beam and allowing soliton creation. The soliton form is highly desirable due to its robustness. Solitons can carry weaker beams, and have therefore been proposed as ideal candidates for data transmission. Furthermore, beams can be steered utilising a variety of different properties of the medium and light. In-plane nematicon steering is important as it has been proposed as a basis for switching and logic operations [6]. With so many swift developments in the experimental field, a full mathematical description of nematicon evolution in all regimes has had to follow. However, by mathematically modelling NLC nematicon problems and solving them numerically, much has already been learned about the underpinning physics. A deeper understanding has been delivered by approximating nematicons using a variety of different techniques. Work by Smyth, García-Reimbert, Minzoni, Worthy, Marchant, Garza-Hume, Bang, Rasmussen, Hu, Assanto and many more has begun to bridge the gap between experimental results and physical descriptions through mathematical modelling. This thesis has been a further extension to the work of those mentioned above.

Two-colour nematicons were created in the laboratory by Alberucci *et al* [17]. It was shown that the additional nonlinear effect of cross-phase modulation (XPM) allowed colaunched beams of different colours to form a vector nematicon. These vector nematicons were effectively steered by changing the wavelengths of the two beams. To induce an appropriate nonlinear response the NLC director had to be pre-tilted. In the experiments this was achieved by coating the boundary interfaces with polyvinyl alcohol (PVA) and then rubbing them, which induces a pre-tilt of $\pi/6$ [17]. This pre-tilt could have been achieved via an applied external static/low-frequency electric field, but it was thought that doing so would cause additional walk-off effects. Essentially then, Chapter 3 addresses the additional vector nematicon walk-off found when a static/low-frequency electric field is used to create a pre-tilt of the NLC director.

Chapter 4 is a similar investigation of the vector nematicon problem of Chapter 3, but in the local nonlinear response regime. This work can be thought of as the complement to that of Chapter 3. Experiments have focused mainly on the nonlocal nonlinear response regime which is a novel feature of the NLC. However, a local response is possible when the medium is cooled or a large pre-tilt induced. The equations governing vector nematicon evolution in the local and nonlocal regimes are derived from the same coupled nonlinear Schrödinger-like (CNLS-like) equations (also coupled to a director equation), but the material response and underlying

physics are completely different. In the local regime beams are stabilised by saturation. As nonlinearity is no longer governed by molecular reorientation, the nonlinear reaction is faster. There are also fundamental differences in the large z evolution of vector nematicons in each regime. Locality allows beams to leak diffractive radiation at a far greater rate during beam evolution and collision, and the inclusion of this radiation in the approximation was shown to make a significant difference to the quality of agreement between numerical solutions of the full governing equations and solutions of the approximate equations, whereas in the nonlocal regime, the inclusion of radiation was shown to be less necessary for good agreement.

Chapters 3 and 4 focused on the steering of nematicons using coupled beams. Chapter 5 offered an alternative approach to nematicon steering. Taking inspiration from experiments conducted by Piccardi *et al* [16], a model of single nematicon beams steered by an index defect was created. Experiments have shown that a highly tuneable index defect can be created in a dye-doped nematic liquid crystal (DD-NLC) by shining a control beam through the nematic cell wall into the nematic cell, this control beam acting on the dye molecules and inducing a reorientation of the molecular director. This technique can increase or decrease the refractive index of the DD-NLC in the defect. The results of Chapter 5 revealed that beams propagating through such refractive index defects experience refraction, allowing large angle deviation of the nematicon path, in accord with experimental results [16]. The work of Chapter 5 revealed that this refraction is caused by a deviation force acting on the beam due to the dependence of momentum on the decay of the reorientation strength in the index defect through the bulk.

To investigate the problems of Chapters 3, 4 and 5 equations governing the evolution of nematicon beams were derived. In Chapters 3 and 4 these equations were derived from the equations governing two-colour nematicons in the absence of an applied static/low-frequency electric field [17]. They can also be thought of as the two beam equivalents of single nematicon equations derived by García-Reimbert *et al* [30]. From these general equations [(3.1)–(3.3)], simplified equations were found in the nonlocal and local limits respectively. The governing equations of Chapter 5 were also a simple extension from those obtained by García-Reimbert *et al* [30]. With appropriate governing equations, soliton solutions could then be sought. Accurate numerical solutions of the full governing nematicon equations were found which revealed the detailed evolution of nematicons and these were used to analyse the accuracy of approximate solutions obtained from simplified nematicon equations. The latter solutions provided far more insight into the mechanics of nematicon evolution.

The approximate method was based on the method of Kath & Smyth [31]. Essentially this is an extended variational approximation where certain appropriate modulation equations are extended to include a radiation loss term derived from an asymptotic analysis of the linearised governing equations. Also, simple trial functions with a hyperbolic secant or Gaussian profile were extended to include a radiation shelf travelling with the beam(s). This radiation shelf was justified by numerical solutions of the full governing equations which revealed a (reasonably) flat finite shelf extending beyond the tail(s) of the beam(s). Further justification lies in the results of Kath & Smyth where a shelf was observed for a perturbed inverse scattering solution of the NLS equation [31]. Once the final modulation equations representing variations of the beam parameters were found, they were solved numerically using the standard fourth order Runge-Kutta scheme, with radiation calculated via numerical evaluation of the radiation integral at each z step. The full governing equations were solved numerically using a pseudo-spectral method, with z stepping performed using the fourth order Runge-Kutta scheme once again, however this time in Fourier space.

The Results sections of each chapter showed that combining an accurate numerical portrayal with an approximate one allows for a detailed mechanical description and understanding of nematicon evolution. Agreement between full numerical solutions and approximate solutions has been, in general, excellent. Additionally, those results that did not agree provided an interesting insight into what was missed by the approximation and how the approximation could have been improved.

6.2 Analysis of Methodology

The extended variational method allows much deeper insight into beam dynamics than can be achieved by a purely numerical approach. However, such a method places severe constraints on the problems under investigation. The experiments conducted by Alberucci *et al* [17], in which experimental two-colour nematicons were created for the first time, could not be replicated exactly for several reasons. Firstly, the variational approximation requires that the governing equations are simple enough for the equivalent Lagrangian formulation to be found. The full nematicon equations were too complex for a variational analysis to be conducted, so limits of the nonlocality/elasticity parameter ν had to be taken for nonlocal and local NLC regimes respectively. Secondly, in Chapter 5 further difficulties in the implementation of the approximate method lay in creating an index defect similar to that introduced experimentally by Piccardi *et al* in a DD-NLC. The experimental defect was created by an elliptical control beam with a Gaussian profile [16]. Such a complicated defect would render the variational problem analytically intractable. Consequently a highly simplified index defect was chosen.

Once the governing equations had been simplified enough so that a variational analysis could be conducted, several approximations had to be made so that modulation equations could be derived. Many of these approximations were common to each of the regimes. Firstly, the radiation shelf travelling with the beam had to be assumed flat. This is clearly not the case as Figure 3.3 shows. However, allowing the shelf shape to vary in the trial function(s) would severely complicate the variational analysis. Secondly, when computing the averaged Lagrangian for hyperbolic secant trial functions, certain integrals were incalculable. As a result, equivalent Gaussians were used to replace the trial functions in these integrals. To minimise the effect that this approximation had on the final results, the equivalent Gaussians were given scaling parameters so that they matched the sech profile as closely as possible. Whilst it is difficult to know exactly what effect, if any, this approximation had, it is reasonable to assume that the damage was minimal. Other significant approximations and assumptions were applied to the radiation calculation, the computation of the shelf lengths, $\tilde{\Lambda}$ and Λ, and the form of the trial functions. Improvements could potentially be made to all of these calculations which would improve the accuracy of the extended variational method in approximating nematicon evolution. For example, the secondary (outer) shelf length $\tilde{\Lambda}$, required in the approximate analysis of nonlocal nematicons, was not directly calculated but was determined from a particular numerical solution of the single nematicon problem [39]. It is possible that an analytical calculation of this value could be made.

The trial functions chosen gave an accurate portrayal of the nematicon beam shape for most quantities analysed, although some improvements could have been made. One such improvement would have been to extend the trial functions to have an elliptical cross-section [24, 43]. This would have allowed the nematicon to *"oscillate in the major and minor axes of the ellipse"* so that beam trajectory distortions, observed particularly in Chapter 3, could have been modelled [24]. Such an elliptical trial function could have been of the form

$$u = a\,\mathrm{sech}\left(\sqrt{\frac{(x-\xi_x)^2}{w_x^2}+\frac{(y-\xi_y)^2}{w_y^2}}\right) e^{i(\sigma+V_x(x-\xi_x)+V_y(y-\xi_y))} \tag{6.1}$$

where w_m, ξ_m and V_m with $m = x, y$ are the widths, positions and velocities of the beam in each direction. Whilst the inclusion of this beam distortion would have undoubtedly improved qualitative agreement, the modulation equations would have been even more difficult to derive and would have been extended and complicated to such a degree that their analysis would have lost any meaning. In choosing trial functions, a fine balance has to be made between accurately portraying beam dynamics and returning simple modulation equations from which a meaningful analysis can be conducted [34].

The extended variational method allowed fundamental conclusions to be drawn for much of the dynamical behaviour observed. The inclusion of a radiation loss term showed that the mechanism allowing initial beams to evolve to the steady state nematicon was radiation. Radiation losses allow the decay of a single beam to the steady state [30, 35, 39], but it had not previously been shown for a two-colour vector nematicon. Another notable general conclusion

was that nematicons have a beam profile very close to a sech or Gaussian profile and that a shelf of radiation does indeed form as an initial beam evolves to the steady nematicon state. As the variational method is highly dependent on the fixed beam profile, the agreement between full numerical and modulation solutions proves the quality of the trial function(s) chosen. Momentum walk-off was calculated via the momentum conservation equation in Chapters 3 and 4. This showed that momentum walk-off was a direct result of the non-symmetric optical parameters of the two beams. Additionally, the refractive walk-off observed in Chapter 5 was shown to be caused by a difference in the rate of change of momentum on each side of the beam which forced the beam to refract. These results were fundamental to the work and the mechanical reasons behind nematicon beam refraction could not have been found if a purely numerical approach had been taken.

Some notable conclusions were also made from what the approximation could not model. Position and amplitude evolution were shown to be directly affected by beam distortions and acceleration when two beams approach collision. Radiative losses resulted from these violent collisions and the subsequent evolution was influenced. Interestingly in Chapter 4 the numerically calculated position, amplitude and width oscillations decayed rapidly in comparison with those of the modulation solutions. However, the higher decay rate observed in the full numerical solutions had no influence on the momentum walk-off which matched exactly that of the modulation solutions.

Radiation loss was shown to be the essential mechanism allowing beams to evolve to steady nematicons. This result is important, yet the effects that losses have were shown to be variable. In Chapter 3 it was not clear whether beams do indeed settle to the steady state or infinitely oscillate around one another, as they do for spinning two-colour nematicons [24]. In the nonlocal regime then radiative losses were shown to be relatively unimportant and were not necessary for good agreement between full numerical and approximate solutions. It should also be noted that radiative losses only affected the accuracy of the modulation solutions over large z for the regimes presented in Chapters 4 and 5. For the short length scales found in experimental situations a standard variational analysis is more appropriate as it is less time consuming and just as accurate.

Clearly there are two key factors in the extended variational method necessary for good agreement between numerical solutions of the full governing equations and solutions of the modulation equations. Firstly, trial functions are required that accurately portray the parameter oscillations displayed in full numerical solutions. This requires that amplitude & width oscillations vary independently of velocity & position oscillations. Including radiation shelves representing radiation travelling with the beams aids agreement between the two solutions. Secondly, diffractive radiation shed by the beams as they evolve must be included in the modulation equations for the large z behaviour to match full numerical results well and to represent the essential mechanism allowing initial beams to develop into steady nematicons. If these requirements are met there is no reason why the same techniques could not be used in various other nematicon problems, or, indeed, other liquid crystal soliton problems.

6.3 Future Research

In-plane interactions of two-colour nematicons in the local and nonlocal regimes have been represented in Chapters 3 & 4. The natural extension of this work would be to investigate multiple colour nematicons. Assanto *et al* investigated the possible application of three nematicons to create an all-optical XNOR logic gate utilising the mutual attraction of nematicons [6]. In this work, a signal beam had one wavelength and the two control beams had another. The presence of one, both or neither control beam changed the output position of the signal beam. The similarity of this problem to the ones investigated here may therefore mean that it would be of interest to investigate this multiple nematicon problem further. One other obvious progression from the work of this thesis would have been to represent two-colour nematicons with angular momentum, or spiralling vector nematicons. But this problem has already been investigated. To find suitable modulation equations for the variational approximation merely required the addition of a y axis position coordinate η_k and velocity U_k in the trial function(s) used in

Chapters 3 and 4, namely

$$u_k = \left[a_k \operatorname{sech}\left(\sqrt{(x-\xi_k)^2+(y-\eta_k)^2}/w_k\right) + ig_k\right] e^{i(\sigma_k + U_k(x-\xi_k)+V_k(y-\eta_k))}, \qquad (6.2)$$

$k = 1, 2$. The calculation of the modulation equations was carried out by Smyth and co-workers in tandem with the two-colour work presented here. Working in this way, mutual verification of equations and results was possible. The full results of the spiralling vector nematicon investigation can be found in Ref. [24].

There are a number of potential avenues of further research involving steering single nematicons. Firstly, the index defect described in Chapter 5 could be refined, mimicking more closely the experimental index defect created by Piccardi *et al* [16]. In the experimental work the index defect lay in the (x, z)-plane at an angle to the propagation direction of the beam. This allowed the beam to experience total internal reflection (TIR), an effect that could not be duplicated in this thesis because the defect lay perpendicular to the z axis. Improvements in the profile and decay of the perturbed refractive index through the bulk could also be made, allowing more direct comparisons with experimental data. Secondly, research into the incorporation of Poynting vector walk-off could be conducted. The current model assumes that Poynting vector walk-off remains constant through the index defect, but this is only an approximation and it would be interesting to observe the combined walk-off and refraction effects in this regime.

The index defect created by Piccardi *et al* is just one of many new ways of steering light that have been found. One experimental set-up looked purely at TIR at the interface between two NLC media with different nonlocality and nonlinearity [68], another similar investigation focused on shining a point beam perturbing molecular orientation across the thickness of a NLC cell and deviating or splitting the nematicon beam path [69]. Beams can also be deviated by altering the optical density of regions of the NLC. This is done by applying different voltages to patterned electrodes which create regions with differing static/low-frequency electric fields [69, 70]. Negative refraction and negative reflection have been reported recently in birefringent NLC utilising beam properties at interfaces [71]. Also, investigations into the nonlinear repulsion of nematicons at the boundaries of NLC cells have been conducted [72]. Many of these experimental advances provide ideal motivation for future work in the mathematical modelling of nematicons.

A more general area of possible future research involving multiple nematicons lies in improving the approximate method for interacting beams. As two beams approach collision, the numerical results showed that they experience an acceleration which could not be incorporated into the variational method, the reason being that acceleration incorporation requires the solution of a moving boundary value problem for which the boundary is undetermined. Overcoming this nontrivial difficulty would be a valuable extension to the method.

There is one large general improvement that could be made to the approach to tackling the nematicon problems visited in this work. Namely, the inclusion of time. Beeckman *et al* investigated how nematicons form in planar NLC cells [15]. In a separate study Strinić *et al* looked into spatiotemporal optical instabilities of nematicons [73, 74]. In both of these works the beam envelope, u, was governed by a NLS-like equation similar to the ones investigated here, but the molecular director was described as a time evolution problem. This allowed both teams to describe the evolution of beams in both space and time. Whilst this approach has clear advantages, the spatiotemporal governing equations cannot be easily approximated, meaning that all of the benefits associated with approximating soliton evolution are lost.

The extended variational method was developed by Kath & Smyth to approximate the evolution of a pulse in an optical fibre [31]. Since then it has been used to approximate solutions for a variety of different soliton problems where evolution is governed by NLS-like equations or CNLS-like equations (the method has also been used to approximate soliton evolution governed by the Sine-Gordon equation [75]) and radiation plays a key role in the evolution. Particular emphasis has been given to nematicons recently, but there is no reason why the method could not be applied to other problems fulfilling these criteria. There are close relationships between the nematicon governing equations and equations governing solitons in completely different media. In fact, the nematicon governing equations are the same as those governing a thermoelastic waveguide [14]. Other similar equations are found governing solitons in colloidal suspensions

[53, 76], media with an optical thermal nonlinearity [14, 77] and photorefractive liquid crystals [78, 79]. Such a diverse range of governing equations suitable for the application of the extended variational approximation suggests a bright future for this approximate method.

Appendix A

Shelf Radius Chapter 3

The shelf radii, R_u and R_v, are determined by linearising the modulation equations about their fixed point ($a_k = \hat{a}_k + a_{k0}$, $w_k = \hat{w}_k + w_{k0}$ and $\sigma_k = \hat{\sigma}_k + \sigma_{k0}$ where $k = u, v$ and $|a_{k0}| << \hat{a}_k$, $|w_{k0}| << \hat{w}_k$ and $|\sigma_{k0}| << \hat{\sigma}_k$), assuming that diffraction and coupling coefficients can be taken as equal for the two beams ($D_u = D_v$ and $A_u = A_v$), as justified by the work of Alberucci *et al* [17]. Linearising in this manner, and after some algebra, the simple harmonic oscillator equation for g_k can be found and is given by

$$g_k'' - \frac{\Theta \Lambda_k \hat{\Sigma}_k^{'}}{I_1^2 \left(\hat{w}_k^2 + 2\hat{a}_k \hat{w}_k \varphi\right)} g_k = 0, \tag{A.1}$$

where

$$\hat{\Sigma}_k^{'} = \hat{\sigma}_k^{'} - \frac{1}{2} D_k \hat{V}_k^2, \qquad \varphi = \frac{D_k I_{22} \Gamma^2 - A_k A^2 B^2 \hat{w}_k^2 \hat{\beta}_k^2 \Gamma \left(2\hat{\alpha}_k + \hat{a}_k W_1\right)}{A_k A^2 B^2 \hat{a}_k \hat{w}_k \hat{\beta}_k \Phi},$$

$$\Phi = 2A^2 \hat{\alpha}_k \hat{\beta}_k^3 + \hat{w}_k \hat{\beta}_k W_2 \Gamma + 2B^2 \hat{w}_k^3 \hat{\alpha}_k W_0, \qquad \Gamma = A^2 \hat{\beta}_k^2 + B^2 \hat{w}_k^2, \tag{A.2}$$

$$W_1 = \frac{4A_k A^2 B^4 \hat{a}_k \hat{w}_k^4}{q\left(I_4 + A^2/4\right)\Gamma^2}, \qquad W_0 = \frac{2q\left(I_4 + A^2/4\right) B^2 \hat{w}_k \hat{\beta}_k^2 + \nu\left(8I_{42} + 1\right) B^2 \hat{w}_k}{2q\hat{\beta}_k \left(I_4 + A^2/4\right)\left(2A^2 \hat{\beta}_k^2 - B^2 \hat{w}_k^2\right)},$$

$$W_2 = \frac{8A_k A^4 B^4 \hat{a}_k^2 \hat{w}_k^3 \hat{\beta}_k}{q\left(I_4 + A^2/4\right)\Gamma^3}\left(\hat{\beta}_k - \hat{w}_k W_0\right), \qquad \Theta = \frac{D_k I_{22}}{2\hat{w}_k^2}\left[P_0 - \frac{\left(P_1 + P_2\right)}{\hat{\alpha}_k \hat{w}_k \hat{\beta}_k}\right], \quad P_0 = 1 - \frac{2\hat{a}_k \varphi}{\hat{w}_k},$$

$$P_1 = \hat{w}_k \hat{\beta}_k \left[\hat{\alpha}_k + \hat{a}_k \left(W_1 + \varphi W_2\right)\right], \quad P_2 = 2\hat{\alpha}_k \hat{a}_k \varphi \left(A^2 \hat{\beta}_k^2 - B^2 \hat{w}_k^2\right)\left(\hat{\beta}_k - W_0\right)\Gamma^{-1},$$

and $'$ denotes differentiation with respect to z.

As in Kath & Smyth, García-Reimbert *et al* and Minzoni *et al* [30, 31, 39, 43] the frequency of equation (A.1) is matched to the nematicon oscillation frequency $\hat{\Sigma}_k^{'}$ given by

$$\hat{\Sigma}_k^{'} = 2A_k A^2 B^2 \hat{\alpha}_k \hat{w}_k^2 \hat{\beta}_k^2 \left(A^2 \hat{\beta}_k^2 - 2B^2 \hat{w}_k^2\right)\left(I_2 \Gamma^2\right)^{-1}, \tag{A.3}$$

which results in an expression for the shelf radius of the beams

$$\Lambda_k = \frac{-\hat{\Sigma}_k^{'} I_1^2 \hat{w}_k \left(\hat{w}_k + 2\hat{a}_k \varphi\right)}{\Theta}. \tag{A.4}$$

Appendix B

Shelf Radius Chapter 4

The shelf radii for the two-colour nematicons are difficult to calculate in this case. Normally one would linearise the modulation equations about the fixed points and $g = 0$, which yield simple harmonic oscillator equations for u and v, then one would match the frequencies of oscillation of these equations, which depend on the shelf radii, Λ_u and Λ_v, to the nematicon frequencies at the fixed points $(\frac{d\hat{\Sigma}_u}{dz}, \frac{d\hat{\Sigma}_v}{dz})$ resulting in an expressions for the shelf radii, as was described in Appendix A for the nonlocal two-colour nematicon problem. However these calculations are laborious and complicated in the local regime due to the number of variables involved in the calculation, the size of the equations being linearised and the relationship between the two separate soliton frequencies, $\hat{\sigma}_u$ and $\hat{\sigma}_v$.

Consequently a simplified approach has been taken. If it is assumed that the nematicons are symmetric the nematicon equations reduce to a coupled pair of local nematicon equations. The shelf radii, R_u and R_v, can then be determined by linearising the reduced modulation equations about their fixed point. Taking $a_k = \hat{a}_k + a_{k0}$, $w_k = \hat{w}_k + w_{k0}$ and $\sigma_k = \sigma a_k + \sigma_{k0}$ where $k = u, v$ and $|a_{k0}| << \hat{a}_k$, $|w_{k0}| << \hat{w}_k$ and $|\sigma_{k0}| << \hat{\sigma}_k$, where $k = u, v$ it is then possible to linearise the modulation equations. The equation for g_u, equation (4.27), can be linearised in this was and then rearranged which yields

$$\hat{a}_u \hat{w}_u^2 I_1 \frac{dg}{dz} = \frac{-192 A_u^4 I_8}{q^3} \hat{a}_u^8 \hat{w}_u w_{u0}, \tag{B.1}$$

$$ID_u = \frac{4 A_u^2 I_4}{q} \hat{a}_u^2 \hat{w}_u^2. \tag{B.2}$$

Equation (B.1) can then be differentiated

$$\frac{d^2 g}{dz^2} + \frac{192 A_u^4 I_8 \hat{a}_u^7}{q^3 I_1 \hat{w}_u} \frac{dw_{u0}}{dz} = 0. \tag{B.3}$$

dw_{u0}/dz is found by linearising equation (4.26)

$$I_1 \hat{a}_u \hat{w}_u \frac{dw_{u0}}{dz} = \Lambda_u g \frac{d\Sigma_{u0}}{dz}, \tag{B.4}$$

where

$$\frac{d\Sigma_{u0}}{dz} = \frac{d\sigma_{u0}}{dz} - \frac{1}{2} D_u V_{u0}^2, \tag{B.5}$$

and a simple harmonic oscillator equation follows directly from (B.3) and (B.4)

$$\frac{d^2 g}{dz^2} + \frac{192 I_8 A_u^4 \Lambda_u \hat{a}_u^6}{q^3 I_1^2 \hat{w}_u^2} \frac{d\Sigma_{u0}}{dz} g = 0. \tag{B.6}$$

An expression for Λ_u is derived directly from the above calculations, namely

$$\Lambda_u = \frac{q^3 I_1^2 \hat{w}_u^2}{192 A_u^4 I_8 \hat{a}_u^6} \frac{d\Sigma_{u0}}{dz} \tag{B.7}$$

By linearising equation (4.28) a simple expression of $\frac{d\Sigma_{u0}}{dz}$ can be derived. Substituting this into (B.6), the resultant shelf radius Λ_u for the u beam can finally be given by

$$\Lambda_u = \frac{I I_1^2 D_u q^3}{384 A^4 I_2 I_8 \hat{a}_u^6}. \tag{B.8}$$

The above expression is the two beam equivalent of that calculated by García-Reimbert *et al* for a single nematicon in the local regime [30]. Obvious symmetric substitutions yield an equivalent expression for Λ_v

Appendix C

Published Papers

In addition to the presentation of research at numerous international conferences, the author of this thesis has also co-authored the following articles

- B. D. Skuse and N. F. Smyth, "Two-color vector-solitons in nematic liquid crystals in the local response regime," *Phys. Rev. A 77*, 013817 (2008).

  URL: http://link.aps.org/doi/10.1103/PhysRevA.77.013817

- B. D. Skuse and N. F. Smyth, "Two-colour nematicon interactions in local crystals," IEEE/LEOS Winter Topicals Meetings Series 2008, 14–16 January 2008, 125–126 (2008).

  URL: http://www.maths.ed.ac.uk/∼noel/twocoloursorrento.pdf

- B. D. Skuse and N. F. Smyth, "Interaction of two-color solitary waves in a liquid crystal in the nonlocal regime," *Phys. Rev. A 79*, 063806 (2009).

  URL: http://link.aps.org/doi/10.1103/PhysRevA.79.063806

- G. Assanto, B. D. Skuse and N. F. Smyth, "Optical path control of solitary waves in dye-doped nematic liquid crystals," *Photon. Lett. Pol 1*, 154–156 (2009).

  URL: http://photonics.pl/PLP/index.php/letters/article/view/1-52

Bibliography

[1] J. Scott Russell, "Report on waves," *Fourteenth meeting of the British Association for the Advancement of Science*, (1844).

[2] A. Hasegawa and F. Tappert, "Transmission of stationary nonlinear optical physics in dispersive dielectric fibers. I. Anomalous dispersion," *Appl. Phys. Lett. 23*, 142–144 (1973).

[3] A. Hasegawa and F. Tappert, "Transmission of stationary nonlinear optical physics in dispersive dielectric fibers. II. Normal dispersion," *Appl. Phys. Lett. 23*, 171–172 (1973).

[4] L. F. Mollenauer, R. H. Stolen and J. P. Gordon, "Experimental Observation of Picosecond Pulse Narrowing and Solitons in Optical Fibers," *Phys. Rev. Lett. 45*, 1095–1098 (1980).

[5] Y. S. Kivshar and G. P. Agrawal, *Optical Solitons. From Fibers to Photonics,* Academic Press, San Diego (2003).

[6] G. Assanto, M. Peccianti and C. Conti, "Nematicons: Optical spatial solitons in nematic liquid crystals," *Optics & Photonics News 14*, 44–48 (2003).

[7] E. Braun, L. P. Faucheux, A. Libchaber, "Strong self-focusing in nematic liquid crystals," *Phys. Rev. A. 48*, 611–622 (1993).

[8] M. Warenghem, J. Henninot, and G. Abbate, "Nonlinearly induced self waveguiding structure in dye doped nematic liquid crystals confined in capillaries," *Opt. Express 2*, 483–490 (1998).

[9] M. Peccianti, A. De Rossi, G. Assanto, A. De Luca, C. Umeton and I. Khoo, "Electrically assisted self-confinement and waveguiding in planar nematic liquid crystal cells," *Appl. Phys. Lett. 77*, 7–9 (2000).

[10] W. Królikowski and O. Bang, "Solitons in nonlocal nonlinear media: Exact solutions," *Phys. Rev. E 63*, 016610 (2000).

[11] C. Weilnau, M. Ahles, J. Petter, D. Träger, J. Schröder and C. Denz, "Spatial optical (2+1)-dimensional scalar- and vector-solitons in saturable nonlinear media," *Ann. Phys. 11*, 573–629 (2002).

[12] W. Hu, S. Ouyang, P. Yang, Q. Guo and S. Lan, "Short-range interactions between strongly nonlocal spatial solitons," *Phys. Rev. A 77*, 033842 (2008).

[13] M. A. Karpierz, "Solitary waves in liquid crystalline waveguides," *Phys. Rev. E 66*, 0336603 (2002).

[14] E. A. Kuznetsov, A. M. Rubenchick and V. E. Zakharov, "Soliton stability in plasmas and hydrodynamics," *Phys. Rep. 142*, 103–165 (1986).

[15] J. Beeckman, K. Neyts, X. Hutsebaut, C. Cambournac and M. Haelterman, "Time Dependence of Soliton Formation in Planar Cells of Nematic Liquid Crystals," *IEEE J. Quantum Electron. 41*, 735–740 (2005).

[16] A. Piccardi, G. Assanto, L. Lucchetti and F. Simoni, "All-optical steering of soliton waveguides in dye-doped liquid crystals," *Appl. Phys. Lett. 93*, 171104 (2008).

[17] A. Alberucci, M. Peccianti, G. Assanto, A. Dyadyusha and M. Kaczmarek, "Two-color vector solitons in nonlocal media," *Phys. Rev. Lett. 97*, 153903 (2006).

[18] M. Peccianti, C. Conti, G. Assanto, A. De Luca and C. Umeton "Routing of anisotropic spatial solitons and modulation instability in liquid crystals," *Nature 432*, 733–737 (2004).

[19] G. Assanto, M. Peccianti, K. A. Brzdkiewicz, A. De Luca and C. Umeton, "Nonlinear wave propagation and spatial solitons in nematic liquid crystals," *J. Nonl. Opt. Phys. Mat. 12*, 123-134 (2003).

[20] M. Peccianti, K. A. Brzdkiewicz and G. Assanto, "Nonlocal spatial soliton interactions in nematic liquid crystals," *Opt. Lett. 27*, 1460–1462 (2002).

[21] A. Fratalocchi, A. Piccardi, M. Peccianti and G. Assanto, "Nonlinear management of the angular momentum of soliton clusters: theory and experiments," *Phys. Rev. A 75,* 063835 (2007).

[22] B. D. Skuse and N. F. Smyth, "Two-color vector-solitons in nematic liquid crystals in the local response regime," *Phys. Rev. A 77*, 013817 (2008).

[23] B. D. Skuse and N. F. Smyth, "Interaction of two-color solitary waves in a liquid crystal in the nonlocal regime," *Phys. Rev. A 79*, 063806 (2009).

[24] G. Assanto, N. F. Smyth and A. L. Worthy, "Two-color, nonlocal vector solitary waves with angular momentum in nematic liquid crystals," *Phys. Rev. A 78*, 013832 (2008).

[25] G. B. Whitham, *Linear and nonlinear waves*, Wiley, New York (1974).

[26] I. C. Khoo, *Liquid Crystals: Physical Properties and Nonlinear Optical Phenomena,* Wiley, New York (1995).

[27] C. Conti, M. Peccianti and G. Assanto, "Route to Nonlocality and Observation of Accessible Solitons," *Phys. Rev. Lett. 91*, 073901 (2003).

[28] G. Assanto and M. Peccianti, "Spatial solitons in nematic liquid crystals," *IEEE J. Quantum Electron. 39*, 13–21 (2003).

[29] C. Conti, M. Peccianti and G. Assanto, "Observation of Optical Spatial Solitons in a Highly Nonlocal Medium," *Phys. Rev. Lett. 92*, 113902 (2004).

[30] C. García-Reimbert, A. A. Minzoni and N. F. Smyth, "Spatial soliton evolution in nematic liquid crystals in the nonlinear local regime," *J. Opt. Soc. Am. B 23*, 294–301 (2006).

[31] W. L. Kath and N. F. Smyth, "Soliton evolution and radiation loss for the nonlinear Schrödinger equation", *Phys. Rev. E 51*, 1484–1492 (1995).

[32] N. F. Smyth and W. L. Kath, "Radiative losses due to pulse interactions in birefringent nonlinear optical fibers," *Phys. Rev. E 63*, 036614 (2001).

[33] J. Yang, "Vector solitons and their internal oscillations in birefringent nonlinear optical fibers," *Stud. Appl. Math. 98*, 61–97 (1997).

[34] B. A. Malomed, "Variational methods in nonlinear fiber optics and related fields," *Progress in Optics 43*, E. Wolf, Elsevier Science, 71–193 (2002).

[35] C. García-Reimbert, A. A. Minzoni, N. F. Smyth and A. L. Worthy, "Large-amplitude nematicon propagation in a liquid crystal with local response," *J. Opt. Soc. Am. B 23*, 2551–2558 (2006).

[36] D. Anderson, "Variational approach to nonlinear pulse propagation in optical fibers," *Phys. Rev. A 27*, 3135–3145 (1983).

[37] D. J. Kaup and A. C. Newell, "Solitons as particles, oscillators, and in slowly changing media: a singular perturbation theory," *Proc. R. Soc. Lond. A 361*, 413–446 (1978).

[38] A. A. Minzoni, "The Mathematical Analysis of the Coupling Between Radiation and Nematicons, Results and Open Questions," LIWAN-2008, SASTRA University, Tamil Nadu, 8 December 2008.

[39] A. A. Minzoni, N. F. Smyth and A. L. Worthy, "Modulation solutions for nematicon propagation in nonlocal liquid crystals," *J. Opt. Soc. Am. B 24*, 1549–1556 (2007).

[40] L. Atkinson, P. J. Harley and J. D. Hudson, *Numerical methods with Fortran 77: A practical introduction*, Longman Group, UK (1989).

[41] M. J. Miksis and L. Ting, "A numerical method for long time solutions of integro-differential systems in multiphase flow," *Comput. Fluids 16*, 327–340 (1988).

[42] B. Fornberg and G. B. Whitham, "A Numerical and Theoretical Study of Certain Nonlinear Wave Phenomena", *Phil. Trans. R. Soc. Lond. A 289*, 373–403 (1978).

[43] C. García-Reimbert, A. A. Minzoni, T. R. Marchant, N. F. Smyth and A. L. Worthy, "Dipole soliton formation in a nematic liquid crystal in the nonlocal limit," *Physica. D 237*, 1088–1102 (2008).

[44] F. If, P. Berg, P. L. Christiansen and O. Skovgaard, "Split-step spectral method for nonlinear Schrödinger equation with absorbing boundaries," *J. Comp. Phys. 72*, 501–503 (1987).

[45] W. H. Press, S. A. Teukolsky, W. T. Vetterling and B. P. Flannery, *Numerical Recipes in Fortran. The Art of Scientific Computing*, Cambridge University Press, UK (1992).

[46] M. Shen, Q. Kong, J. Shi and Q. Wang, "Incoherently coupled two-color Manakov vector solitons in nonlocal media," *Phys. Rev. A 77*, 015811 (2008).

[47] A. Alberucci and G. Assanto, "Propagation of optical solitons in finite-size media: interplay between nonlocality and boundary conditions," *J. Opt. Soc. Am. B 24*, 2314–2320 (2007).

[48] A. Alberucci, G. Assanto, D. Buccoliero, A. S. Desyatnikov, T. R. Marchant and N. F. Smyth, "Modulation analysis of boundary-induced motion of optical solitary waves in a nematic liquid crystal" *Phys. Rev. A 79*, 043816 (2009).

[49] M. Peccianti, A. Fratalocchi and G. Assanto, "Transverse dynamics of nematicons," *Opt. Express 12*, 6524–6529 (2004).

[50] T. R. Marchant and N. F. Smyth, "Nonlocal validity of an asymptotic one-dimensional nematicon solution," *J. Phys. A: Math. Theor. 41*, 365201 (2008).

[51] R. H. Goodman and R. Haberman, "Vector-soliton collision dynamics in nonlinear optical fibers," *Phys. Rev. E 71*, 056605 (2005).

[52] A. W. Snyder and D. J. Mitchell, "Accessible Solitons," *Science 276*, 1538–1541 (1997).

[53] M. Matuszewski, W. Królikowski and Y. S. Kivshar, "Spatial solitons and light-induced instabilities in colloidal media," *Opt. Express 16,* 1371–1376 (2008).

[54] N. I. Nikolov, D. Neshev, O. Bang and W. Z. Królikowski, "Quadratic solitons as nonlocal solitons," *Phys. Rev. E 68*, 036614 (2003).

[55] P. D. Rasmussen, O. Bang and W. Królikowski, "Theory of nonlocal soliton interaction in nematic liquid crystals," *Phys. Rev. E 72*, 066611 (2005).

[56] A. Fratalocchi, M. Peccianti, C. Conti and G. Assanto, "Spiralling and cyclic dynamics of nematicons," *Mol. Cryst. Liq. Cryst. 421*, 197–207 (2004).

[57] A. A. Minzoni, N. F. Smyth and A. L. Worthy, "A variational approach to the stability of an embedded NLS soliton at the edge of the continuum," *Physica D 206*, 166–179 (2005).

[58] C. García-Reimbert, C. E. Garza-Hume, A. A. Minzoni and N. F. Smyth, "Active TM mode envelope soliton propagation in a nonlinear nematic waveguide," *Physica D 167*, 136–152 (2002).

[59] W. Hu, T. Zhang, Q. Guo, L. Xuan and S. Lan, "Nonlocality-controlled interaction of spatial solitons in nematic liquid crystals," *Appl. Phys. Lett. 89*, 071111 (2006).

[60] B. Luther-Davies and G. Stegeman in: S. Trillo and W. Torruellas (Eds), *Spatial solitons,* Springer Verlag, Berlin (2001).

[61] F. Simoni, L. Lucchetti, D. Lucchetta, and O. Francescangeli, "On the origin of the huge nonlinear response of dye-doped liquid crystals," *Opt. Express 9*, 85–90 (2001).

[62] L. Lucchetti, M. Gentili and F. Simoni, "Colossal optical nonlinearity induced by a low frequency external electric field in dye-doped liquid crystals," *Opt. Express 14*, 2236-2241 (2006).

[63] L. Lucchetti, M. Gentili, F. Simoni, S. Pavliuchenko, S. Subota and V. Reshetnyak, "Surface-induced nonlinearities of liquid crystals driven by an electric field," *Phys. Rev. E 78*, 061706 (2008).

[64] A. Fratalocchi and G. Assanto, "Governing soliton splitting in one-dimensional lattices," *Phys. Rev. E 73*, 046603 (2006).

[65] C. García-Reimbert, C. Garza-Hume, A. A. Minzoni, J. A. Reyes, R. F. Rodríguez and N. F. Smyth, "Active propagation and cut-off for low TM modes in a nonlinear nematic waveguide," *Physica D 145*, 144–157 (2000).

[66] M. Peccianti, A. Dyadyusha, M. Kaczmarek and G. Assanto, "Escaping solitons from a trapping potential," *Phys. Rev. Lett. 101*, 153902 (2008).

[67] G. Assanto, A. A. Minzoni, M. Peccianti and N. F. Smyth, "Optical solitary waves escaping a wide trapping potential in nematic liquid crystals: Modulation theory," *Phys. Rev. A 79*, 033837 (2009).

[68] M. Peccianti, G. Assanto, A. Dyadyusha and M. Kaczmarek, "Nonspecular Total Internal Reflection of Spatial Solitons at the Interface between Highly Birefringent Media," *Phys. Rev. Lett. 98*, 113902 (2007).

[69] M. Peccianti, A. Alberucci and G. Assanto, "Nonlinear bouncing of nematicons at the boundaries," *IEEE/LEOS Winter Topical Meeting Series, 2008*, 115–116 (2008).

[70] M. Peccianti, A. Dyadyusha, M. Kaczmarek and G. Assanto, "Tunable refraction and reflection of self-confined light beams," *Nat. Phys. 2*, 737–741 (2006).

[71] M. Peccianti and G. Assanto,"Nematicons across interfaces: anomalous refraction and reflection of solitons in liquid crystals," *Opt. Express 15*, 8021–8028 (2007).

[72] A. Alberucci, M. Peccianti and G. Assanto, "Nonlinear bouncing of nonlocal spatial solitons at the boundaries," *Opt. Lett. 32*, 2795–2797 (2007).

[73] A. Strinić, D. Timotijević, D. Arsenović, M. Petrović, and M. Belić, "Spatiotemporal optical instabilities in nematic solitons," *Opt. Express 13*, 493–504 (2005).

[74] A. I. Strinić, D. M. Jović, M. S. Petrović, D. V. Timotijević, N. B. Aleksić, and M. R. Belić, "Counterpropagating beams in nematic liquid crystals," *Opt. Express 14*, 12310-12315 (2006).

[75] N. F. Smyth and A. L. Worthy, "Soliton evolution and radiation loss for the sine-Gordon equation," *Phys. Rev. E 60*, 2330–2336 (1999).

[76] N. Ghofraniha, C. Conti, C. and G. Ruocco," Aging of the nonlinear optical susceptibility in doped colloidal suspensions," *Phys. Rev. B 75*, 224203 (2007).

[77] C. Rotschild, B. Alfassi, O. Cohen and M. Segev, "Long-range interactions between optical solitons," *Nature Physics 2,* 769–774 (2006).

[78] A. V. Mamaev, A. A. Zozulya, V. K. Mezentsev, D. Z. Anderson and M. Saffman, "Bound dipole solitary solutions in anisotropic nonlocal self-focusing media," *Phys. Rev. A 56*, R1110–R1113 (1997).

[79] M. Segev, G. C. Valley, B. Crosignani, P. DiPorto and A. Yariv, "Steady-state spatial screening solitons in photorefractive materials with external applied field," *Phys. Rev. Lett. 73*, 3211–3214 (1994).